Karlsruhe Institute of Technology

European Organization for Nuclear Research
Organisation européenne pour la recherche nucléaire

Diplomarbeit

Diploma Thesis

June 2014

Advanced Heat Transfer Studies in Superfluid Helium for Large-scale High-yield Production of Superconducting Radio Frequency Cavities

by cand.-Ing. Benedikt J. Peters

Assignment:

Prof. Dr.-Ing. Steffen Grohmann
Karlsruhe Institute of Technology (KIT)
Institute for Technical Thermodynamics and Refrigeration

Second corrector:

PD Dr.rer.nat. Edme H. Hardy
Karlsruhe Institute of Technology (KIT)
Institute for Mechanical Process Engineering and Mechanics

Supervision:

DSc. Karl-Martin Schirm
European Organization for Nuclear Research (CERN)
Beams Department, Radio Frequency Group

Dr.rer.nat. Torsten Koettig
European Organization for Nuclear Research (CERN)
Technology Department, Cryogenics Group

Karlsruher Institut für Technologie

Institute for Technical Thermodynamics and Refrigeration (ITTK)
Head: Prof. Dr. Karlheinz Schaber

Kaiserstraße 12
76131 Karlsruhe, Germany

Phone: 0721 608-42332
Fax: 0721 608-42335
Email: steffen.grohmann@kit.edu
Web: http://www.ttk.kit.edu/

Official in charge: Prof. Dr. Steffen Grohmann
Our reference:
Date: 2013-08-28

Karlsruhe Institute of Technology
Institute for Technical Thermodynamics and Refrigeration

Topic for Diploma Thesis

Advanced Heat Transfer Studies in Superfluid Helium for Large-scale High-yield Production of Superconducting Radio Frequency Cavities

Type: Diploma thesis

Focus: ☒ Literature study ☒ Theory ☐ Design ☒ Experiment

Supervision: Dr. Karl Schirm (CERN, BE Department, RF-Group), karl.schirm@cern.ch
Dr. Torsten Koettig (CERN, TE Dept., Cryogenics Group) torsten.koettig@cern.ch

Assignment: Prof. Dr.-Ing. Steffen Grohmann

Scope of Work

Cavity diagnostics is essential for quality assurance during production. Oscillating superleak transducers of second sound (OST) are extensively and successfully used for quench location on superconducting cavities, e.g. in the ILC high gradient challenge. Despite the success in finding quench spots by triangulation, the accuracy is limited by the fact that the quench information propagates at a velocity faster than for pure second sound. Therefore, a mathematical method using the propagation velocity as a fit parameter is usually applied to derive the quench location. This method can give a good correlation between measured quench spots and actual defects on elliptical cavities, but the actual mechanism of heat transport remains unclear. A better understanding of this process would enable an enhanced detector accuracy and pave the way for application in more complex structures like crab cavities. For this purpose, a dedicated experiment has recently been set up at CERN, consisting of a 3 GHz elliptical cavity with resistors glued to the inner surface for simulating quench spots.

The following issues shall be addressed within this thesis:

a) Become acquainted with fundamentals of heat propagation in superfluid helium

b) Experimental investigations using the CERN set-up, applying e.g. variations in power and pulse lengths of the heat input

c) Data analyses
   - Influence of the set-up geometry on the measured propagation velocity
   - Model development for heat propagation from the inner cavity wall through the helium bath
   - FFT analysis to distinguish between signals created from second sound and possible other effects, such as boiling

d) Participation in quench location tests on cavities in vertical test stands for the SPL and for crab cavity projects
   - Determination of quench spots by triangulation of OST signals
   - Participation in tests with CERN's optical inspection systems to take images of the quench spots

The diploma thesis shall be written in English language. A two-sided summary in German language must be submitted together with the thesis.

Name of Student: Mr. Peters, Benedikt

Start of Work: 01.12.2013

2013-08-28, Prof. Dr. Steffen Grohmann

DECLARATION OF OWN WORK / ERKLÄRUNG ZUM SELBSTSTÄNDIGEN VERFASSEN

I hereby certify that this work has been composed by me and no other than the named sources were used. I also agree that this thesis may be displayed in a library and excerpts may be copied.

Hiermit versichere ich, dass ich die Arbeit selbständig verfasst und keine anderen als die angegebenen Quellen und Hilfsmittel benutzt habe. Alle Zitate und sinngemäß übernommenen Passagen habe ich im Einzelnen unter genauer Angabe der Quelle gekennzeichnet. Ich erkläre mich damit einverstanden, dass die Arbeit in die Bibliothek eingestellt und in Auszügen kopiert werden darf.

Karlsruhe, den 15. Juni 2014

……

(Benedikt J. Peters)

Abstract

Oscillating Superleak Transducers (OSTs) can be used to localize quenches in superconducting radio frequency cavities. In the presented work the occurring thermal effects during such events are investigated both theoretically and experimentally. In the theoretical part the entire heat transfer process from the heat generation to the detection is covered. The experimental part focuses on the effects in superfluid helium. Previous publications observed the detection of an OST signal that was faster than the second sound velocity. This fast propagation could be verified in dedicated small scale experiments. Resistors were used to simulate the quench spots under controlled conditions. The three dimensional propagation of second sound was linked to OST signals for the first time, which improves the understanding of the OST signal and allows to gather information about the heating pulse. Additionally, OSTs were used as a tool for quench localisation on a real size cavity. Their sensitivity as well as the time resolution was proven to be superior to temperature sensors, which were glued to the surface of the cavity.

Zusammenfassung der Diplomarbeit

Thesis summary in German

Supraleitende Hohlraumresonatoren, auch Hochfrequenzkavitäten genannt, sind elementarer Bestandteil vieler Teilchenbeschleuniger. Die Leistung dieser Kavitäten ist häufig durch kleine Oberflächendefekte begrenzt, die bei verschiedenen Schritten im Herstellungsprozess entstehen können. Besonders bei der Produktion von Kavitäten mit hohen Leistungsanforderungen kann die Qualität der Resonatoren daher stark schwanken. Um die gewünschten Anforderungen zu erfüllen, müssen die Resonatoren getestet werden. Nicht nur das Gesamtergebnis eines solchen Tests ist von Interesse, sondern auch Ort und Art des limitierenden Defekts. Eine grobe Lokalisation ist daher notwendig, bevor optische Tests die Ursache des Defekts im Detail ergründen können. Bisher wurde die Lokalisation durch eine große Anzahl von Temperatursensoren realisiert, die die Außentemperatur des Resonators während des Tests in flüssigem Helium überwacht. Während des Betriebs der Resonatoren wärmen sich die besagten Defekte auf und können daher detektiert werden. Diese Methode hat gravierende Nachteile, denn sie ist teuer, muss für Resonatoren mit verschiedenen Formen speziell angepasst werden, benötigt viel Zusatzausrüstung und ist kaum in der Lage transiente Phänomene wie den häufig limitierenden Quench aufzulösen.

Deshalb wurde 2008 eine neue Methode veröffentlicht, um diese Defekte zu lokalisieren. So genannte „Oscillating Superleak Transducers“ (OSTs) sind in der Lage Temperaturwellen in superfluidem Helium zu detektieren, die von Wärmequellen ausgesendet werden. Diese Methode senkt die entstehenden Kosten enorm, braucht wenig Ausrüstung, kann leicht für verschiedene Resonatoren angepasst werden und kann besonders gut transiente Phänomene auflösen.

In der vorliegenden Arbeit werden die auftretenden Effekte bei einem Quench genauer untersucht sowie OSTs zur Quenchlokalisierung eingesetzt. Eine kurze Einleitung erläutert wichtige Hintergrundinformationen zu Teilchenbeschleunigern, Supraleitung und Hohlraumresonatoren sowie Helium als Kühlmedium. Danach werden die Wärmeübergangsvorgänge bei einem Quench theoretisch beleuchtet. Ausgehend von den Heizeffekten am Defekt auf der Innenoberfläche des Resonators über den transienten Wärmetransport durch das Resonatormaterial, den Wärmeübergang in das Helium, die Ausbreitung im Helium und deren Detektion wird der gesamte Prozess beleuchtet. Dabei wird

ein besonderer Schwerpunkt auf den Wärmetransport im superfluiden Helium gelegt, denn dieser funktioniert fundamental anders als sonstige Transportprozesse. Mit dem so genannten zweiten Schall weißt superfluides Helium einen Wärmetransport mit Wellencharakter auf. Diese Schwerpunktsetzung wurde gewählt, da beim Einsatz der OSTs Unregelmäßigkeiten festgestellt wurden, die nicht durch das bisherige Verständnis der Vorgänge im Helium abgedeckt wurden. Es wurde wiederholt berichtet, dass die Temperaturwelle früher als erwartet detektiert wurde.

Der dritte Teil dieser Diplomarbeit versucht den Effekten im Helium experimentell näher zu kommen. Dazu wurde der Quench durch elektrische Wiederstandsheizer simuliert und der zweite Schall per OST detektiert. Dabei wurde der Literaturwert der Geschwindigkeit des zweiten Schalls für niedrige Heizleistungen validiert und somit die Präzision des Messaufbaus bestätigt. Das bevorzugte Material zur Herstellung von supraleitenden Hohlraumresonatoren ist Niob. Mit einem Heizer der auf eine Niobplatte geklebt wurde konnte das Resonatormaterial unter bestimmten Randbedingungen als Verursacher der schnelleren Signalübermittlung ausgeschlossen werden. Eine bisher für OSTs und die Quenchlokalisierung nicht betrachtete Theorie, die eine Abhängigkeit der Geschwindigkeit des zweiten Schalls von der Heizleistung vorhersagt, konnte für die getesteten Fälle als Verursacher der schnelleren Signalausbreitung ebenfalls ausgeschlossen werden. Jedoch wurde die schnellere Signalausbreitung an sich festgestellt. Dazu wurden mehrere Versuchsreihen mit verschiedenen Heizern und Heizleistungen durchgeführt. Ein schon im Theorieteil beschriebener Zusammenhang zwischen der Temperatur des zweiten Schalls und der eingebrachten Heizleistung für den dreidimensionalen Fall konnte durch Variation verschiedener Parameter der Heizpulse bestätigt werden.

Im letzten Teil der Diplomarbeit wurden OSTs für die Lokalisation eines Defekts bei einem Resonator eingesetzt und mit Ergebnissen von Temperatursensoren verglichen. Dies ist erfolgreich gelungen und konnte die hohe Sensitivität der OSTs, verglichen mit den Temperatursensoren, untermauern.

ACKNOWLEDGEMENT / DANKSAGUNG

I would like to express my special appreciation and thanks to Prof. Steffen Grohmann and Dr. Karl-Martin Schirm who made this external diploma thesis possible. They provided the needed working conditions for the presented work and took their time to keep in close touch of the progressing work.

Furthermost I would like to express my deepest gratitude to my advisor Dr. Torsten Koettig for his excellent guidance, knowledge and passion in the field of cryogenics. His practical help and constructive criticism were essential for this work.

Dr. Tobias Junginger was absolutely invaluable for my work in the field of superconducting radio frequency cavities. I am very grateful for his patience and experience, it was absolutely crucial to be able to work in this new field for me.

I would like to thank Dipl.-phys. Sarah Aull and Dr. Alick Macpherson for their helpful advice, their challenging questions and the good working atmosphere they created.

I am indebted to the members of the SRF and MK Sections in building 252, their involvement was always of big help. A special thanks to Dr. Pei Zhang, he always was willing to truly fathom the question at hand. Thanks to Antoine Benoit who was a big help in the field of electronics and programming. His joyful charisma made work much more pleasant.

I also would like to thank the members of the central cryogenic laboratory at CERN. Their experience and help were absolutely necessary for my experiments. I would like to name especially Laetitia Dufay-Chanat who always had an open ear for my questions.

My partner Sonja Wanner helped me through all struggles during the work of this thesis. I am very grateful for her support and care.

Finally I would like to thank my family, my parents and my sister, for all the moral support and the chances they have given me over the years.

COMMONLY USED SYMBOLS

LATIN ALPHABET

Symbol	Name	Value of constant, Unit
$\boldsymbol{A}$	Area	m^2
$\vec{\boldsymbol{B}}$	Magnetic flux density or magnetic induction	$T, kg/(A\,s^2)$
$\boldsymbol{B_{c1}}$	Lower critical magnetic field	$T, kg/(A\,s^2)$
$\boldsymbol{C}$	Capacitance	F
$\boldsymbol{c}$	Speed of light	$2.997\,924\,58 \cdot 10^8\ m/s$
$\vec{\boldsymbol{E}}$	Electric field	V/m
$\vec{\boldsymbol{H}}$	Magnetic field	A/m
$\boldsymbol{h}$	Planck's constant	$6.62606957 \cdot 10^{-34}\ m^2 kg/s$
$\boldsymbol{k}$	Boltzmann's constant	$1.3806488 \cdot 10^{-23}\ m^2 kg/(s^2 K)$
$\tilde{\boldsymbol{M}}$	Molar mass	g/mol
$\boldsymbol{m}$	Mass	kg
$\boldsymbol{N_A}$	Avogadro number	$6.02214129 \cdot 10^{23}\ 1/mol$
$\boldsymbol{P}$	Power	W
$\boldsymbol{p}$	Pressure	$Pa, mbar$
$\boldsymbol{Q}$	Heat	J
$\boldsymbol{Q_e}$	Electric charge	C
$\dot{\boldsymbol{q}}$	Heat flux density	W/m^2
$\boldsymbol{R}$	Resistance	Ω
$\boldsymbol{R_K}$	Kapitza resistance	$m^2\ K/W$
$\mathbb{S}$	Entropy	J/K
$\boldsymbol{s}$	Specific entropy	$J/(kg\ K)$
$\boldsymbol{T}$	Temperature	K
$\boldsymbol{T_c}$	Critical temperature of a superconductor	K
$\boldsymbol{U}$	Voltage	V
$\boldsymbol{U_s}$	Stored energy in a cavity	J
$\boldsymbol{u}$	Standard uncertainty	-
$\boldsymbol{u_C}$	Combined standard uncertainty	-
$\boldsymbol{v_2}$	Second sound velocity	m/s
$\boldsymbol{v_{2,0}}$	Second sound velocity for infinitely small amplitudes	m/s
$\boldsymbol{v_n}$	Velocity of normal fluid component in helium II	m/s
$\boldsymbol{v_s}$	Velocity of superfluid component in helium II	m/s

GREEK ALPHABET AND OTHER SYMBOLS

Symbol	Name	Value of constant, Unit
$\boldsymbol{\Gamma_2}$	Amplitude dependence parameter of second sound	m^3/J
$\boldsymbol{\gamma}$	Ratio of the normal and superfluid density	-
$\boldsymbol{\delta}$	Penetration depth or skin depth	m
$\boldsymbol{\epsilon}$	Electromotive force	$V, kg\ m^3/(A\ s^3)$
$\boldsymbol{\varepsilon_0}$	Vacuum permittivity	$\sim 8.854 \cdot 10^{-12}\ A\ s/(V\ m)$
$\boldsymbol{\varepsilon_r}$	Relative permittivity	-
$\boldsymbol{\mu}$	Permeability	$V\ s/A\ m$
$\boldsymbol{\mu_0}$	Permeability of free space	$4\pi \cdot 10^{-7} V\ s/(A\ m)$
$\boldsymbol{\mu_r}$	Relative permeability	-
$\boldsymbol{\rho}$	Density	$kg\ /\ m^3$
$\boldsymbol{\rho_n}$	Normal fluid density	$kg\ /\ m^3$
$\boldsymbol{\rho_s}$	Superfluid density	$kg\ /\ m^3$
$\boldsymbol{\rho_c}$	Electric charge density	$C\ /\ m^3$
$\boldsymbol{\tau_2}$	Normalized amplitude dependence factor of second sound	-
Å	Angstrom	$10^{-10}\ m = 0.1\ nm$
$\mathbb{R}$	Gas constant	$kJ/(kmol\ K)$

COMMONLY USED ABBREVIATIONS

Abbreviation	Meaning
AB	Allen Bradley Carbon Temperature Sensor
[a.u.]	Arbitrary units
ITS 90	International Temperature Scale from 1990
LHe	Liquid helium
NC	Normal conducting
OST	Oscillating Superleak Transducer
RF	Radio frequency
RRR	Residual resistance ratio
SC	Superconducting
SMD	Surface mount device

TABLE OF CONTENTS

1 Objective

Superconducting RF Cavities are widely used in particle accelerators. Their performance is often limited by the manufacturing process and varies if high specifications are desired. This limitation is often caused by surface defects which can originate from different steps in the production process. In order to insure cavities reaching their specifications they need to be tested. To be additionally able to understand occurring problems, not only the overall performance has to be monitored but also the surface defects have to be localized. A rough localisation of the quench spot is needed before a detailed optical inspection can take place. In the past the localization was done by an array of temperature sensors that monitor the temperature of the outer cavity wall during testing in liquid helium. This method suffers from a series of drawbacks such as high capital cost, need for custom made arrays for different cavity types, big amounts of equipment and the difficulty to observe transient effects such as the often limiting global quench of a cavity.

In 2008 a new method was suggested [1] to localize the defects. It uses Oscillating Superleak Transducers (OSTs) to detect second sound waves in superfluid helium which originate from heating effects such as quenches. This experimental technique has many advantages such as low capital cost, a comparably small amount of equipment, a nearly purely computational adaptation for different cavity types and observation of transient effects.

This thesis tries to broaden the understanding of the occurring heat transfer phenomena. In order to fulfil this goal three approaches were taken in the presented work. Firstly a literature study to understand previous research, secondly lab-scale experiments to test OSTs in controlled conditions and thirdly the use of OSTs for quench localisation in real cavity tests have been performed.

2 Introduction

2.1 CERN

On the 29th of September 1954 the European Organisation for Nuclear Research (originally: Conseil Européen pour la Recherche Nucléaire, CERN) was founded by the ratification of the first twelve member states. Its purpose is the study of fundamental high energy physics and collaboration among European states with at least one particle accelerator [2]. Sixty years after its foundation CERN has 21 member states and operates a big accelerator complex.

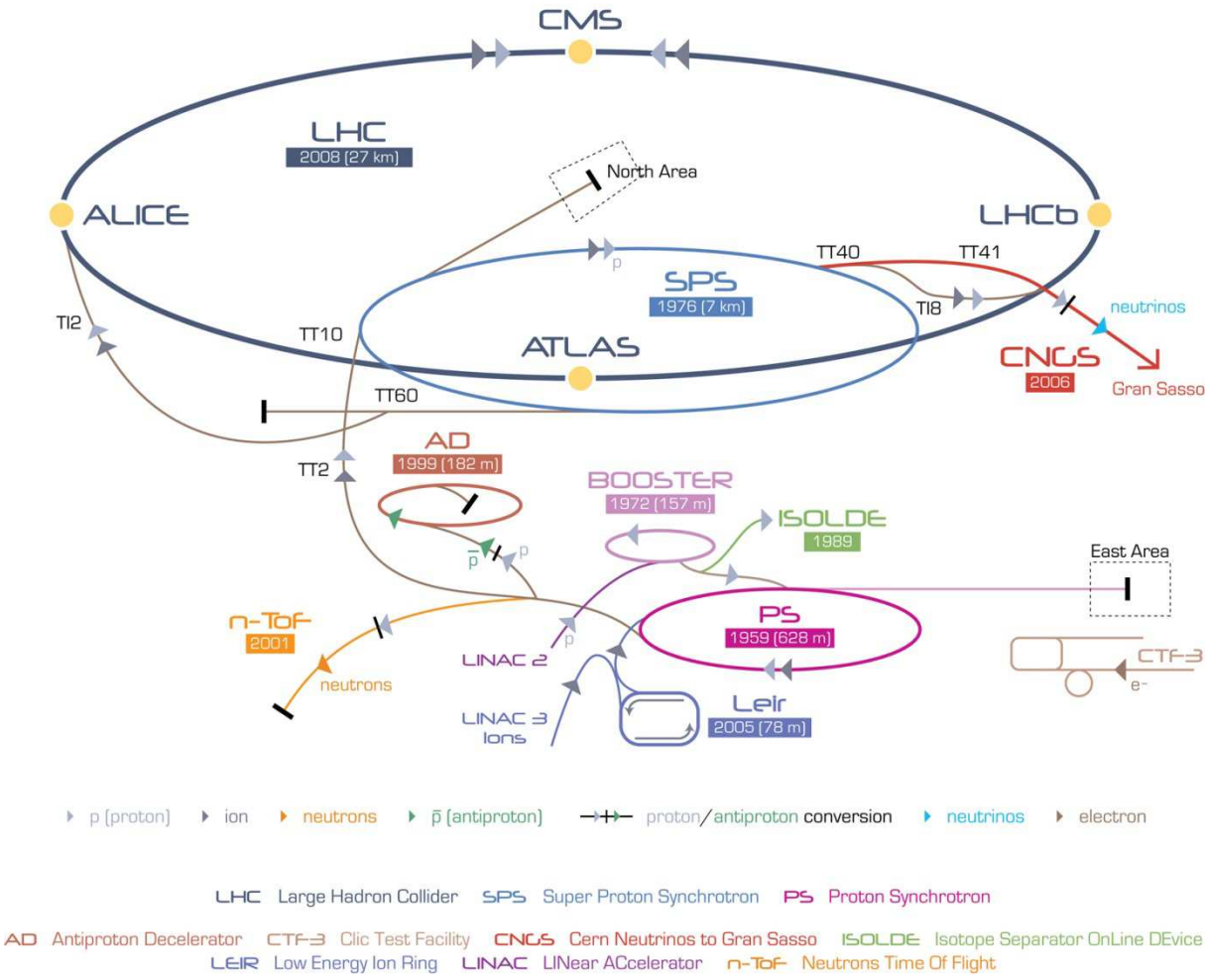

Figure 1: Schematic of the CERN accelerator complex [3].

The Cryogenic expertise of CERN dates back to the 1960s and this technology always gained importance since then. First deployed in bubble chambers as particle detectors, later for the cooling of superconductors it became a crucial part of CERNs technology and experiments. Today the world's biggest and most powerful particle accelerator, the Large Hadron Collider

(LHC), would be not feasible without the utilisation of superconductors and respective cooling technology [4].

2.2 ACCELERATORS

At the beginning of the 20th century Ernest Rutherford started a new scientific era by investigating the structure of matter and atoms. He used α-particles from a radioactive source to gain information about the size of an atomic nucleus [5]. Soon it became clear that higher particle fluxes with higher energies were needed for further studies. In 1927, by then president of the royal society in London, Rutherford gave a widely recognised speech in which he urged the scientific community to develop particle accelerators with higher energies than from natural radioactive decay [6].

Cockcroft and Walton in Cambridge or Van de Graaf in Princeton tried to reach this goal by a high potential difference in which a charged particle gets accelerated. This approach did receive some good results but was finally limited by the high voltage needed causing electrical breakdown by discharge.

The solution for this problem was already demonstrated in the year of Rutherford's speech, but did not have a follow up. Rolf Wideröe, a PhD student at the University of Aachen had accomplished particle acceleration by a varying electric field [7]. In 1929 Ernest O. Lawrence, a professor at the University of Berkeley, found the publication of Wideröe and developed together with one of his PhD students, M. Stanley Livingston, the first cyclotron [8].

The concept of varying electric fields was the breakthrough for high energy particle accelerators. The LHC, the world's most powerful particle collider, still uses this concept and is now able to deliver energies that are a factor of about one million times higher than the described alpha particles by Rutherford.

2.3 RADIO FREQUENCY CAVITIES

In particle accelerators Radio Frequency (RF) cavities are devices made to interact with a charged particle beam via a high frequency electromagnetic field. This interaction often intends to accelerate the beam, but can also be used to decelerate, kick or bunch a beam.

RF cavities consist of an electric conductor that confines a specially shaped empty space. This inner space is designed in such a way that electromagnetic waves of a certain frequency can resonate within them. An example for such a cavity can be seen in Figure 2.

These waves can be described by the Maxwell Equations (2.1); the inner conductor surface gives the boundary conditions for this description. A graphical representation of the solution for these equations for a cavity shape can be found in Figure 3 and Figure 4. The colour and size of the arrows show the magnitude of the field (red highest field, blue lowest field).

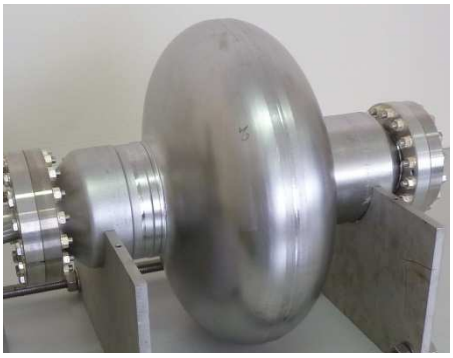

Figure 2: Photo of an elliptical one-cell cavity (for SPL).

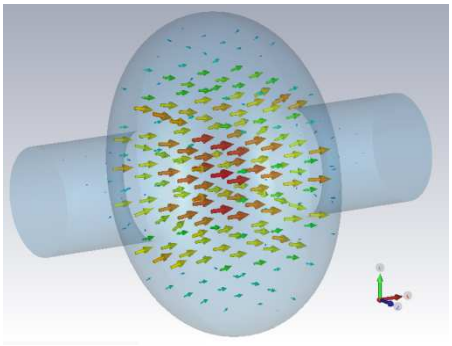

Figure 3: Simulation of the electric field in an elliptical cavity. Courtesy P. Zhang

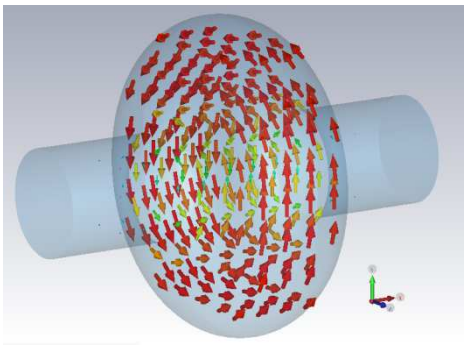

Figure 4: Simulation of the magnetic field in an elliptical cavity. Courtesy P. Zhang

Maxwell's equations in their differential vector form:

$$\nabla \times \vec{B} = \mu_0 \vec{J} + \mu_0 \varepsilon_0 \frac{\partial}{\partial t} \vec{E} \qquad \text{(Ampere's circuital law)} \qquad (2.1)$$

$$\nabla \cdot \vec{B} = 0 \qquad \text{(Gauss' law of flux conservation)}$$

$$\nabla \times \vec{E} + \frac{\partial}{\partial t} \vec{B} = 0 \qquad \text{(Faraday's law of induction)}$$

$$\nabla \cdot \vec{E} - \frac{\rho_c}{\varepsilon_0} = 0 \qquad \text{(Gauss' law for electricity)}$$

To fulfil the boundary conditions for an electric conductor, a surface current has to flow on the inner cavity surface. To reduce the losses of energy due to the electrical resistance of the metal, a good conductor should be used. Often these cavities are made out of copper, but to decrease the losses further also a superconductor can be chosen.

2.4 SUPERCONDUCTIVITY

In 1911, three years after he managed to liquefy helium for the first time, Heike Kammerlingh-Onnes published an unexpected drop in the electrical resistance of mercury at very low temperatures. In this so called superconducting state the electrical resistance is vanishing small. To be more precise the electrical resistance for direct currents is unmeasurable small (practically zero), for alternating currents it is very small but not zero.

Electrical resistance can be explained by the interaction of an atomic lattice and the electrons which get accelerated in an electric field and lose energy to the lattice by interactions. In order to have no electrical resistance the sum of all interactions with the lattice has to be zero. This is how superconductivity is explained. Long time the phenomenon of superconductivity was not understood but in1957 the physicists J. Bardeen, L. N. Cooper and J. R. Schrieffer found an explanation. After these three researchers it is called BCS theory [9]. Crucial for this effect is the creation of so called Cooper pairs, electrons which have opposite spin and momentum. Normally electrons which have a half integer spin obey Fermi-statistics. This implies that they have to obey the Pauli Exclusion Principle and cannot be all in the lowest energy state. When electrons build cooper pairs this new "quasi particle" has a total spin of zero and therefore they obey Bose-Einstein statistics that allows all particles to be in the ground state [10].

Critical parameters of superconductors

The Cooper pairs and therefore superconductivity only exists when certain boundary conditions are fulfilled. The magnetic field, the current through the superconductor and the temperature have to be under a certain limit. These limits are described by a critical magnetic field, a critical current density and a critical temperature. These critical values are the highest allowed value if the other parameters are zero. If the other values are non-zero, which is always the case in practice, breakdown will occur earlier. The three dimensional graph showing the superconducting-normal conducting transition with these three parameters is called critical surface, depicted in Figure 5. Below this surface the material is superconducting. The transition of super- to normal conducting is called quench. In superconducting cavities the critical current is normally not the limiting parameter and thus of minor interest. Niobium is the standard material used for cavities. It is the element with the highest critical temperature $T_{C,Nb} = 9.2$ K and field $B_{C1,Nb} = 195$ mT. As a metal it is easy to shape and its properties are isotropic. For operation the superconducting cavities are immerged in a bath of liquid helium to cool them below the critical temperature.

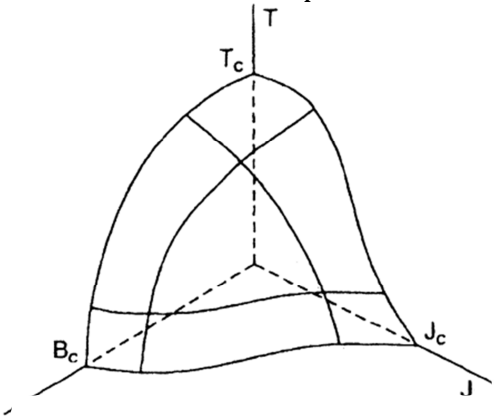

Figure 5: Sketch of a critical surface of a superconductor. [54]

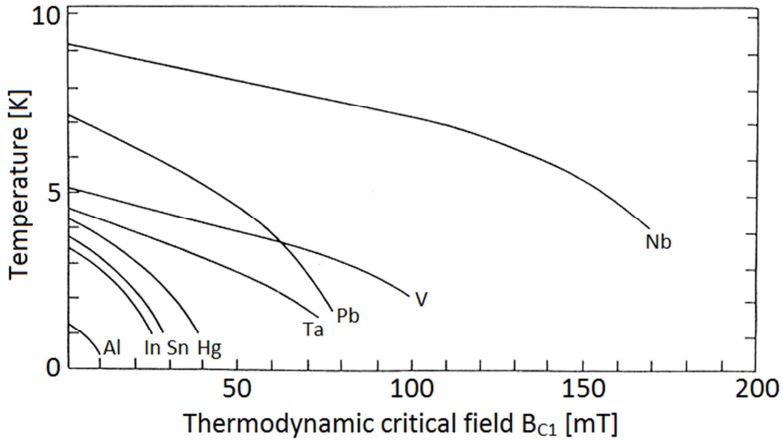

Figure 6: Critical magnetic field vs. critical temperature for metallic superconductors, after [7].

2.5 HELIUM CRYOGENICS

Helium is the second element in the periodic table. It exists in the form of two stable isotopes, helium 4 (^{4}He) and helium 3 (^{3}He). The isotope ^{3}He is extremely rare and is only used for very special purposes[1]. As ^{4}He is considered in this work, the word helium always refers to this isotope. Helium can be liquefied under ambient pressure at a temperature of 4.2 K but will not solidify at this pressure. Thus it is the coolant of choice for applications with temperatures below 4.2 K.

Phase diagram and properties

Besides the fact that helium is the only element which cannot be solidified under atmospheric pressure, it is also the only element which doesn't have a triple point. Instead of the triple point the solid and the vapour phase can be connected with the lambda line. This line marks a transition of the liquid helium with extreme changes in its behaviour. To distinguish the two different states they are named helium I and helium II.

The lambda line is named after the very characteristic heat capacity vs. temperature curve of helium in this temperature range which looks like the Greek letter lambda (Appendix 8.1.2).

In Figure 6 the phase diagram of helium is shown. The usual operating domains for helium II are marked with ① and ②. Helium in its saturated state is marked with the ①, this is the condition that was used in the presented work. The slight pressure difference Δp shown in the detail takes the condition of helium below its liquid level into account. For a volume of helium at a certain height below the surface the mass of helium above adds a static pressure difference. This pressure difference allows a local temperature difference of ΔT before the saturation condition is reached and boiling starts. The second domain, marked with ②, is used for helium II under pressurisation. Thermodynamic correct we would call this a sub-cooled liquid. A few advantages make it favourable to operate in this domain. Probably the most significant role is the amount of energy that can be stored because the heat capacity increases significantly towards the lambda line. As it is much harder to reach the sup-cooled condition, this is only done for well justified applications.

All experiments, presented in this thesis were conducted in saturated helium. In order to reach this regime liquid helium with ambient pressure is filled into the cryostat with the experimental

[1] One of these purposes is very important for cryogenics. ^3He can be utilized in a dilution refrigerator to produce sub-kelvin temperatures.

setup. The condition of the helium at this point is shown by the top right corner of the dotted rectangle in the phase diagram. To reach lower temperatures the pressure over the liquid is reduced by pumping. The removal of enthalpy by the latent heat of helium at its phase transition lowers the temperature of the remaining liquid helium. This process can be pictured in the phase diagram by following the vapour pressure line to lower temperatures and pressures. When the temperature drops below $T_\lambda = 2.1768$ K [11] helium changes from helium I to helium II. When the desired temperature is reached, the pumping is controlled to keep the pressure constant.

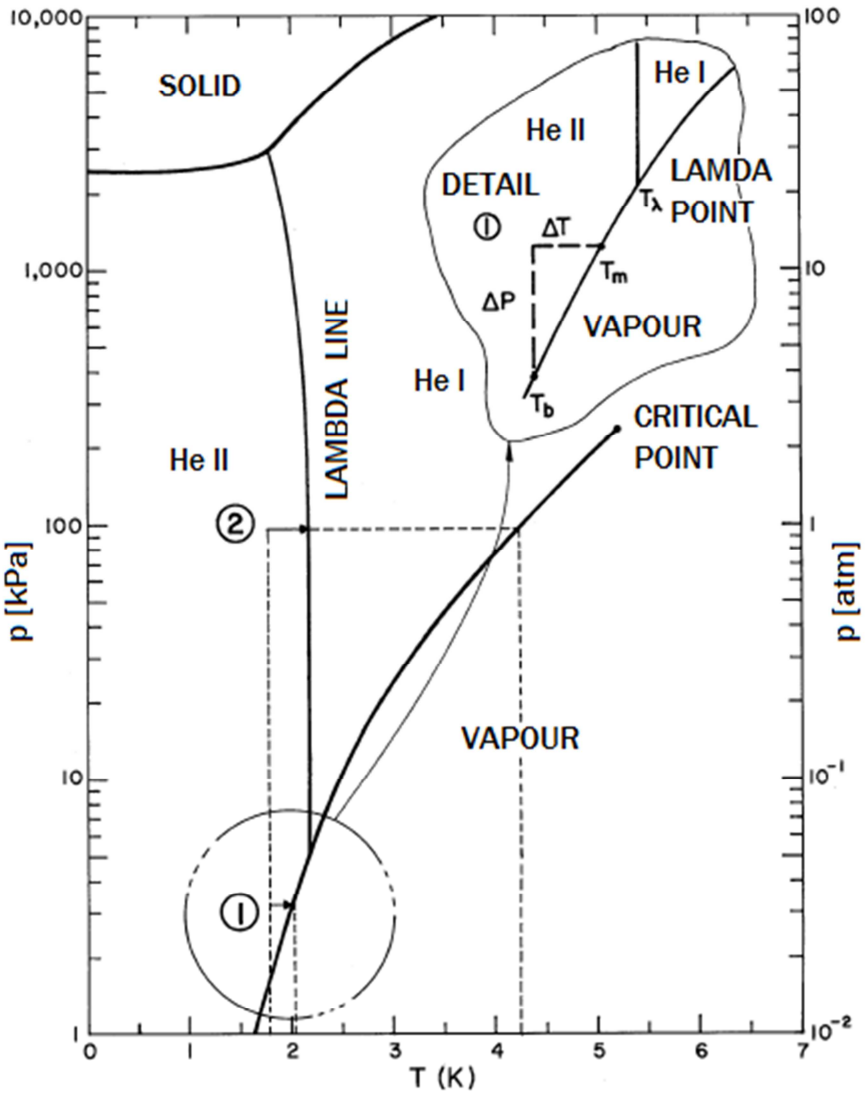

Figure 7: Phase diagram of helium [12].

2.6 HELIUM II

Helium II is the state of liquid helium which is determined by a quantum behaviour called superfluidity. It has remarkable properties. Helium II has the highest known thermal conductance, a very low viscosity in thin channels, which is additionally geometry dependent.

$$\lambda = h/\sqrt{3\,mkT} \qquad \text{(thermal de Broglie wavelength)} \qquad (2.2)$$

At low temperatures the de Broglie wavelength of helium atoms becomes comparable with the distance between the individual atoms. Thus the wave functions overlap and quantum effects determine the macroscopic behaviour of the fluid [13]. For helium the de Broglie wavelength at 2 K is 5.32 Å, whereas the average distance between the atoms is 3.76 Å (Appendix 8.1.3). The exact lambda temperature cannot be calculated with this approach, as effects like the interaction between the helium atoms are neglected. Still this calculation shows the approximate range of the transition and gives an easy explanation why the described phenomena are quantum effects.

Helium II is a strongly interacting quantum liquid, which partly undergoes a Bose-Einstein condensation. This condensation is different from the ones we know, because it is not governed by particle interactions but by its statistics. An ideal Bose-Einstein Condensate (BEC) would have no interaction between the particles in the condensate, but this is not true for helium. The atoms have a slight attractive force for large distances between each other and a strong repulsive force for short distances [14].

Superfluidity

Originally the term superfluidity only described the nearly frictionless flow of He II, but today it refers to the collective quantum effects occurring in helium below the lambda line. Thus helium II itself is called a superfluid. Helium is not the only known superfluid, but the one which was discovered first. A Bose-Einstein Condensate does not have to be a superfluid, actually an ideal BEC should never show this effect [14]. The basic concept of superfluidity is based on the fact, that it is only possible to excite certain energy states in a material. Below a certain threshold it is just not possible to transfer energy to a superfluid. Thus it will not interact [15].

TWO FLUID MODEL

The idea of Bose-Einstein condensation inspired the Hungarian physicist László Tisza to suggest a new model to describe the special properties of superfluid helium [16]. The so called "two-fluid model" characterises helium II as a mixture of two interpenetrating components. The components are called *"normal fluid component"* and *"superfluid component"*. The theory

allocates certain properties to each of these components as given in Table 1. With this model it is possible to describe many phenomena in superfluid helium, an achievement no earlier theory could claim. According to the model the composition of the two fluids changes with temperature and is normally given by the two density fractions ρ_s/ρ and ρ_n/ρ. The equation

$$\frac{\rho_n}{\rho} = \left(\frac{T}{T_\lambda}\right)^{5.6} \qquad \text{For } 1.1\ K \lesssim T \leq T_\lambda \tag{2.3}$$

describes this relationship. For temperatures below 1.1 K. the exponent of the right side of the equation gradually changes to 4. The density ratio of the two components is plotted in Figure 8.

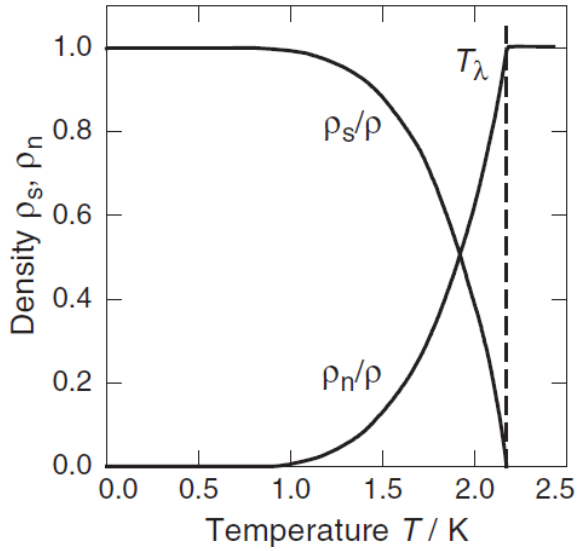

Figure 8: Superfluid and normal fluid density fractions in Helium II [17].

As entropy is only transported by normal fluid, a specific entropy flux is given by [18]

$$\dot{s} = \rho s v_n\,. \tag{2.4}$$

For a closed system where no work is done and no dissipative effects occur one can write [19]

$$dQ = T\ d\mathbb{S}_Q. \tag{2.5}$$

Combining these equations gives

$$\dot{q} = T\ \rho s v_n\,. \tag{2.6}$$

This equation links the two-fluid theory to thermal considerations and explains occurring phenomena satisfactorily. Although this model describes many occurring phenomena quite precisely, it has to be kept in mind that is only a model. There are no separable components in helium, all atoms are indistinguishable [17].

Table 1: Assumptions of the two fluid model.

	Density	**Entropy**	**Specific Entropy**	**Viscosity**
Normal fluid component	ρ_n	$\mathbb{S}_n = \mathbb{S}$	s_n	$\eta_n = \eta$
Superfluid component	ρ_s	$\mathbb{S}_s = 0$	$s_s = 0$	$\eta_s = 0$
Bulk Helium II	$\rho_n + \rho_s = \rho$	$\mathbb{S}$	$s = \rho_n/\rho \; s_n$	η

3 Theoretical Aspects of Heat Transfer

The heat transfer in He II cooled cavities is a very complex process, because very different principles and parameters influence it. The heating occurs due to losses of an electromagnetic field, the heat transport in niobium is described by conduction with changing material properties. The heat transfer at the solid to helium interface is described by two phenomena, the Kapitza resistance and boiling effects. The heat transport in helium II follows totally different principles than in other materials. To draw a conclusion about the events in the cavity the temperature change has to be detected, which can be done with an Oscillating Superleak Transducer (OST).

In this chapter the relevant phenomena are described in the order of occurrence for a quenching event. Therefore a combination of literature study, own theoretical considerations and simulations are presented.

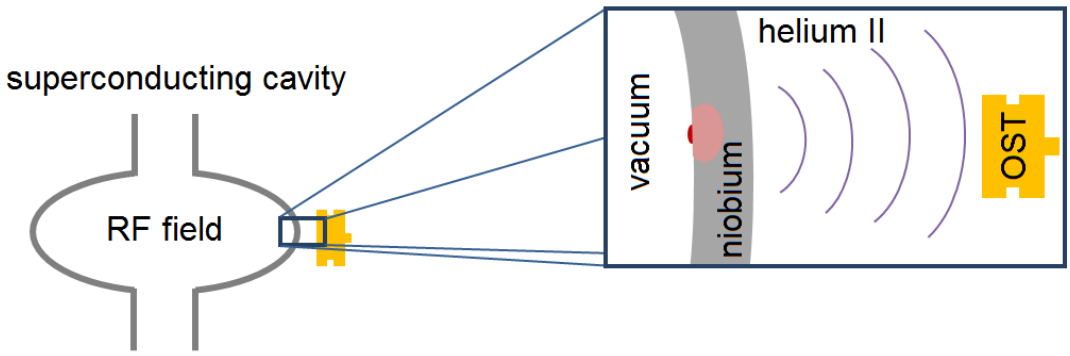

Figure 9: Schematic of heat transfer phenomena at superconducting radio-frequency cavities.

As the literature partly reports significantly faster than expected signals by OSTs (see Section 3.3.2) for quench localisation measurements on cavities [20] [21], special attention is given to all effects that could occur faster than generally expected. The dominating process for the signal propagation is the transport in helium with a velocity of about 20 m/s in the temperature range between 1.5 and 1.9 K.

3.1 Heat Generation in Cavities

An electromagnetic field does not stop on the inner surface of a cavity but decreases in the material in an exponential manner [22]. In Figure 10 this decrease is shown. The blue line shows the maximum field strength at a given point and the green line a temporarily distribution in an oscillating electromagnetic field.

The decay is strongly dependent on material properties and is characterized by the penetration depth or skin depth δ.

$$\mathrm{E(x)} = E_{max} \cdot e^{-\frac{x}{\delta}} \tag{3.1}$$

In normal conductors the skin depth is dependent on the frequency of the applied field, in a superconductor this dependency vanishes for the operating parameters of SC cavities. For niobium in the superconducting state the penetration depth is about 40 nm [10], for normal conducting niobium at 1.3 GHz it is about 17 µm (Appendix 8.1.4.1). As bulk niobium cavities have normally a wall thickness of roughly 3mm, the electromagnetic field can be treated as a surface effect from a thermal point of view.

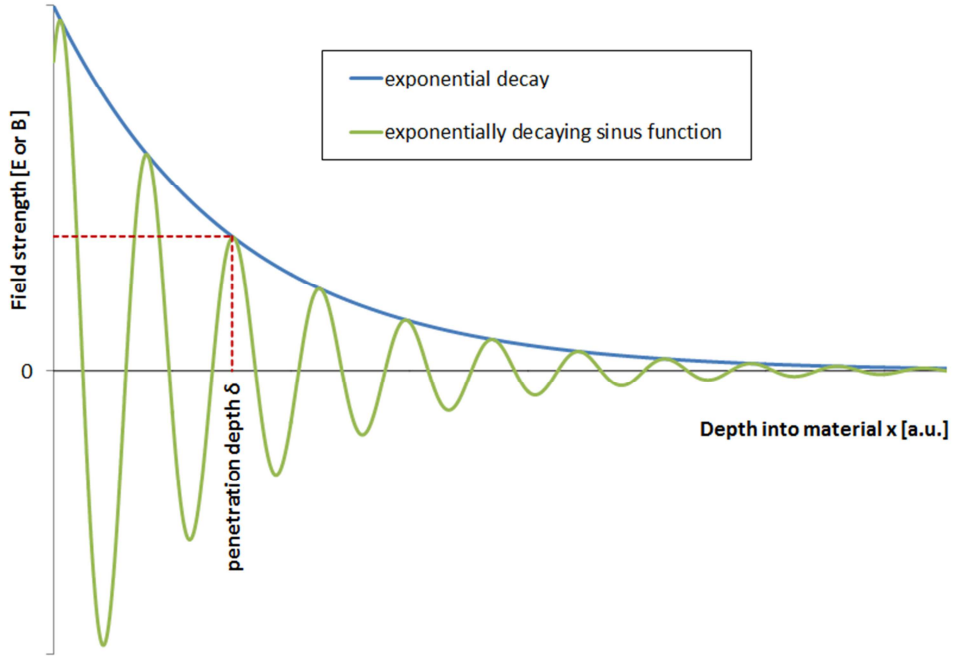

Figure 10: Sketch to illustrate the penetration depth.

In a superconducting RF cavity heating occurs due to resistive parts on the inner surface that interact with the electromagnetic field. This resistance has various origins.

For a homogeneous surface resistance R_A the dissipated power P_{diss} can be written as:

$$P_{diss} = \frac{1}{2} R_A \int_A |H|^2 dA \tag{3.2}$$

In general the surface resistance R_A of a cavity consists of two parts. The resistance which is described by the BCS theory R_{BCS} and a "residual resistance" R_{res} term which is temperature independent and the sum of losses not described by the BCS theory. It is contingent on further material properties such as the purity of the material.

$$R_A(T) = R_{BCS}(T) + R_{res} = A\omega^2 e^{-\frac{\Delta_0}{k_B T}} + R_{res} \qquad \text{For } T \leq T_C/2 \tag{3.3}$$

The BCS term depends on superconductivity related parameters such as the critical temperature T_C and the superconducting energy gap $2\Delta_0$ as well as the frequency of the electromagnetic field. This is the reason why superconducting RF structures for very high frequencies ($\gtrsim 3\ GHz$) don't have an advantage over normal conducting structures and are therefore not used [23].

Quench behavior of SC cavities

If the critical surface of the superconductor is exceeded, the material suddenly becomes normal conducting. This effect is called *quench*. The much bigger electrical resistance of this normal conducting area leads to heating and can cause an increasing normal conducting area. In such a way all the energy stored in a cavity can be dissipated into heat. This effect is called *global quench*. The crossing of the critical surface can be caused by various reasons. Exceeding $B_c(T)$ with the electromagnetic field is one of them; a little normal conducting defect, which gets heated above $T_c(B)$, is another. For most quenches certainly a combination of both effects applies. A local quench does not have to lead to a global quench as long as the surrounding material can transport the heat away from the heating spot. Global quenches are normally triggered during the testing of a cavity to determine its limits. Two cases are possible. Either the electrical field is raised slowly, already leading to local heating on defects until the global quench occurs, or the field is suddenly increased to a value that causes a local or global quench.

Depending on the type, quality and use of a superconducting cavity the dissipated power in a global quench can vary a lot. An example calculation tries to show the relevant quantities for the estimation of such an event. The stored energy U_s in an accelerating cavity (for a particle close to the speed of light) can be calculated with the equation [23].

$$U_s = \frac{{E_{acc}}^2 c^2}{8\pi f^3\, R_a/Q_0} \tag{3.4}$$

E_{acc} is the accelerating field in the cavity, f its frequency and R_a/Q_0 is a common figure of merit for cavities. With the common value of $R_a/Q_0 = 100\ \Omega$, a frequency of $1.3\ GHz$ and an accelerating field of $30\ \mathrm{MV/m}$ one can determine the stored energy in the cavity to be 14.7 J. During a global quench this energy gets converted into heat. The duration of a quench can last from the sub-millisecond range to ten milliseconds. For a global quench of one millisecond the average heating during this time for the previously calculated cavity is $14.7\ kW$.

The evolution of the quench is closely connected to the heat transport in the niobium. This is why further information is given in Section 3.2.1.2.2 "TRANSIENT SIMULATION".

3.2 HEAT TRANSPORT

3.2.1 Heat transport in niobium

A global quench is a transient effect and can therefore not be described like steady state heat transport. The property describing the thermal behaviour of a material for transient effects is called thermal diffusivity a. It takes both the thermal conductivity λ and the volumetric heat capacity c_p into account.

$$\mathrm{a} = \frac{\lambda}{\rho\, c_p} \qquad \text{(thermal diffusivity)} \tag{3.5}$$

At the described temperatures niobium changes its properties quite drastically. Also the boundary conditions, the heat input and the cooling due to the helium bath are necessary for a detailed analysis.

The presented work searched for causes of a “faster than expected“ second sound signal. One hypothesis is that the fastest quenching information does not propagate directly through the niobium and then in direct line of sight to the OST in liquid helium, but travels first faster than second sound in the niobium and then enters the helium where the direct line of sight to the sensor is shorter. Either the high thermal diffusivity (due to low heat capacity) of the superconducting niobium could be the reason for the fast propagation in niobium, or the quench itself propagates faster in the cavity. To check these hypotheses three approaches were taken. An analytical model for the transient heat transport describes the heat propagation through the niobium. The other two approaches used simulations to illustrate the process. Steady state simulations show possible temperature distributions in a niobium wall during operation and a literature study gives results for transient simulations of quenches.

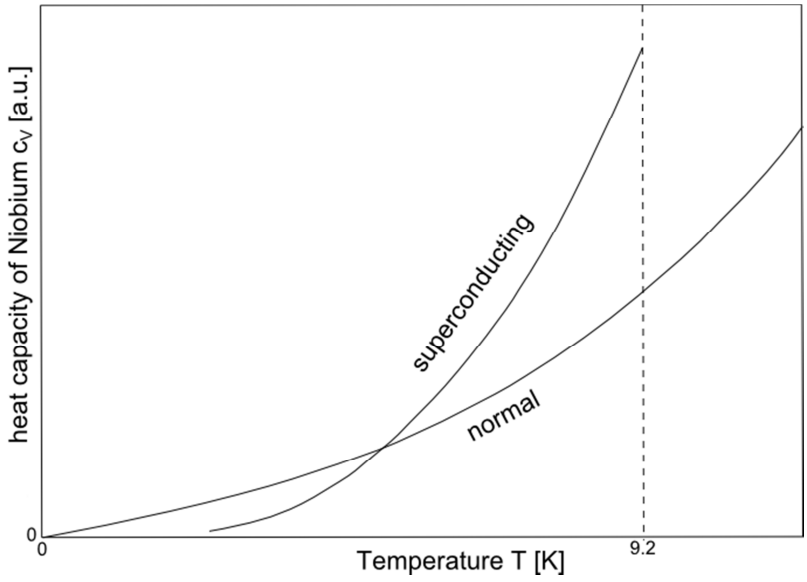

Figure 11: Schematic of heat capacity of niobium in the normal and superconducting state, after [24].

3.2.1.1 SIMPLIFIED MODEL

As mentioned before the thermal diffusivity takes the thermal properties of a material for transient effects into account. It is the only material parameter in the differential equation describing heat transport in a medium. This so called "heat equation" for a homogeneous material and just heat transport is given by

$$\frac{\partial T}{\partial t} = \mathrm{a}\frac{\partial^2 T}{\partial x^2} \qquad \text{(heat equation)} \tag{3.6}$$

for transient solutions in one dimension.

To be able to solve this equation conveniently we assume a one dimensional setup of an infinitely thick niobium sheet with a constant thermal diffusivity for this calculation. These assumptions certainly will not give very accurate results, but it will give a good impression for the approximate time scales.

The thermal conductivity of both normal conducting and superconducting high grade niobium at 2 K is about 11 W/m K [24]. The heat capacity of niobium is very different for the two states. At 2 K the heat capacity of superconducting niobium is 0.015 J/kg K and for normal conducting niobium it is 0.18 J/kg K [25]. The difference of about one order of magnitude in this value can also be found in the value for the thermal diffusivity, which is 850 cm^2/s for the superconducting niobium and 71 cm^2/s for the normal conducting niobium. If one imagines a temperature step on one side of the niobium sheet to the temperature T_S as a boundary condition and an initially constant temperature T_i in the material, the heat equation can be analytically solved as shown in Equation (3.6) [26].

$$\frac{T-T_s}{T_i-T_s} = \mathrm{erf}\left(\frac{x}{2\sqrt{at}}\right) \tag{3.7}$$

In this calculation the erf is the Gaussian error function which is given by [27]:

$$\mathrm{erf}(x) = \frac{1}{\sqrt{2\pi}}\int_{-\infty}^{x} e^{-\frac{t^2}{2}}\,dt\,. \tag{3.8}$$

For a distance of 2 mm from the temperature step to 25 K, the temperature over time looks like shown in Figure 12. One can see the better thermal diffusivity of the superconducting niobium (SC Nb), but for both materials a temperature rise of a few Kelvin occurs far below a millisecond. A temperature rise of 50 mK takes 2.5 µs in the superconducting niobium and 30 µs in the normal conducting niobium which is equivalent to a speed of 800 m/s and 67 m/s. As a temperature rise of 50 mK will certainly trigger a second sound wave in helium II, which is

detectable by an OST, one can see that the heat transport through a niobium sheet will be faster than the second sound velocity.

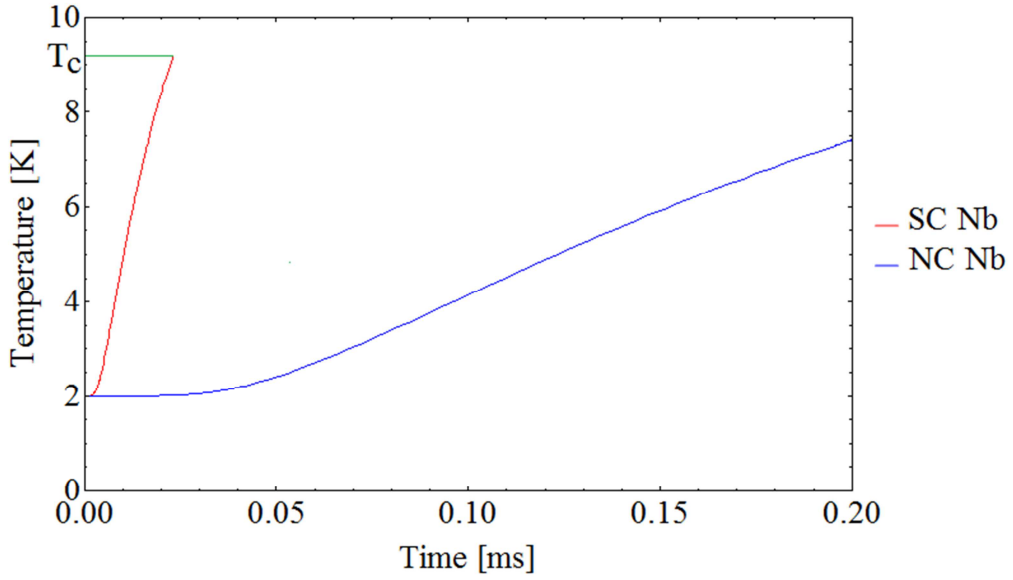

Figure 12: Temperature lapse for the solution of the heat equation with a thermal diffusivity of superconducting (SC) and normal conducting (NC) niobium (Nb). The solution for superconducting niobium was cut at its critical temperature.

The temperature distribution in the niobium obviously doesn't have a constant velocity as in helium II (see Section 3.2.3.1), but follows the error function. The given values for the "speed" are calculated by dividing the distance by the time which a certain temperature rise at this distance needs.

If the calculation is repeated for a distance further away the calculated "speed" drastically decreases as the temperature rise has to heat up more material. The distance where the "speed" is still 20 m/s for a temperature rise of 50 mK is 6.7 cm for normal conducting niobium and 80 cm for superconducting niobium.

These considerations show that a faster signal propagation than 20 m/s is possible. Certainly the calculations cannot be applied directly because of the simplifications that were made. Further investigations have to be done to prove the hypothesis of faster signal propagation due to a high diffusivity.

3.2.1.2 Simulation of quench propagation and heat transport

The chapter about quenches (Heat generation in cavities 3.1) already suggested two scenarios that lead to a global quench. One of them slowly raises the electromagnetic field and the other has a sudden increase of field. In order to get more information about these two scenarios first a steady state simulation was conducted to see the temperature distribution in the niobium before

a quench. Secondly a transient simulation of a quench with a homogeneous temperature profile at the beginning is presented.

3.2.1.2.1 Steady state simulation

A steady state simulation is only possible if the occurring effects equalize. In our case this is the heating of a defect on the inside of the cavity and the cooling on the outside. The presented steady state simulation was computed on the basis of a code by Yi Xie [28]. The used model looks at a flat circular niobium sheet of a defined thickness *z*. This sheet gets heated on one spot on the side that is otherwise insulated and the other surface which is cooled by superfluid helium.

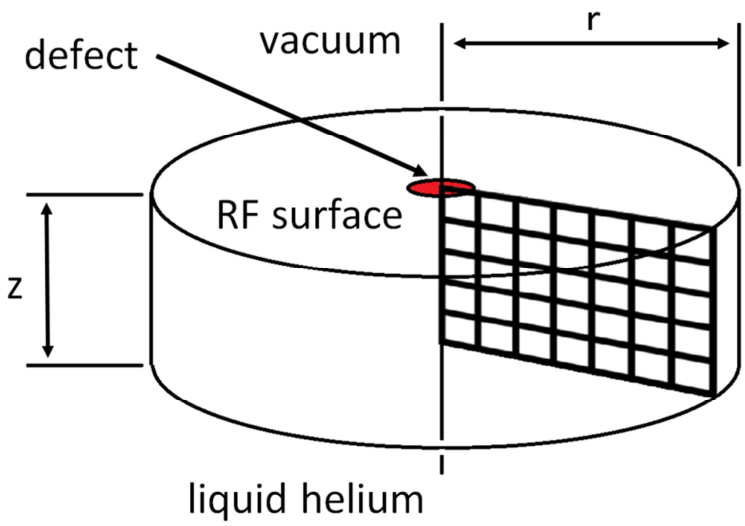

Figure 13: Model for steady state simulation of temperature distribution in niobium.

To get comparable results in the different simulations only two parameters were varied and the others were kept constant. The variables are the thickness of the niobium plate and the temperature of the helium bath. For a real application these are also the parameters that vary. Many cavities are made out of sheet niobium with a wall thickness of a few millimetres. But there are also cavities with complicated geometries and changing thicknesses up to a few centimetres (such as the tested crab cavity, Section 4.5). Therefore, the simulations were done in the range of 2 mm to 3.6 cm. Cavities are often tested at different helium temperatures in a range from 1.5 K up to 4.2 K. As this thesis focuses on phenomena in superfluid helium, the simulations were only done in the temperature range of 1.5 K to 2.1 K.

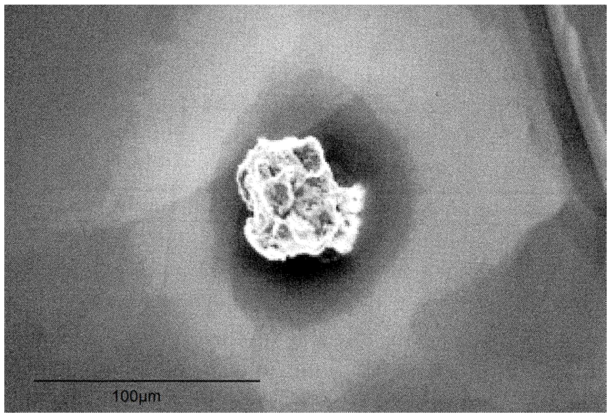

Figure 14: SEM picture of a defect in a single cell cavity. [12]

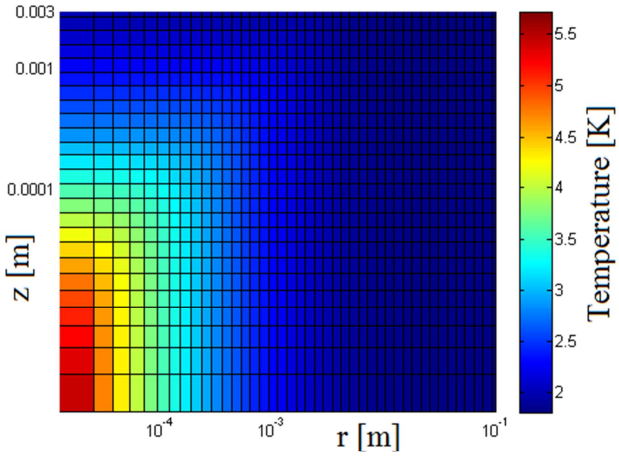

Figure 15: Simulated temperature distribution in a 3 mm niobium plate, cooled with 1.8 K helium. One half of a cut through the plate is shown.

The other parameters that had to be put into the model concern the dimensions of the niobium plate, the kind of defect, the electromagnetic field and the niobium parameters. The plate was set to be 20 cm in diameter, large enough to avoid boundary conditions to play a significant role in the simulation. A very important quality factor for superconducting materials is the residual resistance ratio (*RRR*). A *RRR* of 300 is a common value for high quality niobium for cavities. Thus this value was chosen. The simulations were always done with the common cavity frequency of 1.3 GHz with a rather low peak magnetic field of 50 mT. The low field was necessary to get a stable condition otherwise the heating would have been higher than the cooling capability. The code was not able to calculate this 'run away' scenario. The defect size was chosen to be 50 µm in diameter and 1.5 µm in height because that seems to be in the range of expected defects, compare with Figure 14. The results of the simulations help to understand the temperature distribution in the niobium, see Figure 15. As expected the temperature of the defect spot is severely higher than the surroundings, but lower than $T_C = 9.2$ K. This is clear, because if the temperature of the niobium surrounding the defect spot gets higher than its critical temperature it will change into the normal conducting state. This would lead to a growth of the resistive area which then would increase the heat input and would lead to an accretion of quenched area. This is not a steady state scenario anymore.

In Figure 16 the simulated surface temperatures for a 2 mm thick niobium sheet are shown. The x-axis is in logarithmic scale as most of the temperature changes occur close to the heating spot.

Interestingly the temperature of the heating spot has a small dependency on the bath temperature in the millikelvin range and is roughly 5.72 K for all simulations.

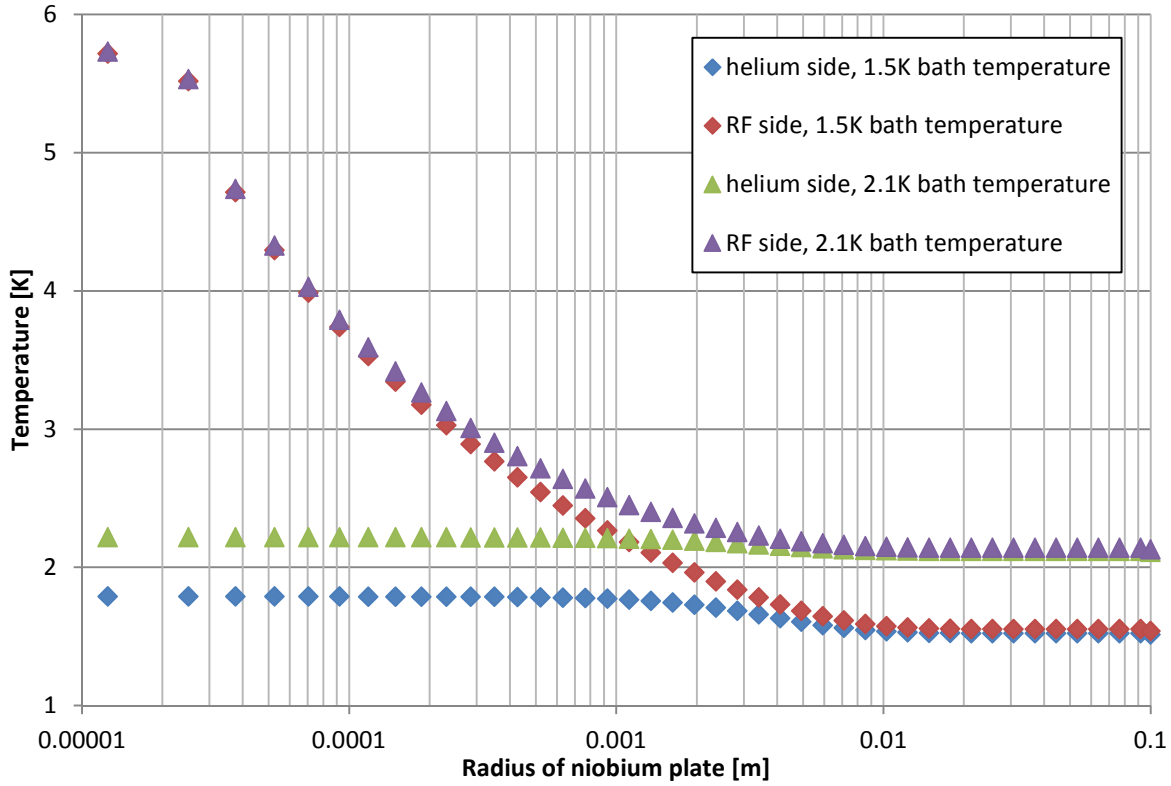

Figure 16: Simulated surface temperatures at a niobium plate for 1.5 K and 2.1 K helium temperature.

Towards the edges of the niobium plate both sides of the sheet have the bath temperature. Coming closer to the middle of the plate both sides of the plate become warmer at approximately 1 cm distance from the middle of the plate. On the helium side a temperature plateau is reached for a distance of 2 mm, which is also the thickness of the plate. This correlation does not hold for thicker sheets where the area of increased temperature is larger than the sheet thickness. Although these temperature simulations do not describe the timescale of heating effects, they give a general insight into the occurring effects and the behaviour of the material. The elevated temperature near the heating spot is closer to the critical surface of the superconductor and will therefore quench at a lower magnetic field.

3.2.1.2.2 TRANSIENT SIMULATION

In the literature a few papers were published about the dynamics of a quench. A very good simulation was conducted by Sang-ho Kim [29]. The used model is comparable with the one in the steady-state simulation. The showed graphs always display the temperature of the heating spot itself and the spot on the helium side of the niobium sheet, also in the middle of the circular plate.

The simulation shows a defect that gets heated by a 70 mT field, which corresponds to a heat input of 0.05 W in the given case. A 2 mm thick niobium wall ($RRR = 270$) in 2 K helium is

thermally stable under these conditions, see Figure 17. The simulation assumes a constant temperature distribution at the beginning of the simulation and is therefore valid if the quench occurs directly when the RF field is applied.

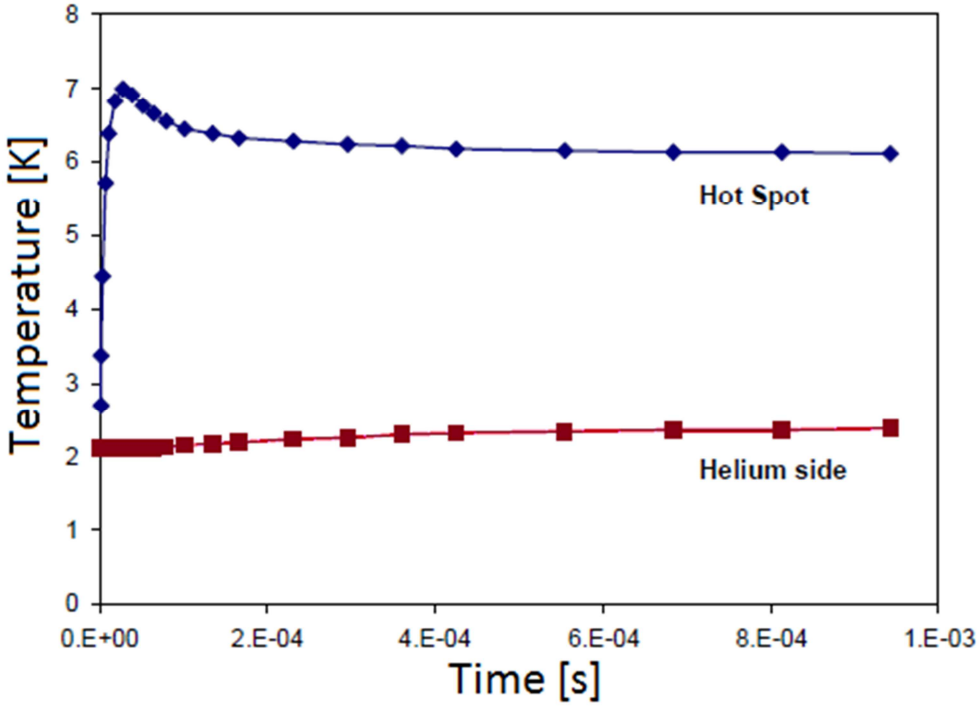

Figure 17: Temperature evolution for a defect heating in a RF cavity which is thermally stable [29].

One can clearly see a little overshoot in the temperature at the beginning of the simulation. The decrease in temperature afterwards can be explained by the better heat conductivity of niobium at higher temperatures.

If the defect on the cavity is a bit bigger and corresponds to 0.1 W of heating power, the system is not thermally stable anymore, but the quenched area increases and leads to a global quench. This is shown in Figure 18. The timescale of this thermal runaway process is in the rage of microseconds. The detailed phases that occur in the simulation are marked in Figure 18.

- In Phase I the spot gets heated to the critical temperature of niobium.
- In Phase II the direct surroundings of the hot spot quench and get heated as well. Thus the cooling of the defect dramatically decreases and its temperature increases.
- In Phase III the higher heat conductivity of the warmer niobium leads to a decrease of temperature. The main quench propagation has not started jet, but the temperature is rising in the adjacent regions.
- At a certain point the quench starts propagating (Phase IV) and leads to a global quench.

One has to point out that the timescale of this effect is very short. It takes less than 25 µs from the beginning of the heating until the quench propagation starts. In another simulation the normal conducting area spread over an area with the radius of 7 cm within1 ms [30] that corresponds to a "speed" of 70 m/s.

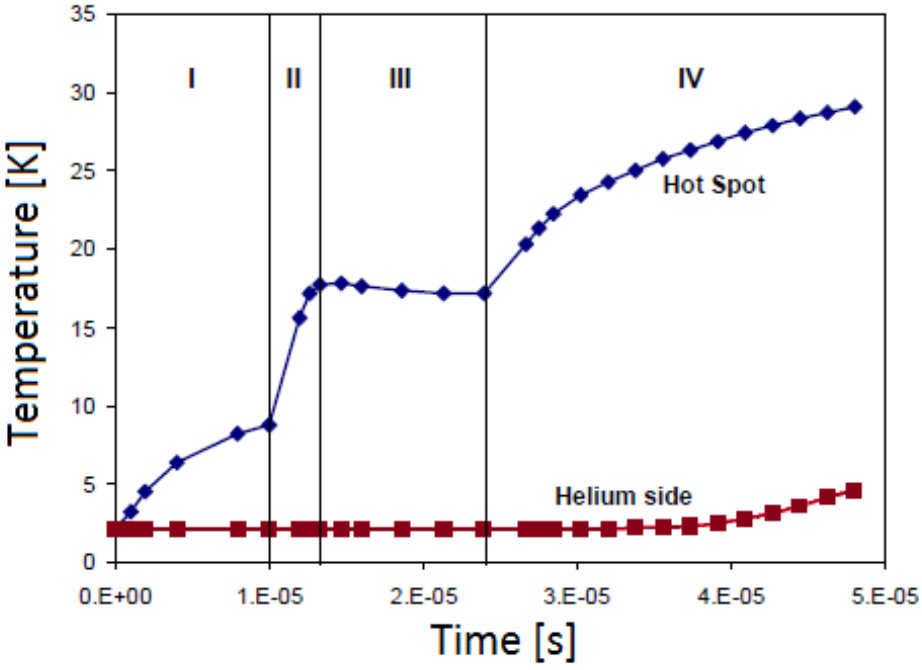

Figure 18: Temperature evolution for a defect heating in a RF cavity that is thermally unstable [29].

3.2.1.3 Conclusion

Both the heat transport by high diffusivity and the expanding quench area can occur faster than the second sound. The expanding quench is certainly the more likely as further heating and the high speed of this effect will be more dominant. Additionally more sophisticated models have predicted it and the further heating on the quenched surface make a signal much easier to detect. Unfortunately, this cannot be the only reason for the faster than expected signal at the OSTs. Experiments at CERN [31], Fermilab [20] and CEA Saclay [21] measured signals with OSTs where the normal speed of second sound did not have a single intersection point with the niobium surface. Therefore some effect in the helium has to allow accelerated signal propagation.

3.2.2 Heat transport across the niobium-He II interface

Various effects occur at low temperatures on a solid-liquid interface. As these effects can only slow the heat transport down, they are discussed very briefly. For low heat fluxes the Kapitza

resistance is an important effect. For higher heat fluxes the different boiling effects can limit the heat transport.

The Kapitza resistance R_K describes a temperature discontinuity ΔT between two different materials, which is dependent on the heat flux $\dot{q}$.

$$\Delta T = R_K \dot{q} \qquad \text{(Kapitza resistance)} \tag{3.9}$$

This boundary resistance was first found for solids and helium but is used for other materials as well. It has its biggest relevance for very low temperature systems (< 1 K) where it can become the dominating heat transfer restriction [32]. The Kapitza resistance is not fully understood, but various theories give well-justified estimations. A theory to describe the upper limit of the Kapitza resistance is the "phonon radiation limit". This theory predicts a $1/T^3$ dependency of R_K, which is quite close to observed values. For niobium the Kapitza resistance with this theory for a bath temperature T in $[K]$, can be obtained by the following equation

$$R_K = 1.92 \cdot 10^{-4}/T^3 \left[\frac{\mathrm{m^2K}}{\mathrm{W}}\right]. \tag{3.10}$$

(Calculated according to [12], with a Debye temperature of 275 K [33]).

For high heat fluxes boiling effects can be observed in helium II. In other liquids boiling occurs only when the vapour pressure rises above the local pressure and thus forms a gas. This condition also holds for helium II, but also another phenomenon can lead to boiling. If the helium II is sub-cooled it is possible, that the lambda line is crossed before the vapour pressure exceeds the local pressure. As the heat transport in He I is worse than in He II, it is likely that the temperature will rise further and the system enters a three phase boiling condition. This can either be with a stable He I layer and nucleate boiling, normally for temperatures close to the lambda temperature, or an unstable process with film boiling. It is important to notice that the transition between helium I and II is a second order phase transition, which allows only a continuous density profile.

Empirically two boiling regimes are distinguished in helium II, they are called noisy and silent film boiling. The origin of the name is easy imaginable, the noisy film boiling process is easily audible. Whether these processes are connected to the earlier named two boiling conditions is not clear [12].

Noisy film boiling is reported to occur at higher immersion depths than silent film boiling. There is an intermediate regime in which either of the two can occur. Zhang [34] identified the boiling regimes as a function of bath temperature, heat flux and immersion depth.

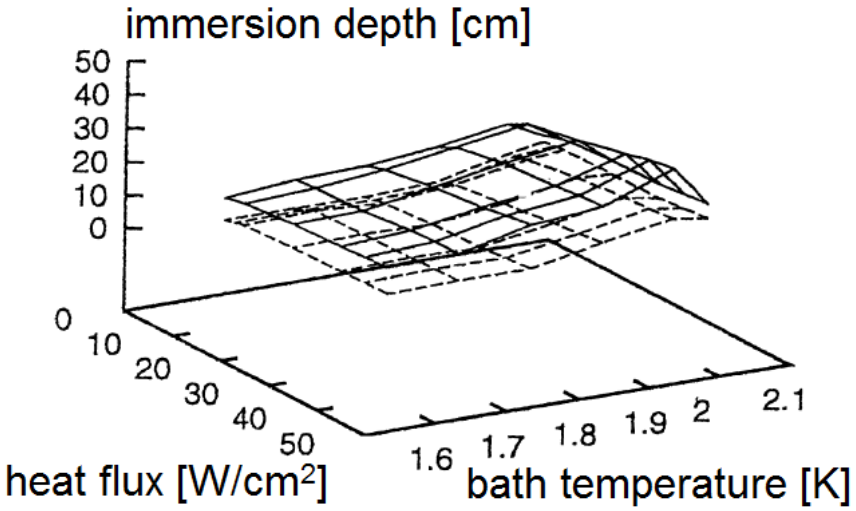

Figure 19: Diagram for different boiling states in helium II. Above the upper surface noisy film boiling occurs, between the two surfaces either regime can be observed and below the lower surface only silent film boiling happens, see [34].

3.2.3 Heat transport in helium II

As mentioned before the thermal conductivity of helium II is higher than in any other known substance. It improves at least five orders of magnitude at the lambda transition [17]. This change is clearly visible when helium is cooled by pumping on a bath. In helium I a violent boiling process is visible, but with the lambda transition the bubbles vanish and the surface calms down. This does not mean the evaporation process has stopped, but the heat conduction within helium II is so large that all evaporation takes place on the surface of the helium bath.

Unlike the heat transfer at higher temperatures helium II does not follow the law of Fourier, Equation (3.11), anymore.

$$\dot{q} = -\lambda \cdot grad\ T \qquad \text{(law of Fourier)} \qquad (3.11)$$

The relationship between the temperature gradient ($grad\ T$) and the heat transfer rate $\dot{q}$ is not linear but has a more complicated dependency [35].

$$grad\ T = A\dot{q}\ + B\dot{q}^3 \qquad (3.12)$$

This indicates that a different approach has to be taken to describe the heat transport in helium II. A and B are other functions, not dependent on T or $\dot{q}$, compare [35].

3.2.3.1 First and second sound

Taking the two fluid theory into account, the thermohydrodynamical equations for superfluid helium may be written in a first approximation as [36]:

$$\rho_s \frac{\partial v_s}{\partial t} = -\frac{\rho_s}{\rho} grad\ p + \rho_s s\ grad\ T \tag{3.13}$$

$$\rho_n \frac{\partial v_n}{\partial t} = -\frac{\rho_n}{\rho} grad\ p - \rho_s s\ grad\ T \tag{3.14}$$

$$\frac{\partial \rho}{\partial t} + \mathrm{div}\ (\rho_s v_s + \rho_n v_n) = 0 \tag{3.15}$$

$$\frac{\partial}{\partial t}(\rho s) + \mathrm{div}\ (\rho s v_n) = 0. \tag{3.16}$$

If one looks at Equation (3.15) one can already see that there are two ways to obtain a constant density ρ in helium. Either the two terms $\rho_s v_s$ and $\rho_n v_n$ are zero, or these terms cancel each other out. As the densities are always positive, only a counter flow of the normal and superfluid component can lead to an equalisation. At a constant pressure, this is a condition for a constant density in compressible fluids, Equation (3.13) and (3.14) show that the velocity of the normal and superfluid component depends on the gradient of temperature but with opposite sign. This clearly indicates that a counter flow can be initiated by a thermal gradient. The given Equations (3.13) - (3.16) can be solved with an ansatz describing ρ and s as a plane wave with a constant speed. The calculation solving the differential equations can be found in [37] and shows that two types of wave phenomena can occur in helium II.

The density fluctuation that is normally called sound can also be found in helium II. Here it is named first sound and the normal and superfluid components are moving in phase. The velocity of first sound is between 220 and 240 m/s below T_λ.

The other phenomenon is consequently called second sound and describes a temperature wave with the components moving in opposite directions. The second sound velocity $v_{2,0}$ as given by the solution of the differential equation is [37]

$$v_{2,0} = \sqrt{\frac{\rho_s}{\rho_n} S^2 \left(\frac{\partial T}{\partial S}\right)_\rho} = \sqrt{\frac{\rho_s}{\rho_n} \frac{T S^2}{c_v}}. \tag{3.17}$$

Its value is far lower than for first sound and additionally much more dependent on the temperature. The $v_{2,0}$ for the relevant temperature range is shown in Figure 20.

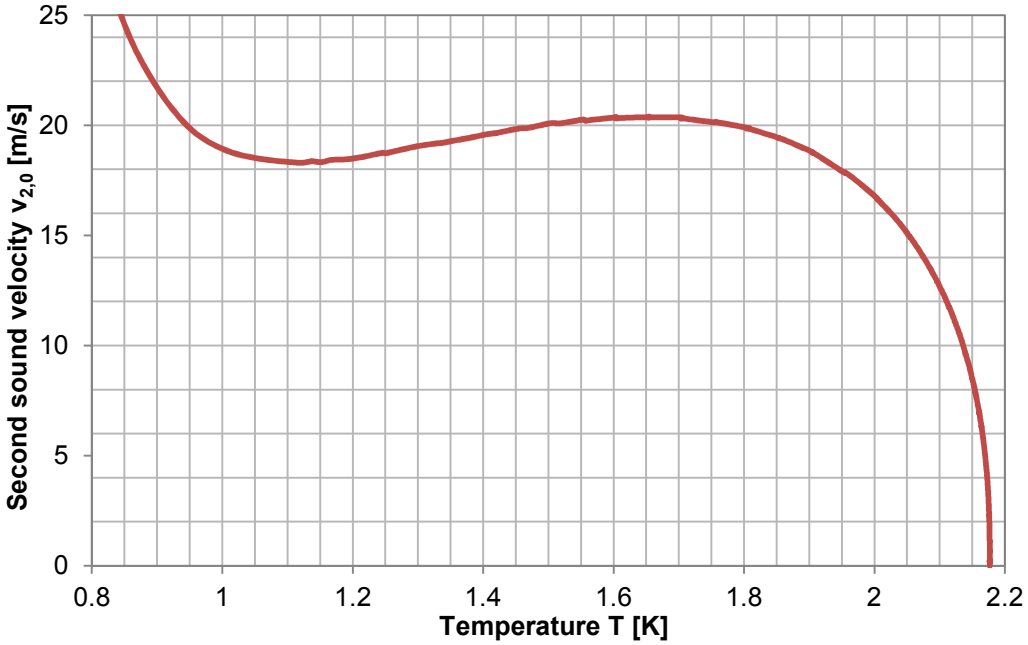

Figure 20: Speed of second sound measured by the resonance method [11].

Towards lower temperatures the second sound has a local minimum at about 1.1 K and then a rapid increase. The maximum value of second sound can be found at 0.4 K with 143 m/s, towards absolute zero the speed of second sound decreases slightly to the theoretical predicted value of $v_2(0\ \mathrm{K}) = \frac{1}{\sqrt{3}} v_1$ [38].

All precise measurements of second sound were made by the so called resonance method (A collection of various measurement results can be found in [11]). This method generates a standing wave by a periodical heating in a confined geometry, often a small cylinder. In that way the nodes and peaks of the wave can be determined most precise and the speed can be calculated.

3.2.3.2 Three dimensional propagation of second sound

The propagation of a one-dimensional wave is still relatively easy to imagine. Its behaviour is dominated by a constant speed, and its shape will not change. For a three-dimensional geometry this is more complicated. To be able to make some predictions about this case the spherical symmetric propagation of a single heat pulse is calculated.

A few assumptions are made for this evaluation. First the temperature of the heat wave is expressed as the deviation θ of the bath temperature T_0.

$$T = T_0 + \theta \tag{3.18}$$

The second assumption is to have a pure second sound wave with no change in pressure or density. With this simplification Equation (3.14) becomes

$$\frac{\partial \overrightarrow{v_n}}{\partial t} + \gamma \, s \, grad \, \theta = 0. \tag{3.19}$$

where γ expresses the ratio of the superfluid to the normal fluid component. One has to keep in mind: the normal fluid velocity is a vector in the three-dimensional case.

Applying the same simplification as in (3.19) to Equation (3.16) and introducing $s_1 = \partial s / \partial T$ we get

$$s_1 \frac{\partial \theta}{\partial t} + s \, div \, v_n = 0 \tag{3.20}$$

Changing the vector operators into polar coordinates and eliminating v_n, as can be found in [39], one obtains

$$\frac{\partial^2 (r\theta)}{\partial r^2} - \frac{1}{{v_{2,0}}^2} \frac{\partial^2 (r\theta)}{\partial t^2} = 0. \tag{3.21}$$

With the definition of $v_{2,0}$ as given in Equation (3.17).

A solution for this differential equation can be found with a reciprocal decaying temperature change, depending on time, radius and speed.

$$\theta = \frac{1}{r} g' \left(t - \frac{r}{v_{2,0}} \right). \tag{3.22}$$

With this description of θ one can find an expression for the normal fluid velocity, which is given as

$$v_n = \frac{\gamma S}{v_{2,0} r} \, g' \left(t - \frac{r}{v_{2,0}} \right) + \frac{\gamma S}{r^2} \, g \left(t - \frac{r}{v_{2,0}} \right). \tag{3.23}$$

As heat flux and the normal fluid velocity are directly related by Equation (2.6) one can state how heating and the shape of the temperature wave are connected. To be able to know the initial heat flux on the heater, its surface area has to be known. For a spherical heater with a radius of r_0, the equation yields.

$$\dot{Q}(t) = 4\pi r_0 \rho T_0 s^2 \gamma \left[\frac{1}{v_{2,0}} g' \left(t - \frac{r}{v_{2,0}} \right) + \frac{1}{r_0} \, g \left(t - \frac{r}{v_{2,0}} \right) \right] \tag{3.24}$$

If the size of the heater is negligible, one can write

$$lim_{r_0 \to 0} \dot{Q}(t) = 4\pi\rho T_0 s^2 \gamma \, g(t) \tag{3.25}$$

Comparing the function of $\theta(t, r)$ in Equation (3.22) and $Q(t)$ in Equation (3.25) clearly shows that the shape of temperature pulse is directly dependent on the time derivative of heating power.

This theory was affirmed by numerous papers such as [40]. Figure 21 shows a plot from this publication which nicely shows a measurement depicting this relationship.

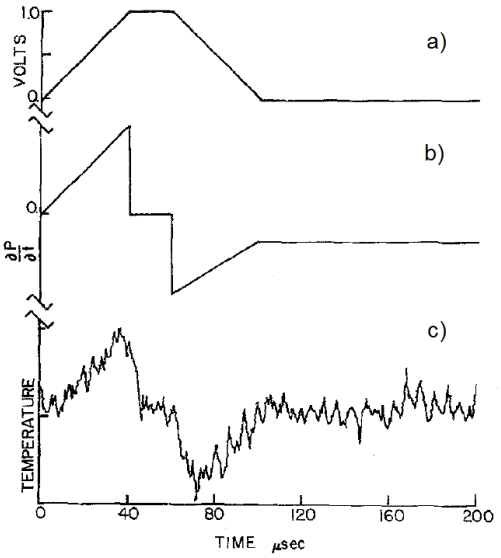

Figure 21: Heating and measured second sound pulse, after [40]:

a) The input voltage pulse to create heating with a resistor immerged in He II. One has to consider the heating power is $P = U^2/R$.

b) The time derivative of the input power.

c) The measured second sound pulse at 1.449 K and 10.8 atm. (the signal was already post processed)

Except for a) the units are arbitrary.

One can clearly observe that the signal is reduced to the change of heating power while propagating in 3D. Since large computing power is nowadays available, the thermohydrodynamical equations of helium can be solved in a numerical way without the simplifications as it was done by Zhang and Mukarami [41]. Figure 22 shows a series of 2D slices of a 3D second sound wave at different times. It is a simulation of a second sound wave in helium with an initial bath temperature of 1.6 K. The simulated pictures show the left side of a symmetrical problem. The heater had a squared surface of 25 mm side length (black line at bottom), the pulse was send for 0.5 ms starting at t = 0. The heat flux density was 10 W/cm^2.

The time in the first slice is exactly the end of the heating pulse. One can clearly see the heated helium and how far it propagated. After three quarters of a millisecond one can see the evolving cooling front, which starts at the edge of the heater. On the third slice the second sound, with both the heating and the cooling front can be clearly seen. They propagate nearly spherically with the strongest deviations of the surrounding bath temperature in perpendicular direction as shown in the slice after two milliseconds.

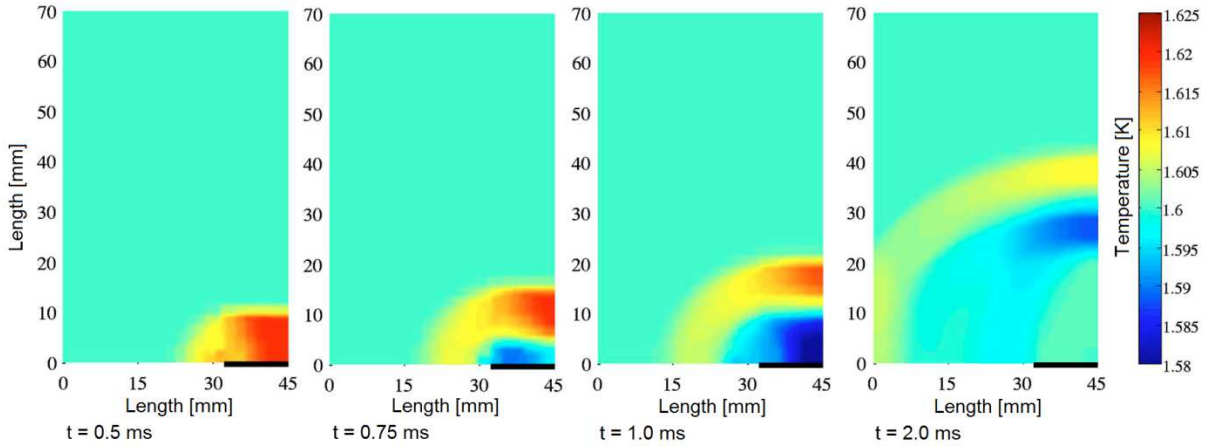

Figure 22: A series of 2D slices of a 3D second sound wave at different times, from [41].

3.2.3.3 Amplitude dependence of second sound

In 1951 two papers in the Proceedings of the Physical Society London by Temperly [42] and Osborne [43] theoretically described and experimentally proved a concept that shows the dependency of the second sound velocity on the amplitude of a heating pulse. While Osborn's experiment only qualitatively shows the concept, Dessler and Fairbank [44] published a quantitatively verification of the theory a few years later on the basis of Dessler's PhD thesis. Temperly's theory was later improved for lower temperatures by Khalatnikov [45].

The second sound velocity v_2 for a certain bath temperature is given as

$$v_2 = v_{2,0} + \tau_2 v_n \,. \tag{3.26}$$

$v_{2,0}$ is the second sound velocity for infinitely small pulses at a given temperature, τ_2 is a dimensionless factor that is only dependent on temperature and material properties and v_n is the velocity of the normal component in helium II. This velocity is a direct function of the heat flux in the second sound wave as already shown in Equation (2.6), see Section 2.6.

$$\dot{q} = \rho s T v_n \tag{2.6}$$

The idea of the amplitude dependence is based on two assumptions. First for high heat pulses the temperature of the second sound wave is higher than the surrounding bath, so its speed will be also different. Second, entropy is only transported by the normal fluid component. As the proportion of normal to superfluid component rises with the temperature, this slows down the normal fluid and has to be taken into account. These two assumptions can be unified into one equation:

$$\tau_2 = \frac{sT}{c_v}\frac{\partial}{\partial T} ln\left({v_{2,0}}^3 \frac{c_v}{T}\right) \tag{3.27}$$

In Figure 23 this formula is plotted, the data points given show the experimental results of Dessler and Fairbank.

As one can see in Figure 23 at three temperatures the value of τ_2 is zero and therefore will not alter the speed of the second sound.

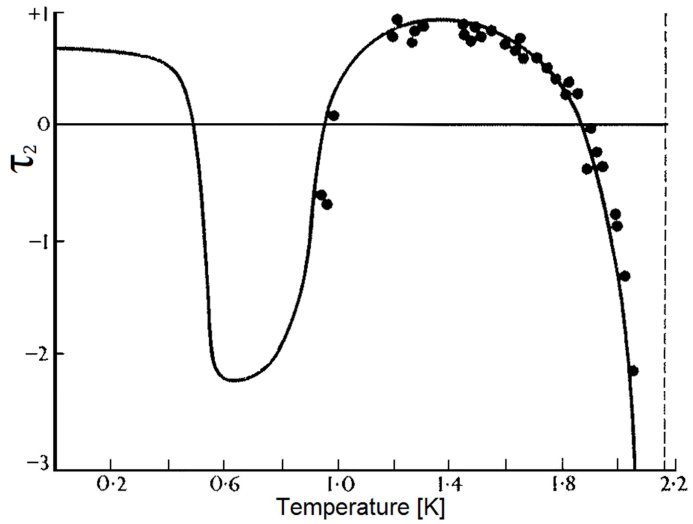

Figure 23: The amplitude dependence factor τ_2 [37]. Data points are from Dessler and Fairbanks publication, the solid line is described by Khalatnikov's theory, see Equation (3.27).

If cavities are cooled with superfluid helium, their usual operating temperatures lie between 1.6 and 2 K. In this region the amplitude dependence factor is zero at 1.88 K. At lower temperatures the factor will accelerate the v_2, at higher temperatures it will slow it down. Although the amplitude dependence factor τ_2 is most extreme for temperatures close to T_λ, the actual change in v_2 is not very pronounced because the speed of the normal component is not very high. This is caused by the high percentage of normal fluid component and therefore high specific entropy. This shows that although it was possible to describe the change of the v_2 via this theory, this abstract factor is hard to imagine. This is the reason that Dessler and Fairbank introduce a new factor which combines τ_2 and v_n.

$$\Gamma_2 \left[\frac{\mathrm{m}^3}{\mathrm{J}}\right] = \frac{v_2 - v_{2,0}}{\dot{q}} \tag{3.28}$$

This simplifies the calculation of the velocity of second sound to

$$v_2 = v_{2,0} + \Gamma_2 \dot{q}\,. \tag{3.29}$$

The plot of this factor (Figure 24) shows clearly that for a given heating power the deviation of the low amplitude pulse decreases drastically between 1.1 K and 1.88 K.

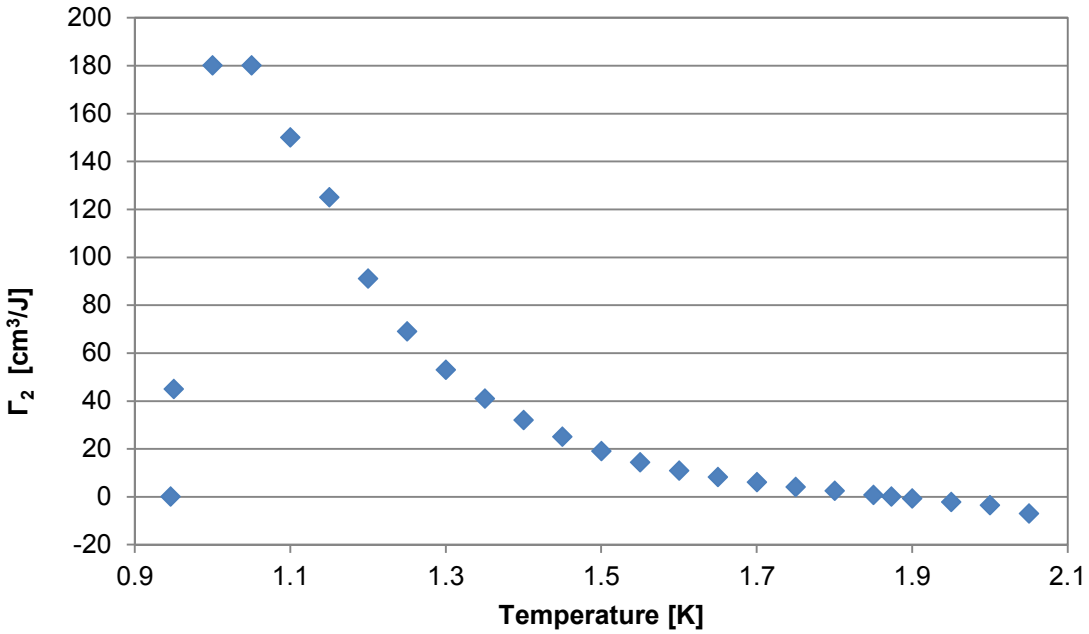

Figure 24: The amplitude dependence parameter Γ_2 as measured by Dessler and Fairbank. [44]

To simplify the measurements, the experiment of Dessler was done in a tube with constant cross-section. In this way the heat flux density was constant over the whole measured distance.

In contrast the investigated case has a three dimensional geometry with changing cross section. To be still able to compare the theory with the experimental results the effect of the changing geometry has to be taken into account. The simplified calculation can be found in Appendix 8.2.1.

3.2.3.3.1 Questioning the Applicability of the Theory

Although the amplitude dependence of second sound could be an explanation for a faster second sound wave, some doubts question the applicability of this theory on the investigated scenario.

The measurements by Dessler had a totally different setup. They were done in a channel with a constant cross section and measured the relative velocities of a short, high amplitude heat pulse which travelled on a longer low amplitude one. The relative movement gave the earlier discussed values. If one looks at a triangular temperature pulse with the amplitude dependence at different times of flight one gets changing pulse shapes over time. This is depicted for a channel with a constant cross section in Figure 25. For a symmetrical temperature excursion at t_1 and a positive amplitude dependence, the high temperature part of the pulse will travel faster and change its shape like in t_2 and t_3. At t_3 the temperature has a discontinuity and does a

temperature step on the leading edge. The observed second sound speed has not changed so far, only the leading edge became steeper. The open question is what happens at a time $t > t_3$. According to the theory one would obtain a pulse shape as shown in purple. As two different temperatures at one spot are thermodynamically impossible, the pulse has to look different than shown. Most likely the temperature step will still determine the pulse shape, but it is not clear how far the pulse has travelled up to that time. The most likely position is $x_{4,2}$, because the shaded areas have the same size (assuming the heat capacity over this temperature range is constant). This would mean the pulse has travelled faster than the literature value of second sound (which would be $x_{4,1}$), but not as fast as the amplitude dependence predicts $x_{4,3}$.

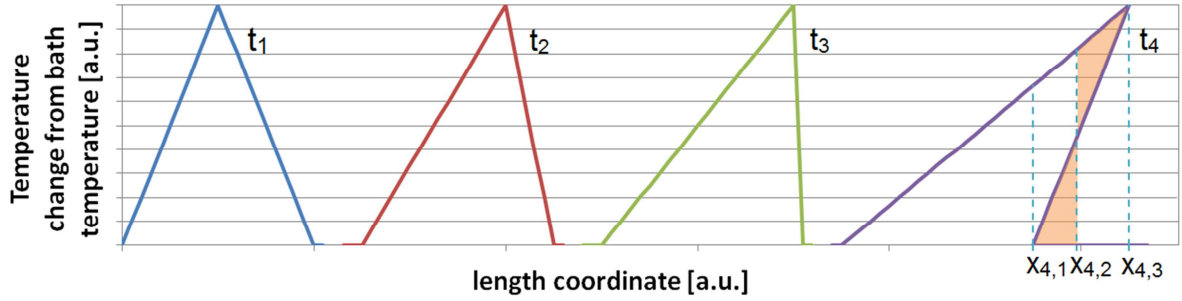

Figure 25: Changing pulse shape with positive amplitude dependence over time. The pulse travels from left to right.

3.3 DETECTION OF HEAT TRANSPORT

There are many different ways to measure temperature in cryogenic conditions. The main two techniques used in the experimental section are described.

3.3.1 Temperature sensors

A very precise way to measure temperature of the whole helium bath is by measuring the vapour pressure. Especially in helium II this method is very precise as the temperature gradient in the liquid is negligible. The vapour pressure – temperature relationship is so convenient, that the temperature between 1.25 and 5.0 K is even defined by this pressure (Appendix 8.1.1.1) [46].

The second type of measurement makes use of a temperature dependent electric resistivity of certain materials. They can be read out via a so called four-point measurement. A well-defined small current is send by two wires through the resistor and the other two wires read out the voltage drop over the resistor. With these two values the resistance can be calculated via the simple Equation (3.30).

$$R = U/I \tag{3.30}$$

By calibrating the resistance vs. temperature in a test with a different temperature sensor (often the described vapour pressure method is used) one obtains a curve which can be used to determine the temperature of the sensor.

3.3.2 Oscillating Superleak Transducers

A very sensitive sensor to detect second sound is the Oscillating Superleak transducer (OST). The idea for this sensing element evolved at the eleventh International Low Temperature Conference in 1968 in discussions between D.O. Edwards and I. Rudnick [47]. It makes use of the unique properties of superfluid helium. The OST has the same setup like a capacitor microphone with a metal coated membrane and a solid back electrode. A movement of the membrane is detected by measuring the change in capacitance of the device. The specialty of an OST over a normal capacitor microphone is its membrane. Very small holes make it very hard for normal fluids to pass through them. But the superfluid component of helium II, with its zero viscosity, can flow through the holes (Figure 27).

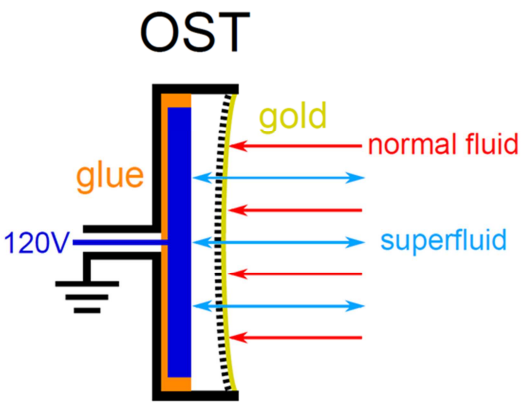

Figure 26: Working principle of a OST. [33]

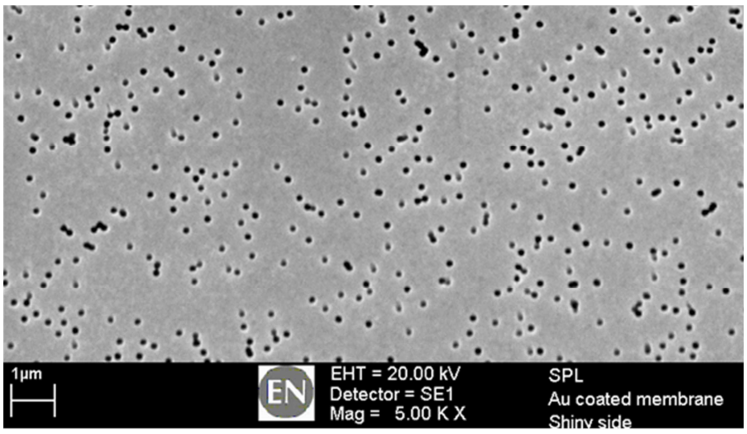

Figure 27: SEM picture of a gold coated OST membrane.

A change in temperature is equivalent to a change of the normal to superfluid component ratio in helium. A temperature wave therefore has a shifted normal-superfluid component ratio in comparison to the bath temperature. If a second sound wave reaches an OST this ratio on the two sides of the membrane is different. This difference is the driving force for superfluid component to flow through the membrane. As the normalfluid component cannot pass the membrane, a pressure difference is the result. The resulting force moves the membrane. This principle is schematically shown in Figure 26.

To detect the change in capacitance a certain setup is needed. The electronic circuit can be found in the Appendix 8.3.3. The circuit basically allows loading the OST with 120 V by a battery to charge the sensor and read out voltage changes on the OST due to a change in capacitance.

The capacitance C of a parallel plate capacitor is given by

$$C = \varepsilon_0 \varepsilon_r \frac{A}{d} \tag{3.31}$$

and defined as

$$C = \frac{Q_e}{U}. \tag{3.32}$$

These two equations can be combined to

$$U = \frac{Q_e\, d}{\varepsilon_0 \varepsilon_r A}. \tag{3.33}$$

If one assumes that the area of the OST as well as the permittivity of the medium stays constant and for a fast process the charge is also approximately constant, the change in voltage is directly proportional to the change in distance between the capacitor plates. The constant charge is a valid assumption, as the loading resistance is high [48].

With the explanations up till now the words Superleak (membrane with small holes) and transducer (changing movement of membrane into electrical signal) were explained.

The word oscillating becomes clear when one looks at a signal of an OST. A short temperature pulse in He II gives an oscillating voltage change on an OST due to a movement of the membrane as a signal. A group of scientists at the University of Göttingen identified the movement as oscillations of a circular membrane, which could either be the whole membrane or only parts of it. They did that by identifying the ratio between different frequencies in the OST signal as the characteristic eigenmodes of a circular membrane [49]. The first twelve eignemodes are displayed in Figure 28. A three dimensional snapshot of the first two is also shown. For the others only the two dimensional representation is depicted. The lines and circles show the nodal lines and circles where the amplitude is zero if only this harmonic is exited. The neighbouring fields always move in opposite directions. The numbers below the pictograms display the relative frequency in comparison to the (0, 1) mode. This relationship between the frequencies was observed by the researchers in Göttingen.

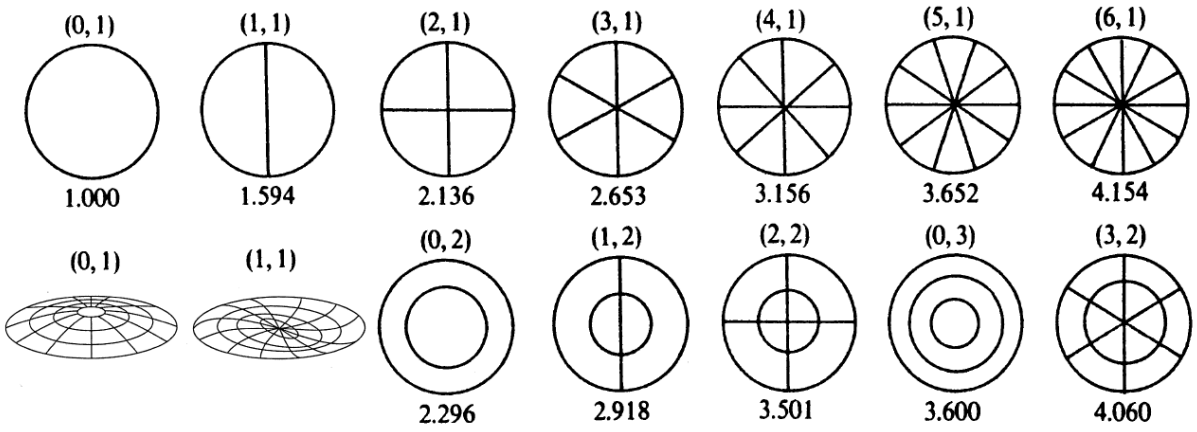

Figure 28: Graphical representation of the first 12 eigenmodes of a membrane. For the first two a three dimensional representation is given. The modes are named in the form (m, n), where m is the number of radial nodal lines and n is the number of nodal circles. The numbers below the representations give the relative frequency in comparison to the (0, 1) mode. After [50] and [51].

The original paper suggesting and describing the OST as a measuring device for second sound gives a different explanation. The transducer is modelled as a Helmholtz resonator to explain the oscillation [52]. This model takes other entities into account such as properties of the enclosed fluid, in the presented case helium. The paper gives also experimental evidence of its theory. Sherlock and Edwards varied the temperature in their measurements and showed that the change in the main frequency of the OST response can be explained by their model.

So the literature does not give a coherent explanation for the oscillating phenomenon. Further research has to be done to understand the OST signal in more detail.

4 Experimental Aspects of Heat Transfer

The experimental work has been done both in small cryostats dedicated to this research and in an industrial style test facility used for cavity tests. In order to investigate transient heat transfer phenomena in a controlled environment a test stand in the central cryogenic laboratory of CERN (Building 165, Meyrin site) was refurbished and upgraded. Resistors were used to simulate heating spots in superfluid helium.

To validate the previous measurements in a different setup and to test with higher heating powers, a collaboration with CEA Saclay made this possible. CEA stands for “Commissariat à l’énergie atomique et aux énergies alternatives” (Eng.: Alternative Energies and Atomic Energy Commission) and is a French government-funded technology research organisation with ten research centres in France [53]. One of these is CEA Saclay, close to Paris.

The application of OSTs for cavity tests was done in CERNs Cryogenic test facility SM18. The measuring system was improved and employed for the cavities that were tested there during this thesis.

4.1 TEMPERATURE SENSORS

Two different kinds of measurements were used to determine temperature during the conducted experiments. The overall temperature of the helium bath was measured and controlled by the pressure of the vapour space above the helium bath. The used pressure sensors are a temperature compensated Capacitance Gauge CMR 361 ($1 \cdot 10^{-2} - 110$ hPa) by Pfeiffer and a MKS Baratron® Type 626B ($5 \cdot 10^{-2} - 100$ Torr). The relationship between pressure and temperature is calculated by the ITS 90, see Appendix 8.1.1.1.

All other temperature measurements for the presented work make use of temperature dependent electric resistivity. Four sensors were used in the various setups. If the temperature was used for measurements and evaluation of occurring effects either an already calibrated sensor was used or a calibration curve was produced with the vapour pressure as a reference value. Table 2 gives an overview of the various sensors that were used.

Table 2: Important properties of the used temperature sensors. The given values just intend to give approximate ranges and are not universally applicable.

Resistor	Dependency	Temperature Range	Resistance range
Allen-Bradley Carbon Resistor	$R = A\exp(B/T) + C$	$1.2 - 325$ K	$10\,000 - 500\ \Omega$
Cernox™ 1050	No standard curve	$1.2 - 325$ K	$10\,000 - 50\ \Omega$
Ruthenium Oxide resistor	No standard curve	$0.01 - 40$ K	$1\text{M}\Omega - 1\text{k}\Omega$
Pt100	Linear	$80 - 273$ K	$20 - 100\ \Omega$

4.2 TEST STANDS IN THE CENTRAL CRYOGENIC LABORATORY OF CERN

The small scale experiments of the presented work were conducted in the central cryogenic laboratory of CERN. Here 11 cold tests in 3 cryostats with a 6 different experimental setups were tested.

4.2.1 Measuring second sound

To determine the second sound velocity the values for the time of flight of the second sound pulse had to be determined as well as the distance between the OST and the heater. The distance between the OST and the heater was measured at room temperature. As the OST is not point like, but has a membrane with an active diameter of 19 mm, the distances of the sides of the OST to the heater were measured (a and b) and then the distance to the middle of the membrane was calculated by trigonometric functions.

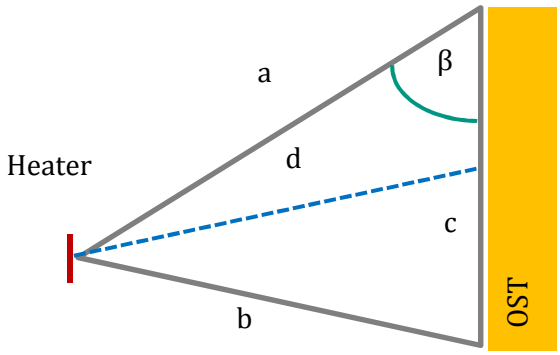

Figure 29: Sketch to demonstrate distance measurement heater - OST.

The used equation is given in (4.1). It was obtained using the law of cosine and equalizing the angle β for different triangles.

$$\mathrm{d} = \sqrt{\frac{a^2}{2} - \frac{c^2}{4} + \frac{b^2}{2}} \tag{4.1}$$

The time of flight for the propagating second sound signal was obtained by taking the difference between the rising edge of the heating pulse and the onset of the signal on the OST.

4.2.2 Niobium plate

To be able to study the phenomena occurring on cavities, a heater was glued to the surface of a niobium plate. Three OSTs were positioned around the plate to investigate occurring phenomena. The questions of particular interest were:

1. Can we measure the second sound velocity as published in literature?
2. Is the speed of heat propagation in niobium faster than the second sound?

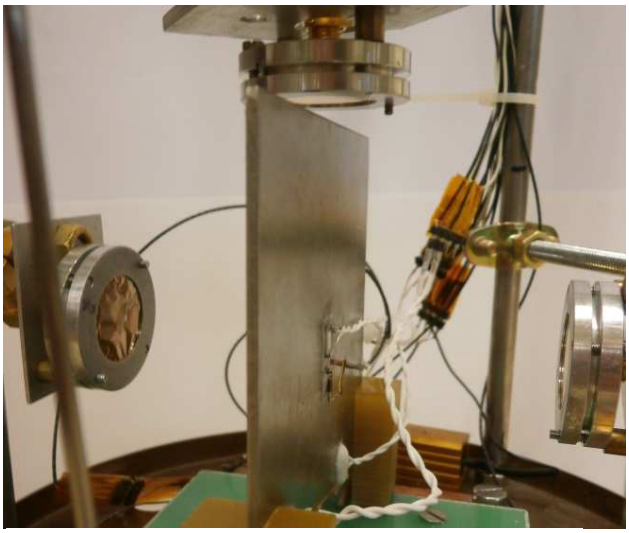

Figure 30: Measurement setup with a heater glued to a niobium plate and OSTs in three positions around it.

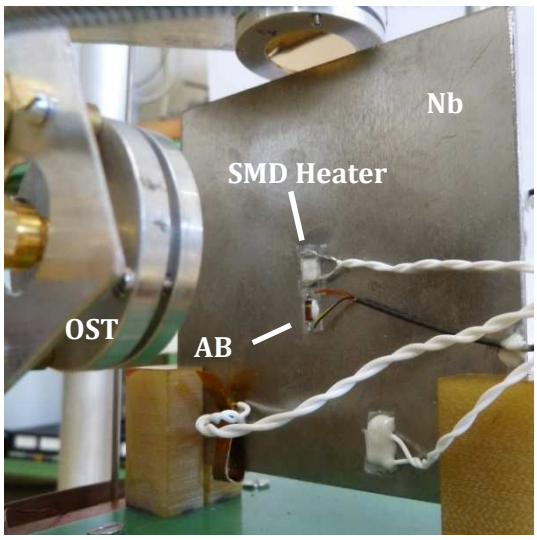

Figure 31: Close up of SMD heater and AB temperature sensor on niobium plate.

In Figure 30 and Figure 31 one can see the experimental setup for the test with the niobium plate. The 2 mm thick niobium plate has a SMD heater with a resistance of 68 Ω glued to its surface, the heating side is facing the plate. Right below it one can see an Allen Bradley (AB) temperature sensor that was also connected to the plate (also in Figure 31). Not visible on this photo is another AB temperature sensor which was glued to the other side of the plate. Around the plate three OSTs are placed to detect the second sound. One in direct line of sight, one along the niobium plate and one on the other side of the niobium plate.

4.2.2.1 LITERATURE VALUES OF SECOND SOUND

In this experiment a fairly accurate measurement of the second sound velocity was obtained as can be seen in Figure 32. For these results the OST in direct sight of the heater was used. The error bars in the figure, as in this whole document, represent three times the standard uncertainty of the measurement and are calculated according to the GUM [54], see Section 4.6.

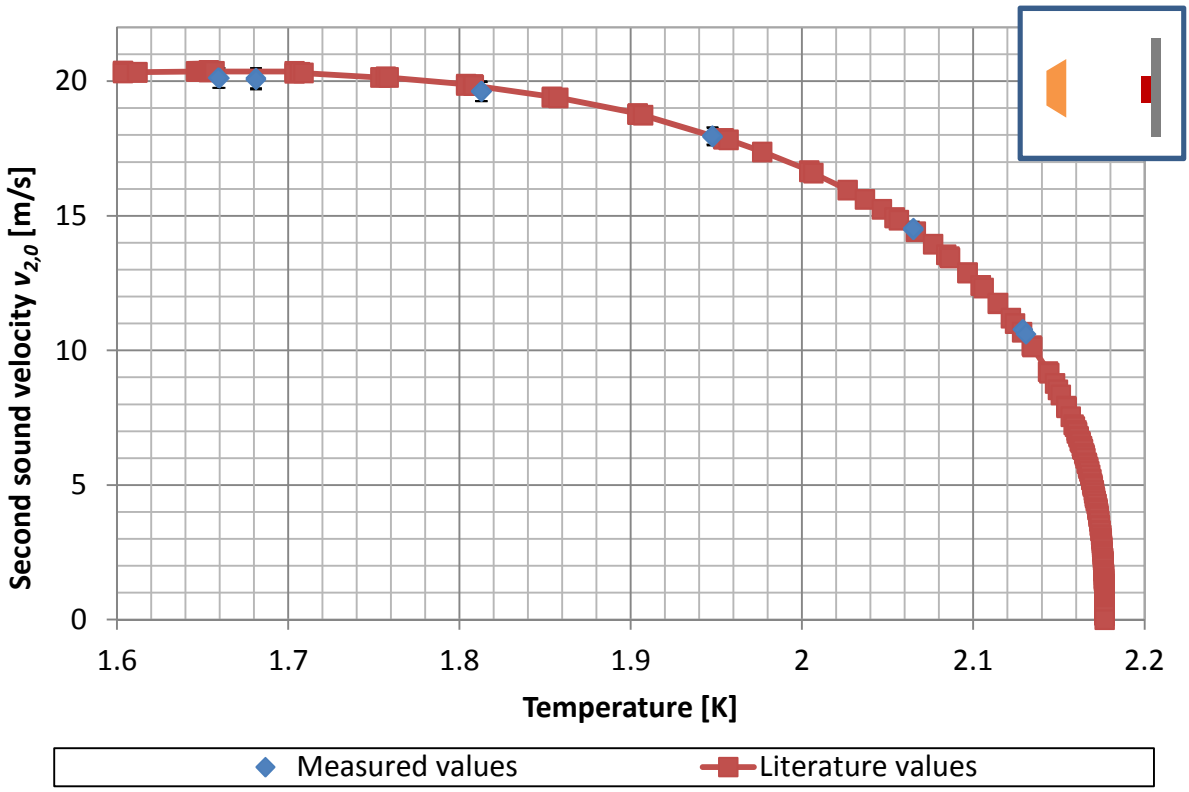

Figure 32: Measured second sound velocity by pulse method. The error bars for the deviation in speed are already in the graph but partly smaller than the markers. The literature values are obtained from [11]. The sketch in the upper right corner demonstrates the position of the OST in respect to the heater location.

The temperature was determined by the vapour pressure, measured by a sensor on the top of the cryostat. The ITS 90 (Appendix 8.1.1.1) was used to calculate the temperature of the bath. These results show that the setup allows quite accurate measurements and no significant systematic errors were made.

4.2.2.2 HEAT PROPAGATION IN NIOBIUM

If the temperature information travels faster in the niobium than in the superfluid helium, OST 2 in this setup should receive an earlier second sound signal than calculated for the direct line of sight and the second sound velocity. The niobium could warm up faster than the traveling second sound wave (see, 3.2.1.1) and at the upper edge of the niobium plate it would emit a new second sound wave which then gets detected by the OST 2. In Figure 33 one can see a part of

measured OST responses. The graph shows the part of the OST signal where the second sound wave arrives. The three vertical stripes show the theoretical arrival for a second sound wave traveling the shortest distance between the heater and the OST. The signals are partly magnified for better display, this is also the reason for the different noise levels for the different OSTs (OST 2 was magnified by a factor of 5, OST 3 by a factor of 20).

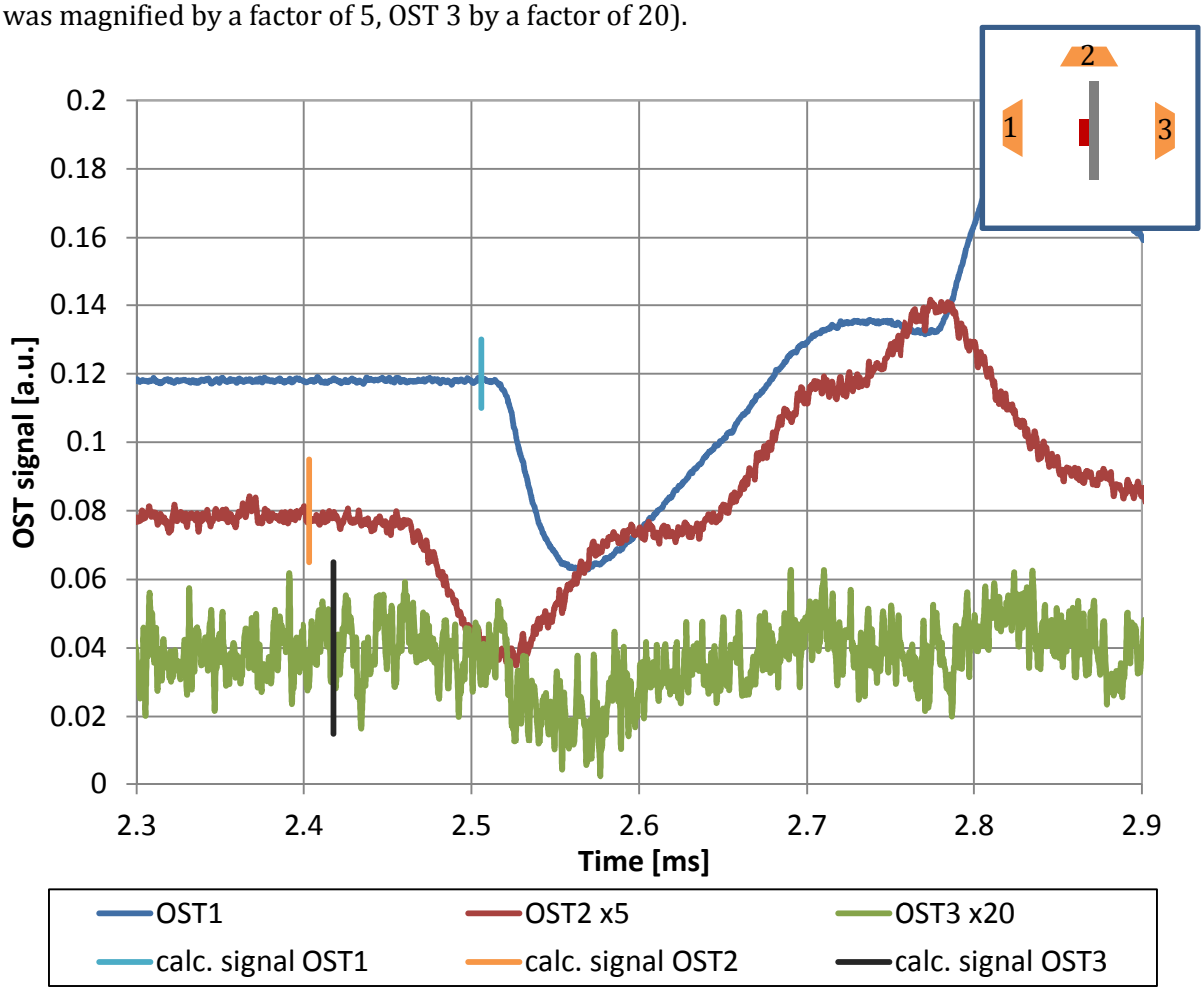

Figure 33: Zoom on the OST data from 2.3 to 2.9 ms after the beginning of the heating pulse. Pulse duration of 250 µs, heating power of 2.9 W and bath temperature of 1.95 K. The calculated signal was computed with a second sound velocity of 18.02 m/s. The signals were magnified for better display. The sketch in the upper right corner demonstrates the positions of the OSTs in respect to the heater location.

For all the OSTs one can see that the bend down of the measured values don't happen at the theoretical predicted point, but a few fractions of a millisecond later. OST 1 has the smallest delay between theory and measurement. OST 2 has a quite noticeable delay of about 50 µs and for OST 3 the signal is so weak, that it is hard to determine the onset of the signal bending down, but also at least 50 µs.

OST 1 is in direct sight of the heater so it is clear that the delay should be shortest. Various reasons are probably the origin of this setback. It can be caused by the heat capacity of the

heater which has to warm up to create a temperature gradient which is needed for heat transfer. This is quite important because the heating surface of the SMD resistor faces the niobium plate thus the heat has to be transported through the heater before it can trigger a second sound wave. The Kapitza resistance will also limit the amount of heat that is transported over solid liquid interface (see, Section 3.2.2). The sensitivity of the OST is also a limiting factor. OST 2 has a bit longer delay. The same delaying factors named for OST 1 matter in this case. The sensitivity aspect seems to be of even bigger importance as the heater does not face the OST directly (compare with second sound wave simulation, Figure 22) thus the temperature rise is not as big. An additional aspect seems to be the copper wires on the heater, which are attached on the side of the heater pointing towards OST 2. These wires are soldered to the heater which guarantees good thermal contact. The high thermal conductivity of the copper will cool the heater so it will take longer to heat up the heater on this side. The soldering patches are also not coated by the resistive layer so the distance from OST to the heater body is probably shorter than the distance between the OST and the heat source (resistive layer). So the result of this measurement does not give the information weather faster signal propagation occurs in the niobium, it only states that this effect has a smaller influence than the named delay mechanisms if it has any at all. OST 3 receives only a very weak signal, which is also delayed. In order to avoid electrical shortcuts a thin insulation layer was glued between the heater and the niobium plate. These interfaces (heater - glue - insulation material - glue - niobium) can cause the delay as well as the Kapitza resistance. For this OST signal the detection threshold of the OST has the biggest influence as it is already hard to detect the arrival of the signal. This OST was put there not to detect fast signal propagation, but to prove that at least some heat was transported through the niobium plate. This OST signal proves exactly that. The second sound wave moving around the niobium plate would need much longer than the observed signal. (The second sound signal, which travels around the plate is also detectable. It gives a quite strong signal on this OST, but takes about the double time to reach the sensor.)

4.2.2.3 Amplitude dependency

As the theory (Section 3.2.3.3) suggests, one should be able to find a linear rise or fall in the second sound velocity for changing heating powers. For this measurement the heater on the niobium plate and the OST in direct line of sight was used, because it gave the clearest signals. The measurements were done at six different temperatures. The signal generator, which was used for the heating pulses, was able to deliver a voltage of up to 10 V. For the used 15 mm^2 big SMD heater of 68 Ω resistance, this corresponds to a maximum heat flux of 9.8 W/cm^2. Figure 34 shows the different measured second sound velocities. As expected they show different

values for different temperatures. For this heating range v_2 is constant over all heat fluxes within the accuracy of the measurement.

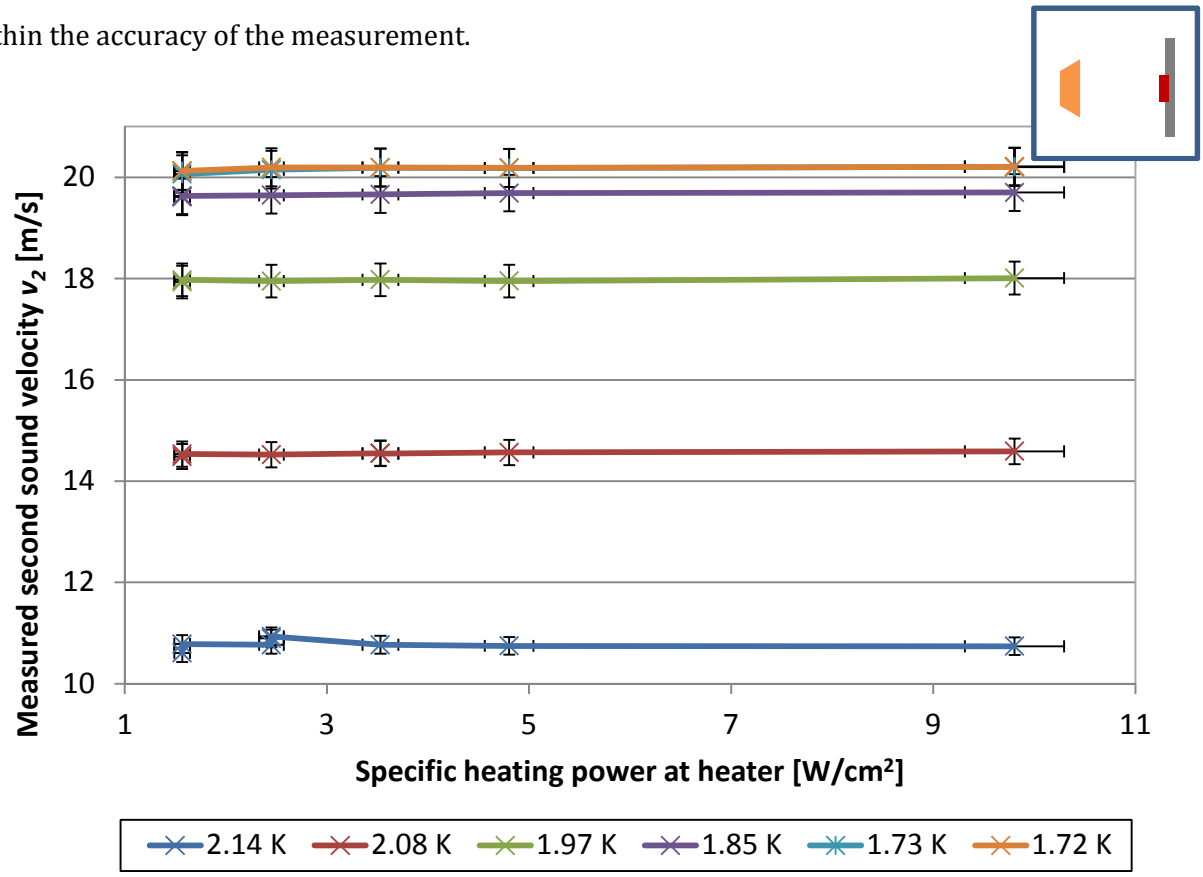

Figure 34: Second sound velocities vs. the applied specific heating power.

In superconducting cavities the heating power is much higher, so it is possible that the amplitude dependence can influence the result, but in this setup the effect is too small to be detected.

4.2.3 Three OSTs in a row

As the heating power was probably not sufficient to detect the amplitude dependence in the niobium plate experiment, a new setup was build. Besides the higher heating power of up to 80 W/cm^2 the experiment was also conducted in a bigger cryostat with a more precise pressure regulation. Better pressure regulation corresponds to better temperature stability of the bath (less than 0.02 mbar fluctuations with superfluid bath). Two heaters were mounted in the setup; a SMD heater for DC heating pulses and a RF heater. The DC heater had two cables sending the heating pulse and two cables to measure the voltage drop over the heater connected to it. The RF heater broke early in the experiment and therefore could not be used (see Appendix 8.3.1). As the heat flux is the relevant variable for the amplitude dependence this influence should become smaller with increasing distance from the heater in a three dimensional geometry. In order to detect this effect the setup included three OSTs behind each other. The

distance between the heater and the first OST as well as one OST to the next one was always chosen in the range of 5 cm.

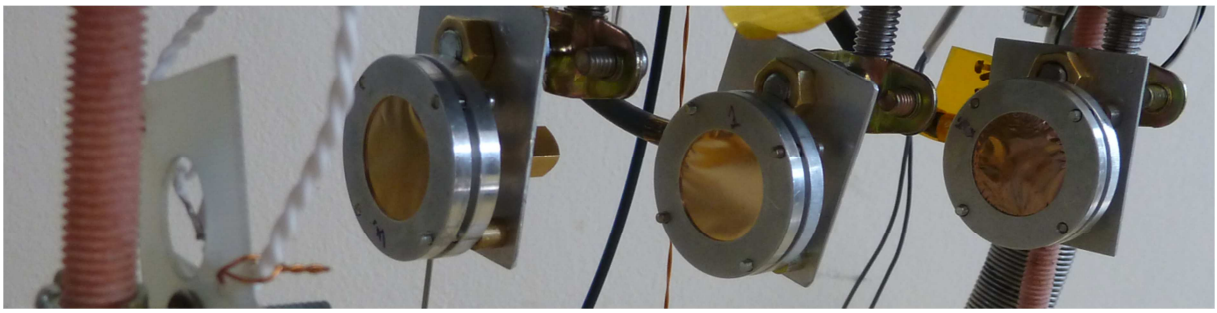

Figure 35: Photo of the measurement setup with three OSTs in a row. On the left side the heater is connected, a part of it can be seen through the hole in the fiberglass mounting plate.

4.2.3.1 Measurement

The second sound velocity was measured with the DC heater for 10 temperatures and heating powers between 1.6 W/cm^2 and 80 W/cm^2. The measured curve is shown in Figure 36 and consists of 276 data points.

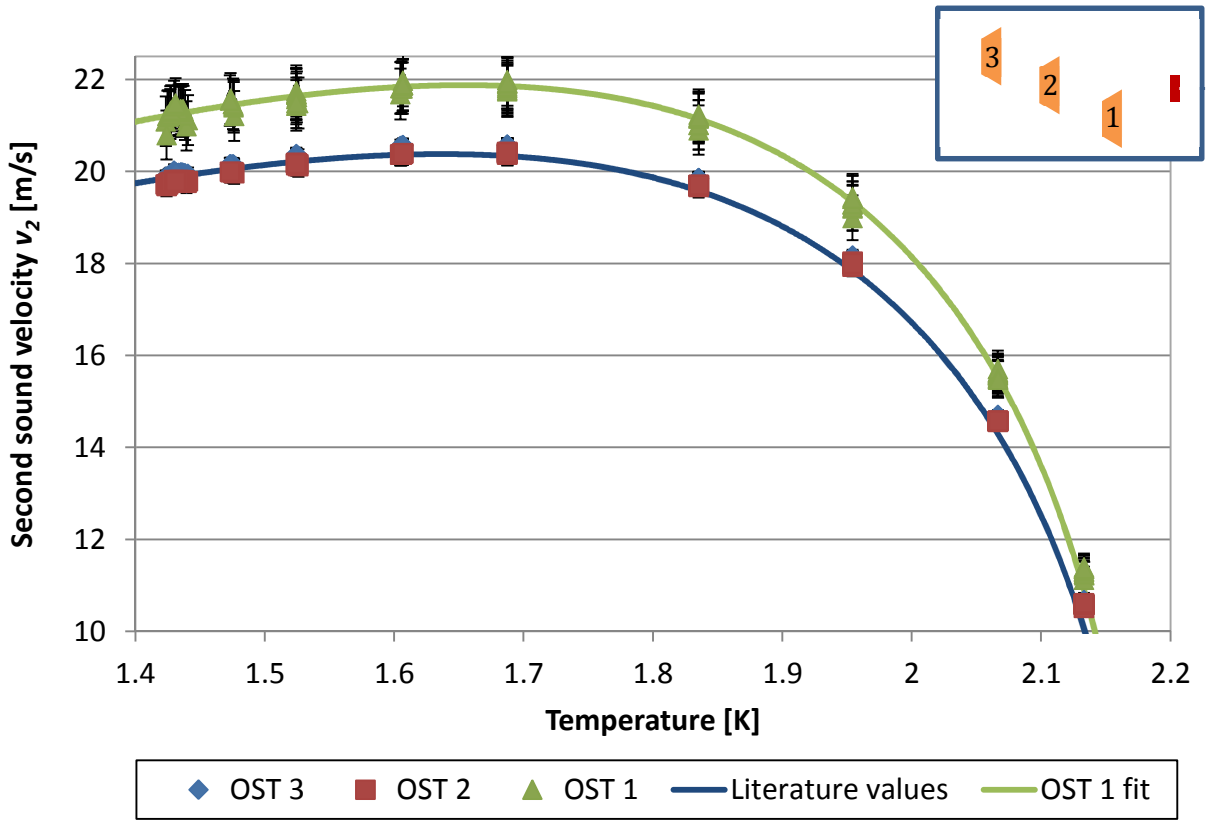

Figure 36: Measured values for the second sound velocities in the three OST experiment.

The graph shows the speed of second sound vs. the temperature of the helium bath. The dark blue line represents a fit of literature values [11]. One can see that the measured second sound velocities for OST 2 and OST 3 match the literature quite well. Striking is the faster signal

measured at OST 1. It is significantly higher than the literature values at all temperatures. Close to the lambda temperature the difference is smallest and increases towards lower temperatures. To be able to draw further information out of this the difference between the measured values and the literature values for the second sound velocities Δv_2 is plotted in Figure 37.

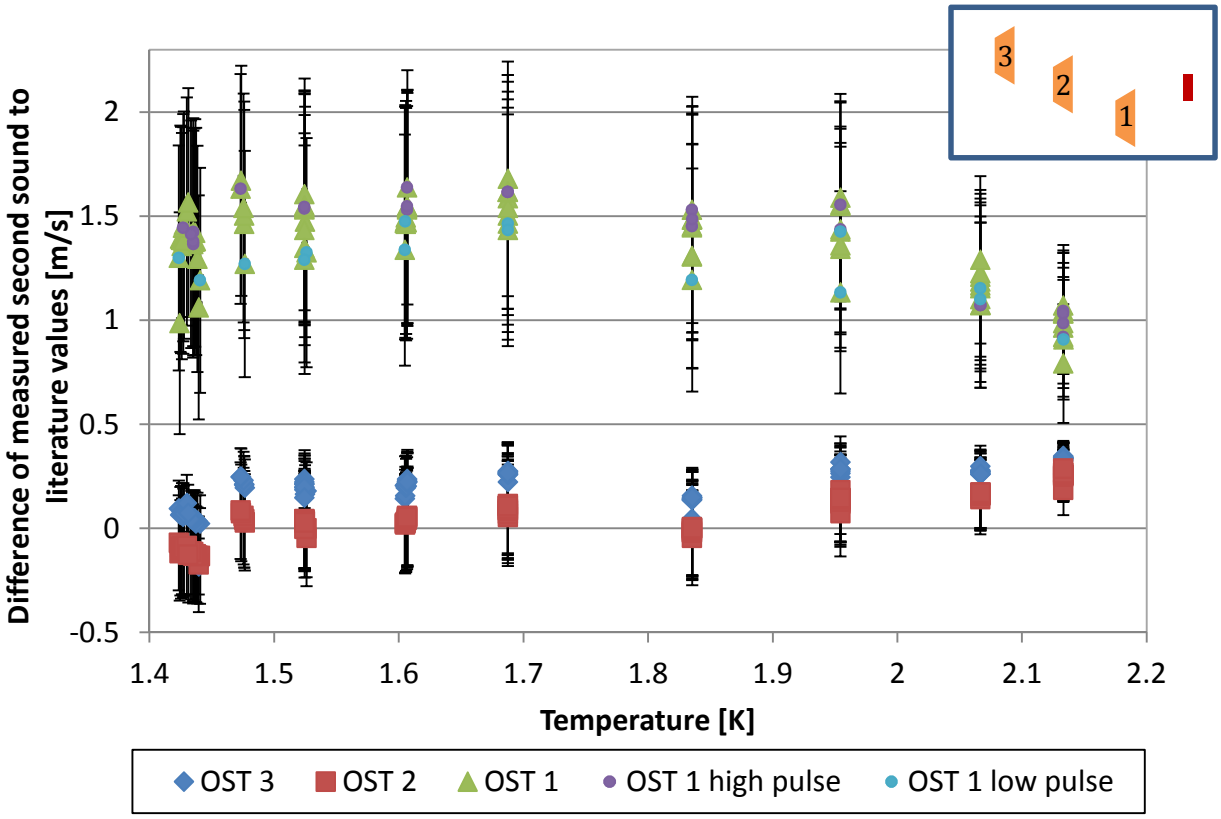

Figure 37: Difference between the measured second sound velocity and the literature for the three OST experiment, heating powers ranged from 1.58 to 78.52 W/cm².

The graph shows clearly the fast propagation for OST 1. From the amplitude dependence we would expect the closest OST, OST 1, to show the highest second sound velocity, but even more clues speak against this theory as the main reason for this effect. First the signal is faster for all measured temperatures. The amplitude dependence predicts only a faster propagation for temperatures between 0.9 and 1.88 K. Below and above these thresholds a slower propagation is expected. Second the OST 1 should have the most extreme variation from the literature values, followed by OST 2 and then OST 3. For all measurements this is not the case. OST 3 shows always faster signals than OST 2. For this argument one has to note that this tendency could also be explained by systematic errors, as the calculated errors of these OSTs nearly always overlap. Third the deviation should be linearly dependent on the applied heat flux. As described before various heat fluxes were applied, varying a factor of up to 50. To illustrate this, the highest and the lowest applied heat fluxes were marked for OST 1. Except for the measurements at 2.07 K, always the high heat fluxes led to faster signal propagation. To investigate this even further Figure 38 plots the results from OST 1 over the applied heat fluxes.

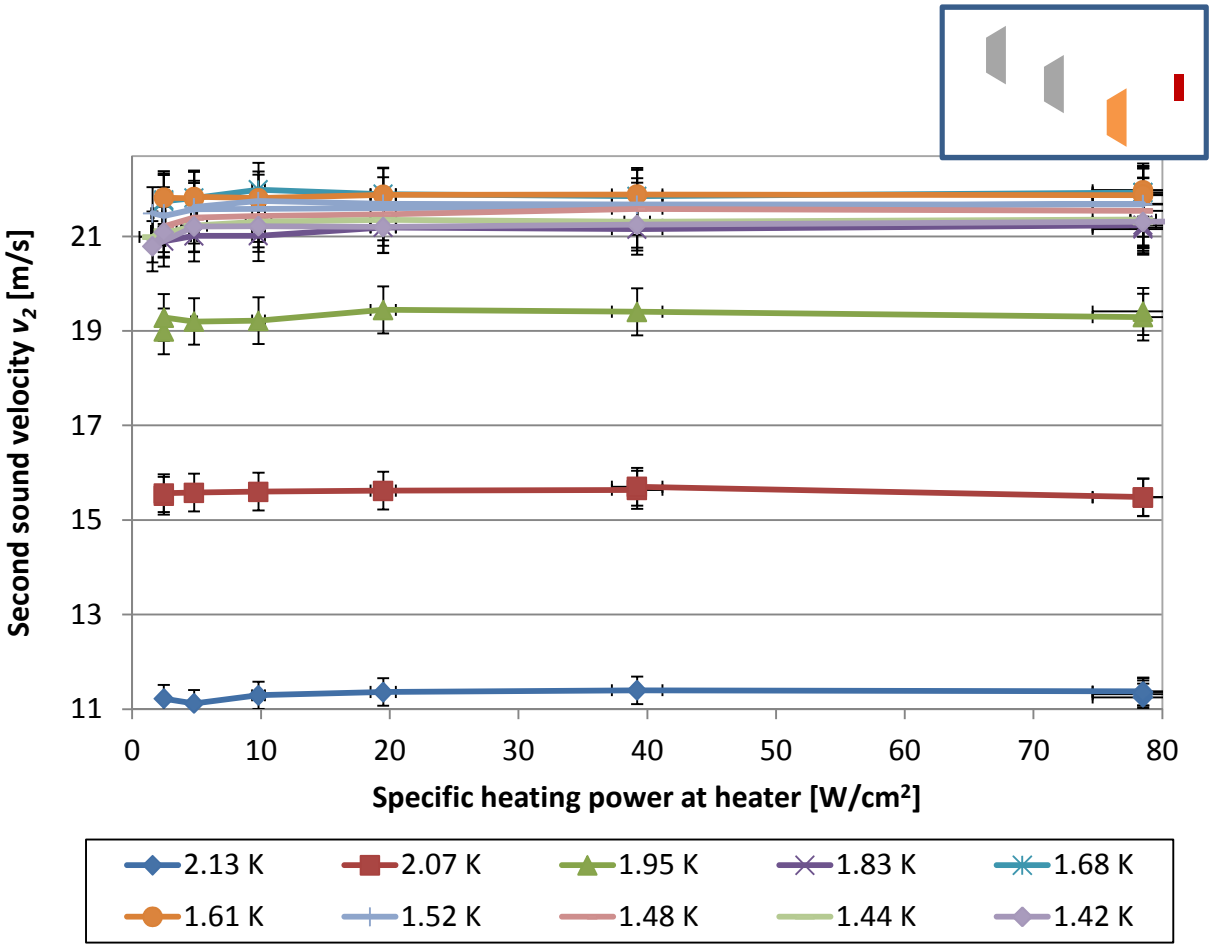

Figure 38: The measured second sound velocities in relation to the applied heat flux for OST 1 in the three OST experiment.

With slight variations at small heating powers the second sound velocities seem to be quite constant over the whole heating range. To be able to evaluate this in more detail Figure 39 gives a detailed view for the measurements at lower temperatures. The error bars were left out for better display.

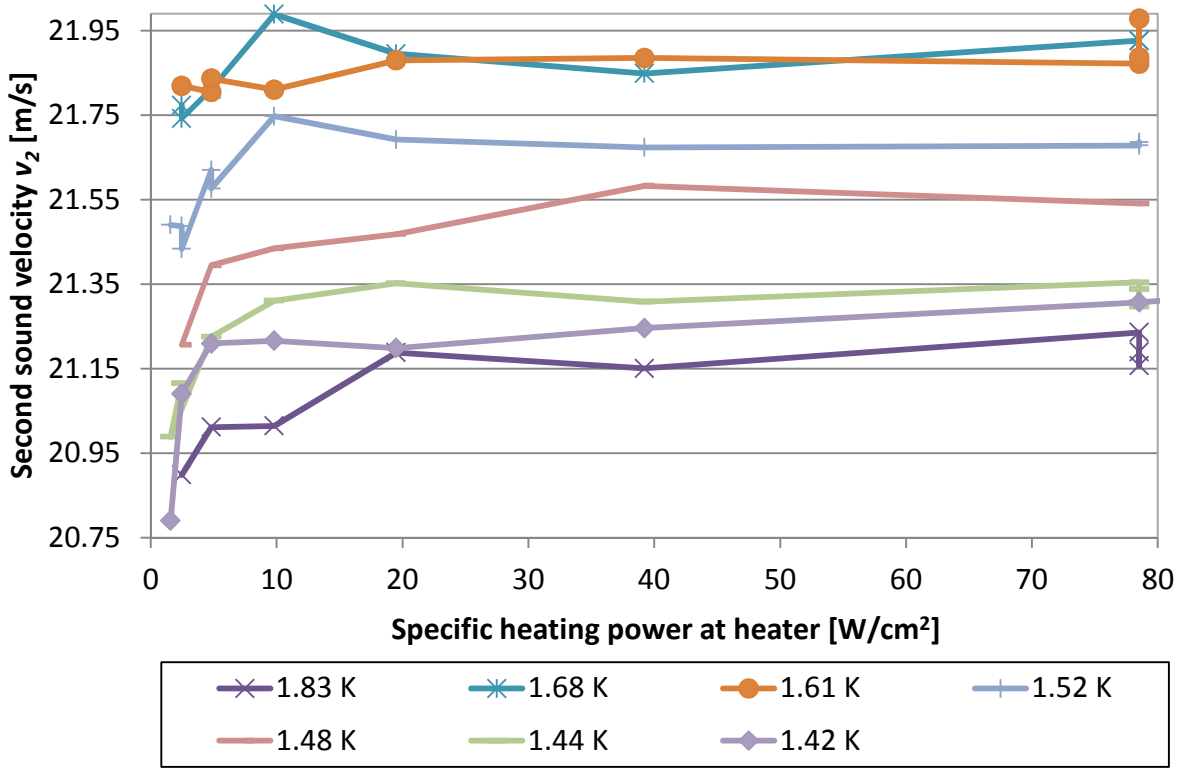

Figure 39: Detailed view of the measured second sound velocities for the measurements above 20 m/s.

The curves have similar shapes especially if their error bars are taken into consideration. This is shown for the temperatures 1.42 and 1.68 K in Figure 40. The theory for the amplitude dependence describes a linear dependence on the change in second sound velocity with heat flux. This could explain the slight rise in the high heat flux region ($\dot{q} > 30$ W/cm^2) of the graph, but does not cover the steep rise on the low heat flux side of the graph.

The most likely interpretation for this is related to the data analysis. One has to keep in mind that higher heat fluxes give much clearer signals on an OST. The low power side of the graph were the lowest signals detected on the OSTs. To determine the speed of second sound the onset of a signal had to be defined. As the pulse itself was not so big, part of the pulse was certainly within the noise level of the measurement. This led to the problem that the onset was probably detected to late, so the time which the signal took for a given distance was shorter. This is equivalent to a lower measured velocity. To avoid this problem, measurements with higher heating powers seemed sensible.

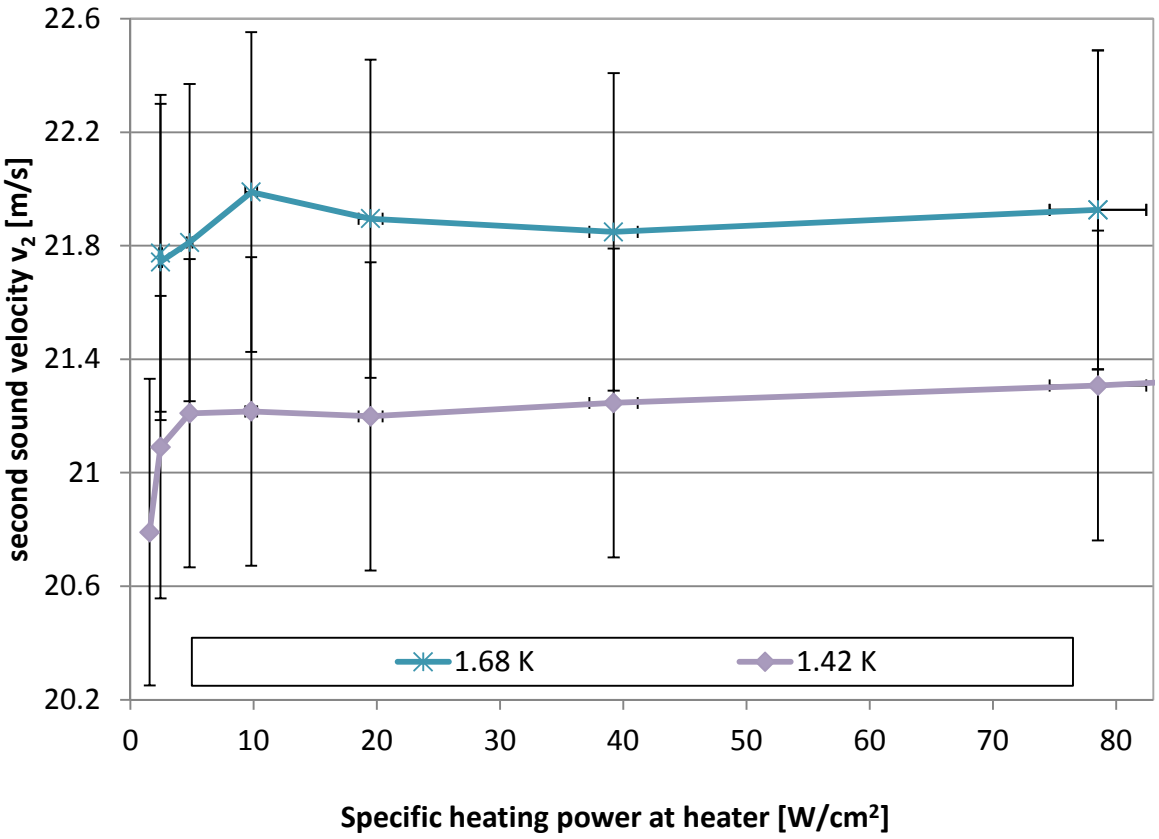

Figure 40: Measured second sound velocities at 1.42 K and 1.68 K.

4.2.4 Combined experiment with three OSTs in a row

As the cryostat that could house the three OSTs in a row setup in a horizontal position was needed for cavity tests, the two tests were combined in one cryostat but measured at different times. This can be seen in Figure 41. The 1.3 GHz niobium-coated copper cavity is in the middle of the cryostat insert and at the bottom one can see the three OSTs. Figure 42 shows for the same setup the view along the cavities. The black DC Heater with its four white cables can be seen as well as the new RF Heater with its black coaxial cable. The RF heater was produced by the company “Bourns”. It is specified for heat loads of up to 100 *W* at room temperature. During the tests in liquid helium a power of up to 350 W was applied, the heater did not show any signs of damage. It is important to note that the OST positions were switched in their order to avoid specific effects of individual sensors.

Figure 41: Photo of combined experiment setup.

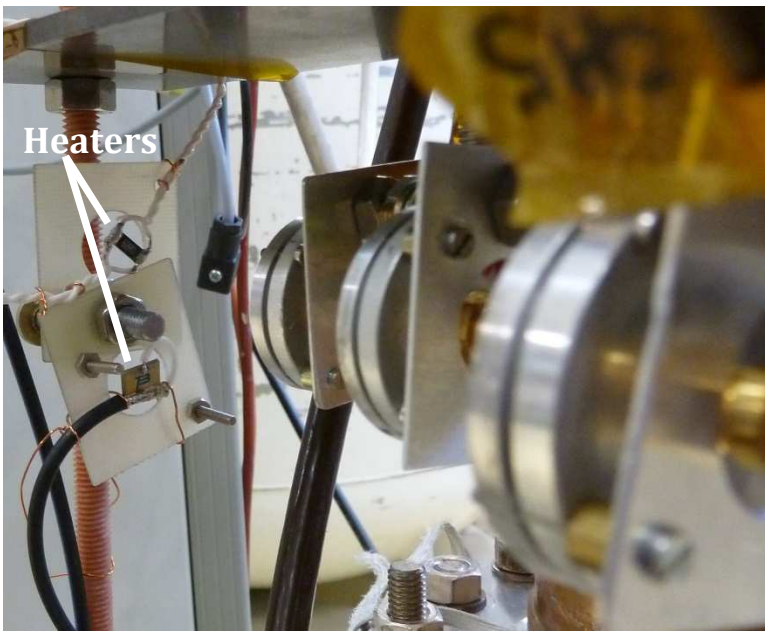

Figure 42: Photo looking along the three OSTs on the heaters (DC top, RF bottom).

4.2.4.1 MEASUREMENT

For this measurement about 500 OST responses on heating pulses have been evaluated. The data was taken at 5 temperatures. The temperatures were chosen to be close to the lambda temperature (2.165 K), close to the zero transition of the previously mentioned amplitude dependence (1.89 K), close to 1.8 K (1.77 K) as it is a very common cavity testing temperature and at temperatures below this value, as the amplitude dependence strongly increases for lower temperatures. The lowest obtainable temperature with this setup was 1.45 K. The applied heating power ranged between 1 and 350 W, which corresponds to a heat flux between 2 and 700 W/cm^2.

The measured results give a similar curve as the previous measurements, see Figure 43. The OST closest to the heater (OST 1) always had faster signals than the second sound literature values, OST 2 always had the lowest measured value and the OST which was furthest away (OST 3) gave intermediate results. In this measurement the values of OST 3 were not much closer to the OST 2 values as in the previous measurement, but well in between the values of the other two OSTs. To get more insight again the difference of the measured second sound velocity to the literature values is plotted in Figure 44. The highest signal speed was observed at 1.67 K for all three OSTs and decreases for higher and lower temperatures. Close to the lambda temperature the signals of OST 2 and OST 3 are all lower than the literature value.

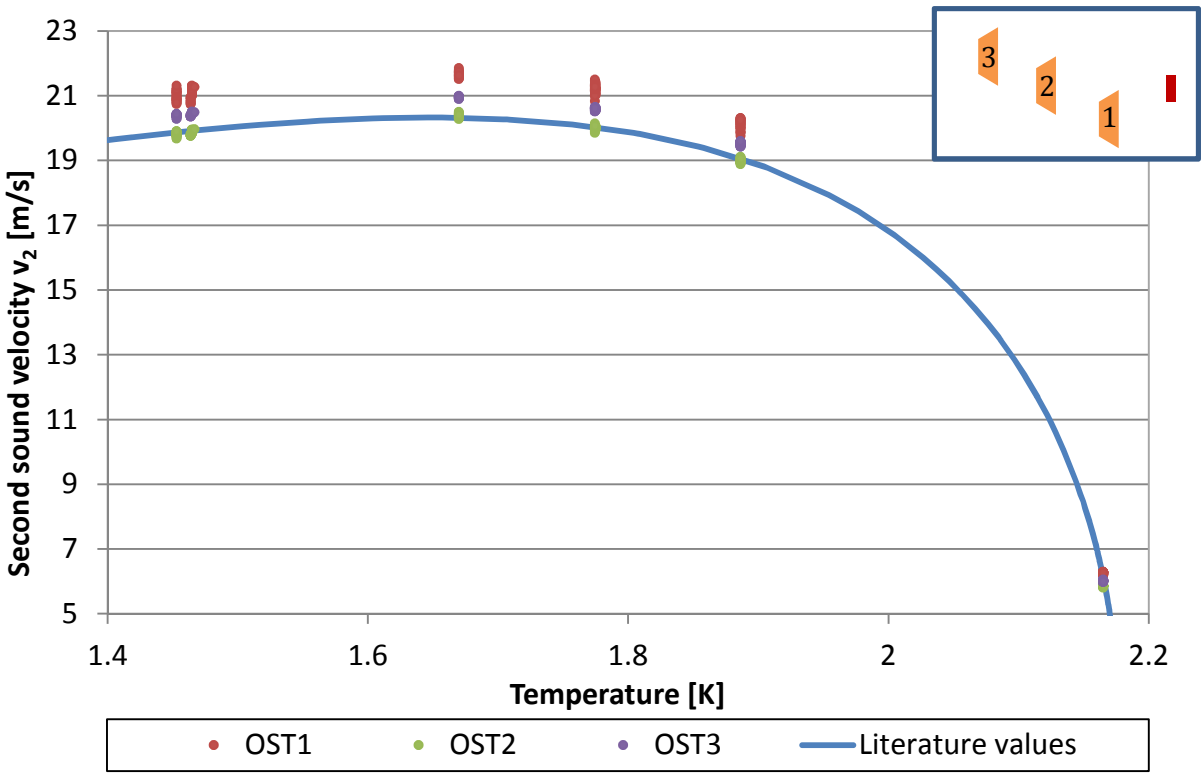

Figure 43: Results of the combined experiment, heating powers ranged from 2 to 700 W/cm^2.

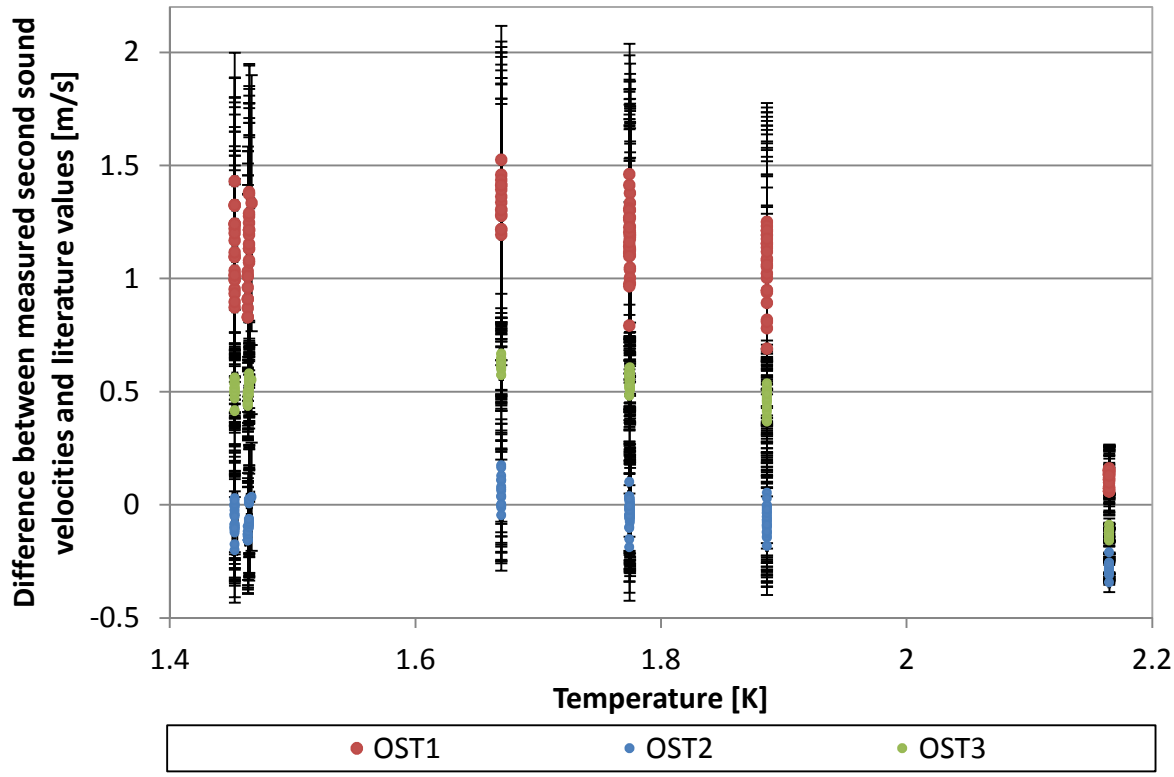

Figure 44: Difference between the measured second sound velocity and the literature for the combined experiment vs. the temperatures of measurement. Heating powers ranged from 2 to 700 W/cm^2.

The measured values spread over nearly 0.5 m/s for OST 1, OST 2 has a smaller spread and for OST 3 the values lie closest together. This can be also seen in the estimation for the uncertainty of the measurement and it is obvious that absolute errors in the measurement of the distance heater to OST and for the time of flight result in smaller relative errors for longer distances and times of flight. To evaluate this quite wide spread of data the deviation between $v_{2,0}$ and the measured value is plotted against the applied heating power for OST 1 in Figure 45.

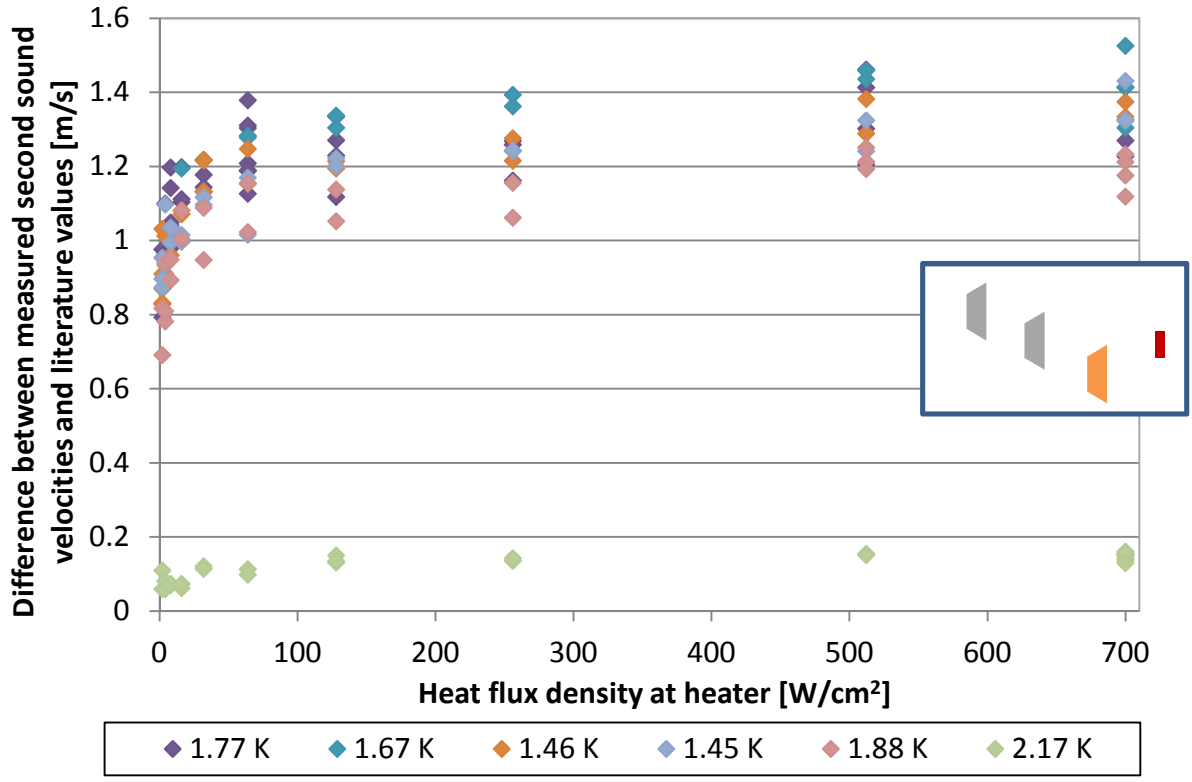

Figure 45: Difference between the measured second sound velocity and the literature for the combined experiment over the applied heating powers for OST 1.

One can see in Figure 45 that the wide spread of measurement points in Figure 44 is clearly related to the different heating powers that were applied. The devolution of the second sound values over the applied heat flux is similar as in the previous measurement with less heating power. At lower heating powers the deviation of v_2 from the literature values is smallest, then rises quickly to higher values and seems to develop linear with a slight rise of v_2 with rising heating powers. This applies to all temperatures except for 2.17 K. The measured values for this temperature are only slightly faster than the literature values and do not change a lot over the heating range.

These measurements clearly show that the amplitude dependence can't explain the change of the second sound velocity. The amplitude dependence suggests no change for v_2 at 1.88 K and a positive one for lower temperatures. But at 1.88 K the change of the second sound velocity is

about the same as for lower temperatures. With little variance v_2 is higher than expected from previous known theories. Several indications give rise to the assumption that other than the discussed effects alter the second sound velocity.

As most of the measurements give similar results except for the measurement close to the lambda temperature an important question is to find an explanation for this different behaviour. The amplitude dependence could give part of the explanation. At 2.17 K the amplitude dependence factor τ_2 is highly negative and thus slows down the second sound wave with higher heating powers. The second sound wave will flatten out and on the back side of the heating pulse a temperature step should be observable. This could lead to a delayed detection of the second sound pulse. As the theory predicts a delayed signal for these conditions but all measurements were significantly faster than the literature value of the second sound except for the measurement close to the lambda temperature is just not as fast as the others, one conclusion can be drawn. It is likely that all measurements were influenced by an accelerating effect other than the amplitude dependence but it still can be observed, in this case as a decelerating component.

4.3 CEA – SACLAY TEST FACILITY

Although high attention was paid to avoid systematic errors, it is hard to be sure that they did not influence the given results too much. One possibility to cross check is to reproduce these results with a different setup. This is one of the reasons why a testing series was done at CEA Saclay. The other reason was to use devices that were capable to deliver higher heating power.

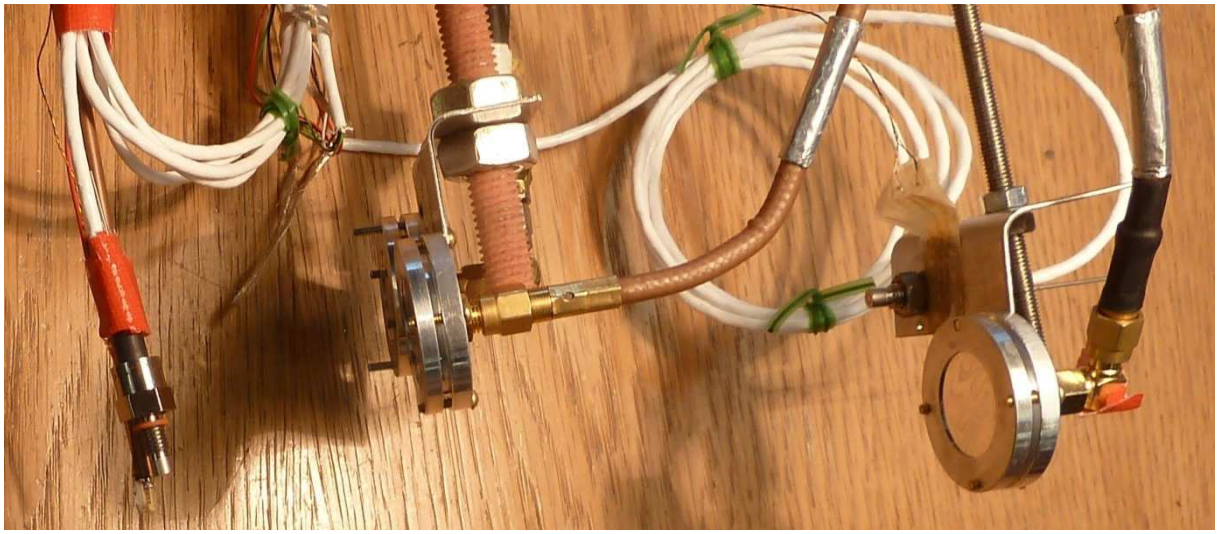

Figure 46: Measurement setup used at CEA Saclay for second sound experiments. The heater is located on the left, the OSTs are fixed in two distances from it.

Instead of the OSTs produced at CERN, OSTs from Cornell University were used. As can be seen in Figure 46 only two OSTs were mounted in a row. The smaller cryostat did not allow more OSTs behind each other. Besides the OSTs also two Cernox™ bare chip sensors were used. Unfortunately they weren't sensitive enough to give any signal. The heat pulse was created by a high power pulsed RF amplifier, capable of pulses of up to 1 kW power for a duration of up to 1 ms. The detailed data analysis for this experiment still has to be done, but preliminary results affirm previous measurements. For all experiments the measured second sound velocity was higher than the literature values.

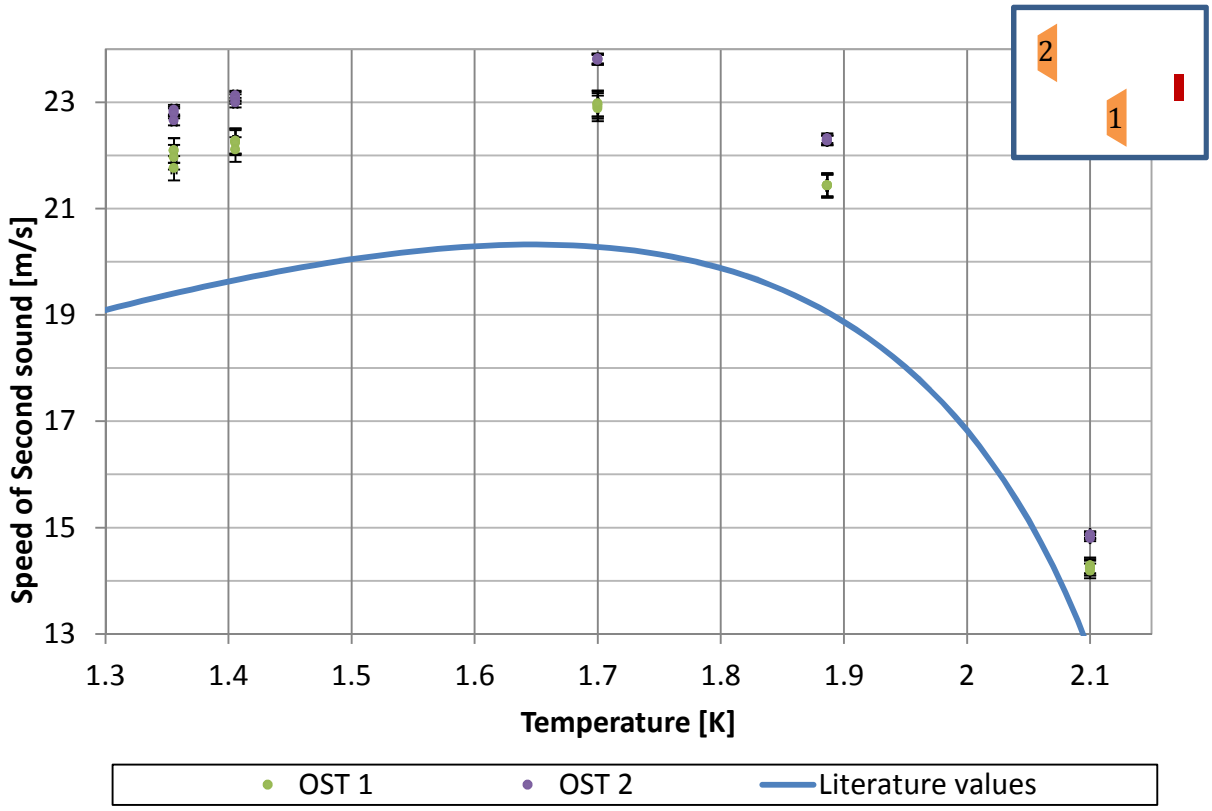

Figure 47: Preliminary results of OST measurements at CEA Saclay.

4.4 FURTHER TESTS AT THE CENTRAL CRYOGENIC LABORATORY OF CERN

4.4.1 Influence of the heat pulse on the OST signal

As described in the theory chapter, second sound pulses vary a lot dependent on the confinement of the helium. The two extreme cases are the one-dimensional geometry, which can be realized within a tube with a constant diameter. The three dimensional geometry is characterized by no special space constriction. To test the theory the parameters of the heating pulses were varied and the OST response was evaluated. Besides the strength of the signal no significant difference between the signals of the three OSTs could be seen, so the following graphs show only OST 1, which had the clearest signal. The temperature of the helium bath was always 1.89 K to avoid shape derivations by the amplitude dependence of second sound, compare Section 3.2.3.3.

In Figure 48 two measurements of the response of the OST on rectangular heating pulses are displayed. The OST signals and the heating pulses were measured. To make the edges of the heating pulses more visible, the data points were joined by dotted lines. One can see the little overshoot on the leading edge of the pulse and that the pulse does not fall exactly to zero after going down, but applies a little negative voltage after the pulse for the same duration as the positive pulse. These are features of the used pulse generator. They are not regarded as a problem, but have to be kept in mind. The measured data points for the OST are not connected which allows to see both the resolution of the measurement as well as the two measured signals, even when they have the same shape.

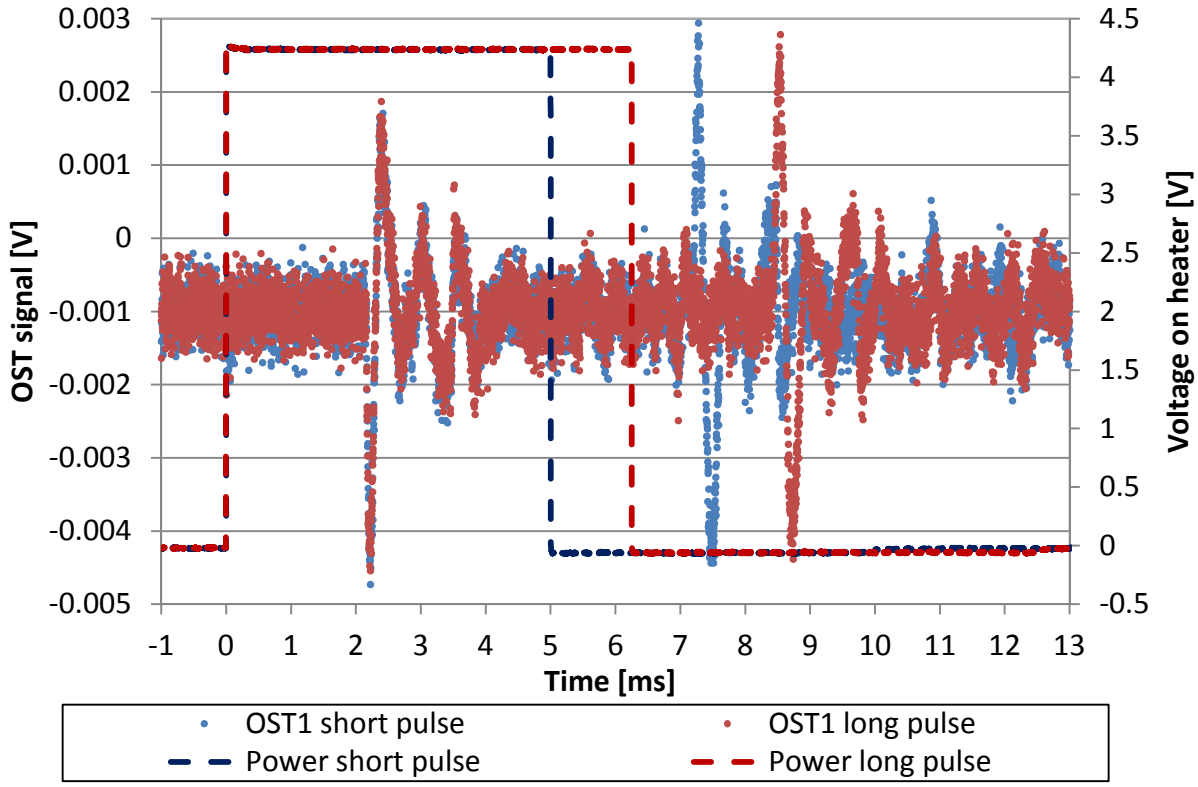

Figure 48: Data of two measurements of second sound, all parameters exept the pulse length were kept constant.

The leading edges of the heating pulse are set to be at the same time. A bit more than two milliseconds afterwards the second sound wave reaches the OST and gives a characteristic oscillating signal. This is reproducible as can be seen from the two OST signals that have exactly the same shape. Although the heating is still on, the oscillation decays and vanishes in the noise level. Only when the heating is switched off, it takes again about two milliseconds to receive the corresponding signal. Interestingly, this time the signal first goes up and not down.

This behaviour can be explained by the behaviour of the OST membrane and the second sound propagation in the three dimensional case. The theory of second sound propagation in the three dimensional case already suggests that the temperature excursion is dependent on the change of heating (see Section 3.2.3.2). This is the reason why only the changes in heating can be seen. Although the oscillation of the membrane is not fully understood, the direction of the first excursion can be explained. If the second sound has a higher temperature than the bath temperature, it has a higher content in normal fluid component and a lower content in superfluid component. When this wave reaches the membrane, the superfluid fluid component flows from the inside of the OST through the membrane trying to equalize the ratio difference. In the same manor the normal fluid component tries to flow into the OST, but is blocked as it can't permeate the small holes in the membrane. Both movements press the membrane closer to the backplane and thus increase the capacitance of the sensor. The result is a measurable voltage

drop. If the heating is switched off, the temperature of the wave is lower than the bath temperature and the exact opposite as described above happens, so the measured voltage increases.

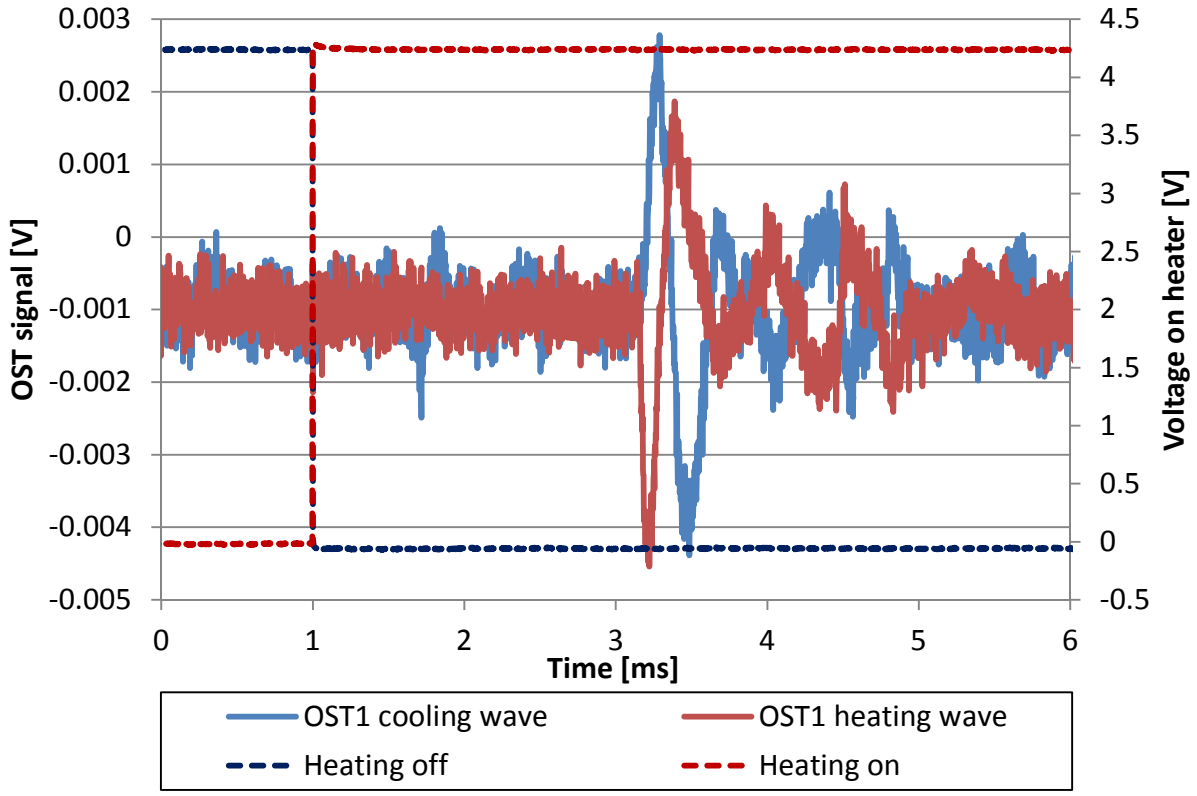

Figure 49: Measured OST behaviour for a rising and falling edge of a heat pulse. At a time of 1 ms the heater is swiched on (red dotted line), or swiched off (blue dotted line)

This is also shown in Figure 49. Here the data from the "long pulse" in Figure 48 is shown again, but the rising and falling edge of the heat pulse with the corresponding OST responses were moved in time. Both edges are now on the one millisecond mark. One can see the OST signals look as if they were mirrored. The response starts at the same time and the first peak has the same shape. The second peak is shaped a bit differently, but afterwards the signals are again surprisingly similar.

One can only speculate about the reasons for the different shapes of the second peak. Quite likely is the theory, that the driving temperature difference of the cooling curve is bigger and therefore the pulse is larger. The heating pulse elevates the temperature at the OST a bit ($T = T_0 + \theta$). As the cooling curve has a lower temperature than the bath temperature ($T = T_0 - \theta$), the temperature difference is bigger ($\Delta T = 2\theta$). This could explain the little bigger first and second peak of the cooling wave response.

Until now only a second sound shock wave with a step in heating power was investigated. This had the advantage that no information was overlapped by the oscillating behaviour of the OST and thus wasn't altered. The disadvantage was that only little information about the temperature of the helium could be obtained. In Figure 50 a sinus shaped voltage pulse ($U \propto \sin(t)$) of one millisecond length was send to a resistive heater. The heat generation is shown in red in the figure, it is dependent on the square of the voltage ($P \propto \sin(t)^2$). As the temperature change is dependent on the change of heating ($\theta \propto \sin(2t)$) and the OST response is reciprocal to the temperature, the inversed slope of the heating power is shown in purple.

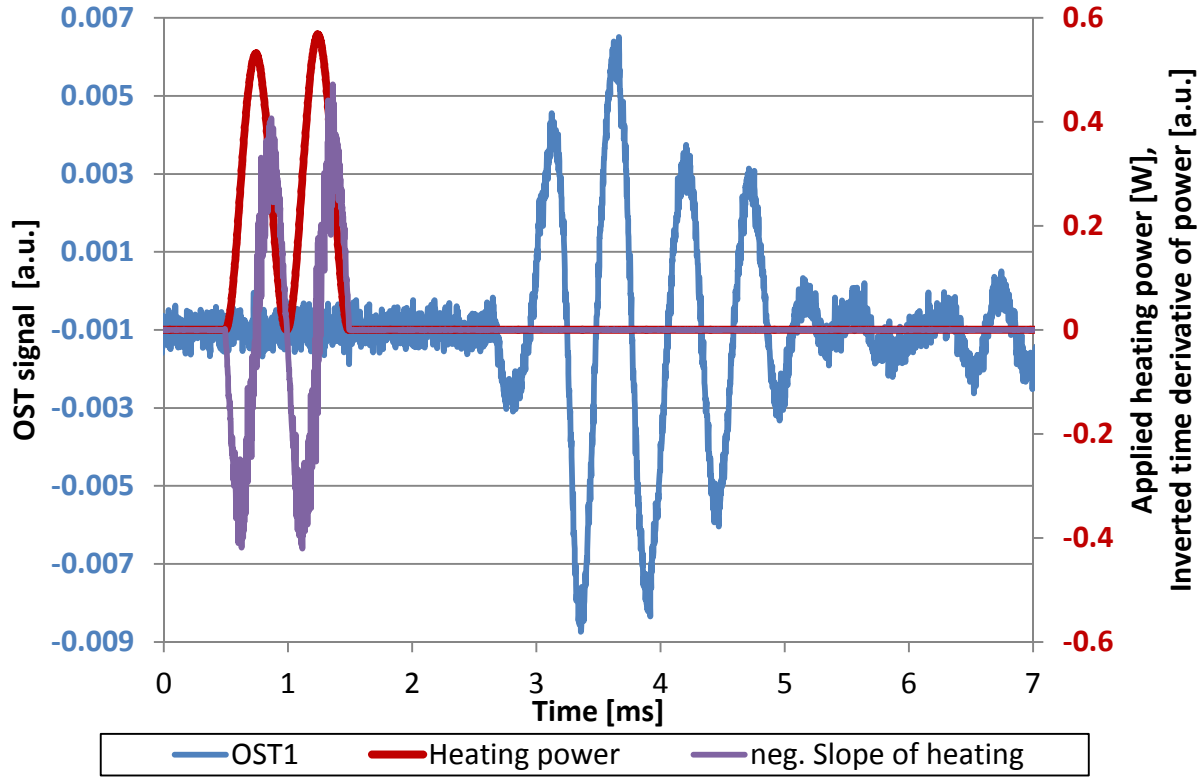

Figure 50: OST response on a sinusoidal voltage pulse on a resistive heater with a pulse length of one period.

The second sound wave again arrives a bit more than two milliseconds after the heating started. This time the OST response is not the same as for the shock pulses. The first up and down peaks are not the largest, the oscillating seems to have a uniform frequency and decays after four periods quite fast. The frequency of the heating is exactly twice the heating frequency, which proves the theory of the temperature distribution in three dimensional second sound. Unfortunately the other features such as the oscillations for four periods and their decay in the OST response can't be explained up to now. Thus further investigations are required.

4.4.2 Measurements in the glass cryostat

With the investigation of the pulse shape a new point of view on the subject is given, not only the time of flight of the second sound is looked at but also what kind of temperature wave is created and how the OST does respond to that. To reveal more of this information, a test in a glass cryostat was prepared. The two main questions that were tried to be answered are:

1. How does the OST membrane behave in superfluid helium?
2. Can one see boiling effects in the helium?

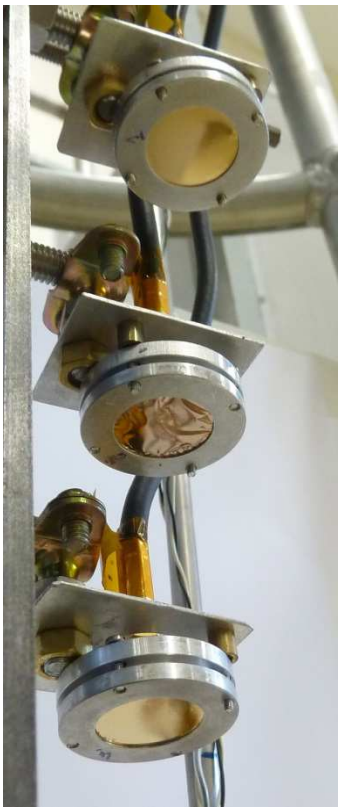

Figure 53: Photo of the three OST membranes in the test setup at room temperature.

Figure 52: Test setup for test in the glass cryostat.

Figure 51: Setup in the glass cryostat. At the top one can slightly see the helium level and much lower the nitrogen level.

The importance of these questions arose from the investigation of the OST signals. As boiling can store energy in the phase transition it can influence an OST signal quite strongly. The oscillation of a membrane tightly attached to a backplane is different to a loose membrane and thus this information is needed. In the previous measurements the OSTs were selected according how well they seemed to work. The “best” OSTs all had membranes which looked quite different at room temperature (see Figure 53). One was absolutely flat, one was heavily wrinkled and the last one had a single dent in it (bottom to top). Their performance did not change noticeably when the position of the OSTs was switched. Previous to this experiment an OST membrane was

cooled down in liquid nitrogen to check its behaviour. In previous experiments some heat pulses were accompanied by easily audible noise and first sound could be detected on the OST traces. Boiling effects were the most likely explanation for this behaviour, so this should be investigated.

In Figure 52 one can see the test setup. The glass cryostat was not wide enough to house the three OSTs in a horizontal position. In this case the static height of the liquid column could have some influence on the signal. At the bottom one can see the heaters. The black heater with the four white cables for DC pulses and the yellowish heater with the one black coaxial cable for the high power RF pulses. This setup was placed in the glass cryostat. Most of the glass surface of the cryostat was mirrored to minimize the incoming heat load due to radiation, but two windows were left free to allow sight on the experiment. The cryostat consisted of the inner helium vessel, surrounded by a liquid nitrogen shield. These two "layers" of the cryostat had vacuum insulated parts between them and to the outside. One can see the whole setup in Figure 51. The test setup is placed in the cryostat, which is then filled with helium. The helium level can be seen quite close to the top of the photo. Due to the small density difference between the liquid and the gaseous helium, this boundary is quite hard to see, but the refraction can be seen on the black cables. On the height of the second OST the liquid nitrogen level is quite easy to spot. The little bubbles in the nitrogen show it is in boiling condition.

4.4.2.1 Observations

When the OST membrane was cooled down in liquid nitrogen, it immediately curled up. This is not very surprising as gold and polymers have quite different thermal expansion coefficients. The gold coated side of the membrane was outside when the membrane curled, so this confirms that the polymer contracts more than the gold [55]. The membrane also was still easily bendable with tweezers, so a movement of the membrane at low temperatures seems to be no issue.

Figure 54: Photo of the RF heater in superfluid helium, no heating.

Figure 55: Photo of the RF heater in superfluid helium, heating of 350 W for 0.5 ms.

Except for the heavily wrinkled OST membrane, the membranes were absolutely flat in superfluid helium. Even the wrinkled one was nearly totally flat, only a little groove, which covered less than 5% of the surface, could be seen. One could not see a difference between the polarized and unpolarised membranes. As the membranes were clamped into the aluminium body of the OST at room temperature, the bigger contraction of the membrane in comparison to the aluminium body of the OST probably caused the membrane to flatten out.

For high heat fluxes, the boiling was again audible and also visible. A small vapour cloud formed very fast on the whole surface on the heater and then moved up and formed a spherical, milky-looking phase which rose a few millimetres and then disappeared. It was not clearly visible weather this phase consisted of one big bubble or many little bubbles. Figure 54 and Figure 55 show two photos of the RF heater in superfluid helium. One shows the heater without and the other one with applied power. The milky phase above the heater gives clear evidence of boiling. The photos were extracted from single frames of a video which was taken. The time between the two pictures was just 67 ms (two frames). Another 67 ms after the second picture the bubble was gone already. Signs of this boiling could be seen for heating powers above 44 W for heating durations of 3 ms, and above 233 W for 0.5 ms. The resistive part of the heater had a surface of 0.5 cm^2. For long heating durations (~5 ms) even sparks could be produced on the heater surface.

These results suggest that boiling effects will play an important role for quenching studies on SC cavities. One could also misinterpret a first sound wave as a second sound wave on an OST. As the first sound wave is about ten times faster than a second sound wave, this could be an explanation for "faster second sound" results.

4.5 CRYOGENIC TEST FACILITY SM18

In between the two main sites of CERN, Meyrin and Prévessin, one can find the cryogenic test facility SM18. It consists of three parts, the cryogenic systems which can deliver a cooling power of up to 6 kW at 4.5 K, the magnet and the cavity testing facilities. Here the crab cavity tests were done. They are described in the following.

Crab-cavity test

Crab cavities are devices to tilt the beam to get a higher interaction rate of particles in the interaction point of a circular collider, see the working principle in Figure 56. They are operated in a different electromagnetic mode than accelerating cavities. For the High Luminosity LHC upgrade these cavities are planned to be used. Up till now this type of cavities were only used for

Lepton colliders. To be able to use crab cavities in a hadron collider, prove of principal tests will be done at the SPS Accelerator at CERN in 2017 and 2018.

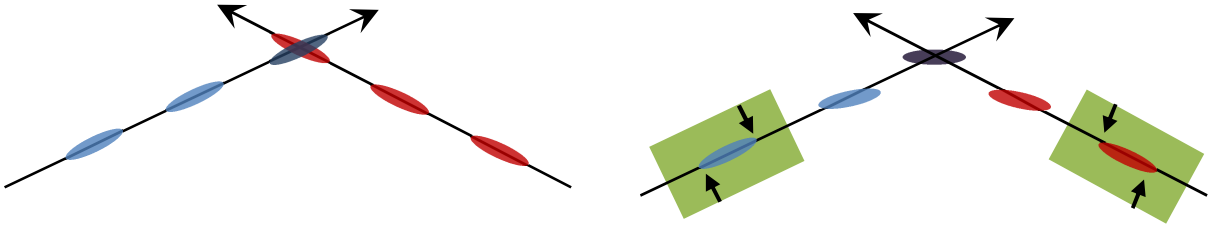

Collision of two particle beams without crab cavities. Only a part of the particle bunches can interact.	Collision of two particle beams with crab cavities. The whole particle bunches can interact.

Figure 56: Collision principle of bunched particle beams with and without crab cavities.

At the moment three different designs for this purpose are developed including the auxiliary equipment (RF-tuners, cryostats etc.). One of the designs was made by the University of Lancaster and was tested at CERN. This UK 4-Rod Cavity was made out of bulk niobium. It was assembled by electron beam welding the parts, which were made by bending sheet niobium and milling out of a niobium block, in Figure 58 and Figure 57 one can see the parts and the finished cavity.

Figure 57: Niobium parts of UK 4-Rod Cavity [21].

Figure 58: Photo of UK 4-Rod Cavity [20].

4.5.1.1 Instrumentation for tests

For the cold tests the cavity was equipped with 13 Allen-Bradley temperature sensors, which were glued to the surface and 7 OST Sensors to detect the quench spot during its performance test at cryogenic temperatures.

The decision how the sensors were placed (especially the temperature sensors) was based on the simulation of the electromagnetic field in the cavity, see Figure 59. The region of the high magnetic field was chosen because the magnetic field itself can lead to a quench of the cavity. The high electric field region was also monitored because this region was most likely to be heated by field emission, which also could lead to quenching. These thoughts led to a distribution of temperature sensors as shown in Figure 60.

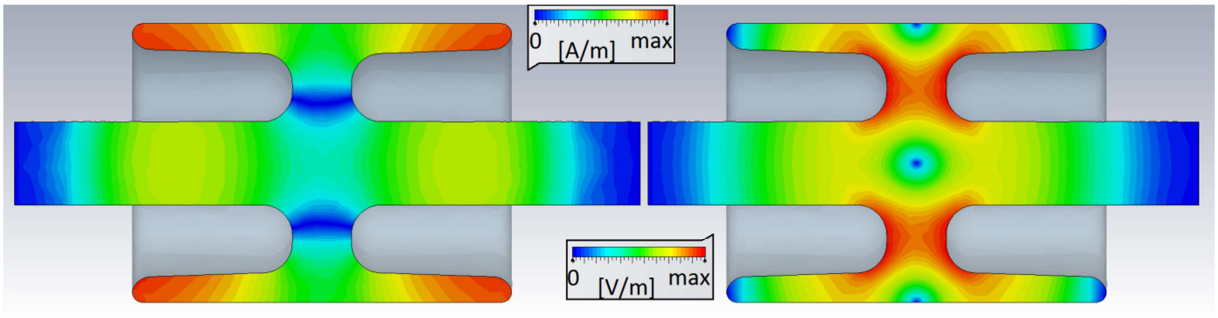

Figure 59: Simulation of the magnetic (left) and electric (right) field in the Crab Cavity, courtesy P. Kardasopoulos.

The cavity had to be mounted in a vertical position like shown in Figure 60 because the cryostat was not wide enough for a horizontal test. This led to the concern that gas bubbles could get trapped in the two bottom rods of the cavity, which then insulate the top of the rods. To evaluate this problem a test with an upside-down glass beaker was done in a glass cryostat. This experiment clearly showed that the beaker was full of gas during the cool down from 4.2 K, but as soon as the helium crossed the lambda transition the helium vapour was condensed within a few seconds.

Four OSTs were placed facing into the rods and the other three facing the rounded parts of the side of the cavity (see Figure 60). In this manner the quench spot cannot be localized by triangulation. For a triangulation process three OSTs have to be in direct line of sight to the quench spot. The difficult geometry of the cavity with the four rods made this practically impossible. Besides the space around the cavity, missing cabling made it impossible to have more OSTs around it. But even the knowledge about which OST receives the second sound signal first as well as the amplitude of the pulse can give information about the quench spot.

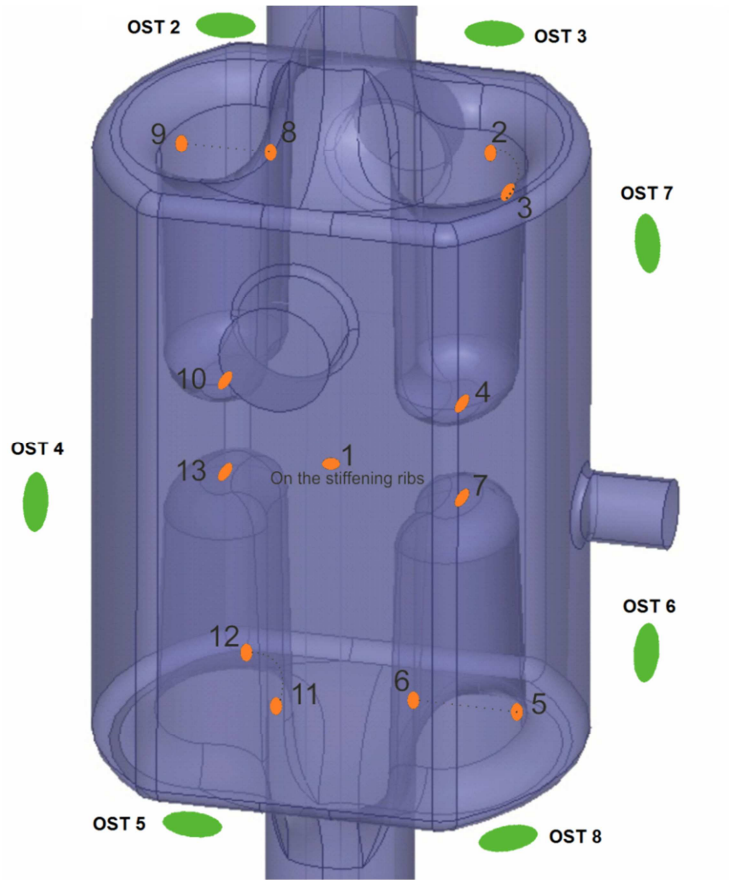

Figure 60: Position of Allen-Bradley Sensors (orange) and of the OSTs (green) on the UK 4-Rod crab cavity.

4.5.1.2 OST Measurement

The performance of the crab cavity was limited by a global quench. If the stored energy in the cavity was raised above 6 J, the cavity quenched globally. The process was monitored by the OSTs and is plotted in Figure 61.

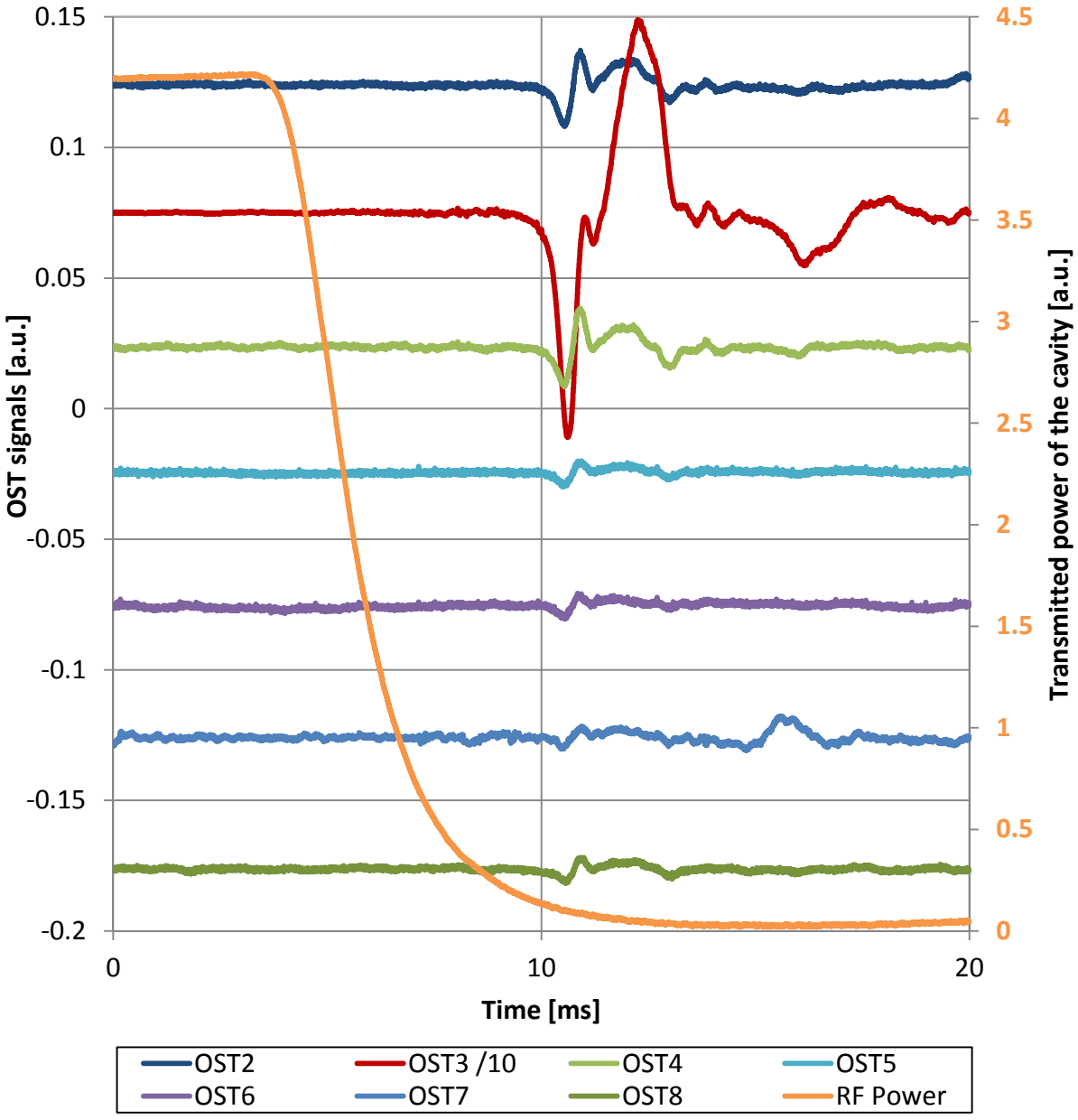

Figure 61: Signals of the seven OSTs for a global quench of the Crab Cavity. The transmitted RF power is also plotted to indicate the quench. The signal of OST 3 was divided by a factor of ten for better display.

The orange curve, which depicts the transmitted RF power through the tested cavity, indicates the quench. The transmitted power is directly proportional to the stored energy in the cavity ($P_t \propto U_s$). So at the beginning of the trace the stored energy in the cavity is about constant, then the cavity quenches and dissipates the stored energy in an exponential manner.

One can clearly see a signal on all OSTs at roughly the ten millisecond mark. The strongest signal can be seen on OST 3, for better display in this graph its signal was divided by a factor of 10. It is by far the strongest signal. On OST 7 one can also see a second signal at the 15 ms mark which interestingly does not go down but up. This upward bend of the curve could be detected in repeated measurements but not in all of them. The arrival of the second sound wave at the OST is marked by a decreasing measurable voltage. The onset of the bend down thus marks the arrival time. Although the arrival time was similar for all OSTs they were not precisely at the same time. The first signal arrives at OST 3 closely followed by OST 2 and 4. The other OSTs all responded a bit later, after the 10 ms mark.

The strong signal of OST 3 is only explainable by a second sound wave that has a much higher temperature deviation of the bath temperature in comparison to the other curves. This gives rise to the assumption that the quench originated close to the OST and thus was heated most. As the second sound signal can be seen on all OSTs at roughly the same time only two possibilities can explain this behaviour. Either the heating spot is at the same distance of all OSTs or there are multiple origins of second sound on the cavity. The first assertion is not possible because there is no such spot. The second explanation is quite likely because quench propagation in a superconducting cavity takes place in the timescale of tens of microseconds, which is much faster than the second sound propagation. This shows that most of the inner cavity surface, if not all, quenches and gets heated. Then the question is why is the signal of OST 3 so much stronger than the signals of the other OSTs, if the whole cavity quenches very fast. The main explanation for this could be the heating prior to the quench. Before a spot does quench it has to be heated to a temperature above the critical surface (see Section 2.4). This means the whole region around the heating spot already has a temperature close to the critical temperature before quench propagation starts. Not much heat is needed to quench the region. The other possible reasons are that the region of the quench origin is a high field region so the heating is anyway very strong, especially when the niobium is normal conducting at this place. This also applies to three other areas in the cavity, see Figure 59, but the spot also gets heated first when the stored energy in the cavity is biggest which corresponds to a high magnetic field. As the dissipated power depends of the squared magnetic field, see Equation (3.2), this can have a big influence.

4.5.1.3 COMBINED TEMPERATURE SENSOR AND OST MEASUREMENT

For the tests in superfluid helium only one Allen Bradley temperature sensor did show a temperature change. Normally the sensors were monitored every minute by a programmable logic controller (PLC). For the quench monitoring they were connected to a precise current source and the voltage change was observed with an oscilloscope. AB 3, one of the sensors directly below OST 3 showed the temperature change.

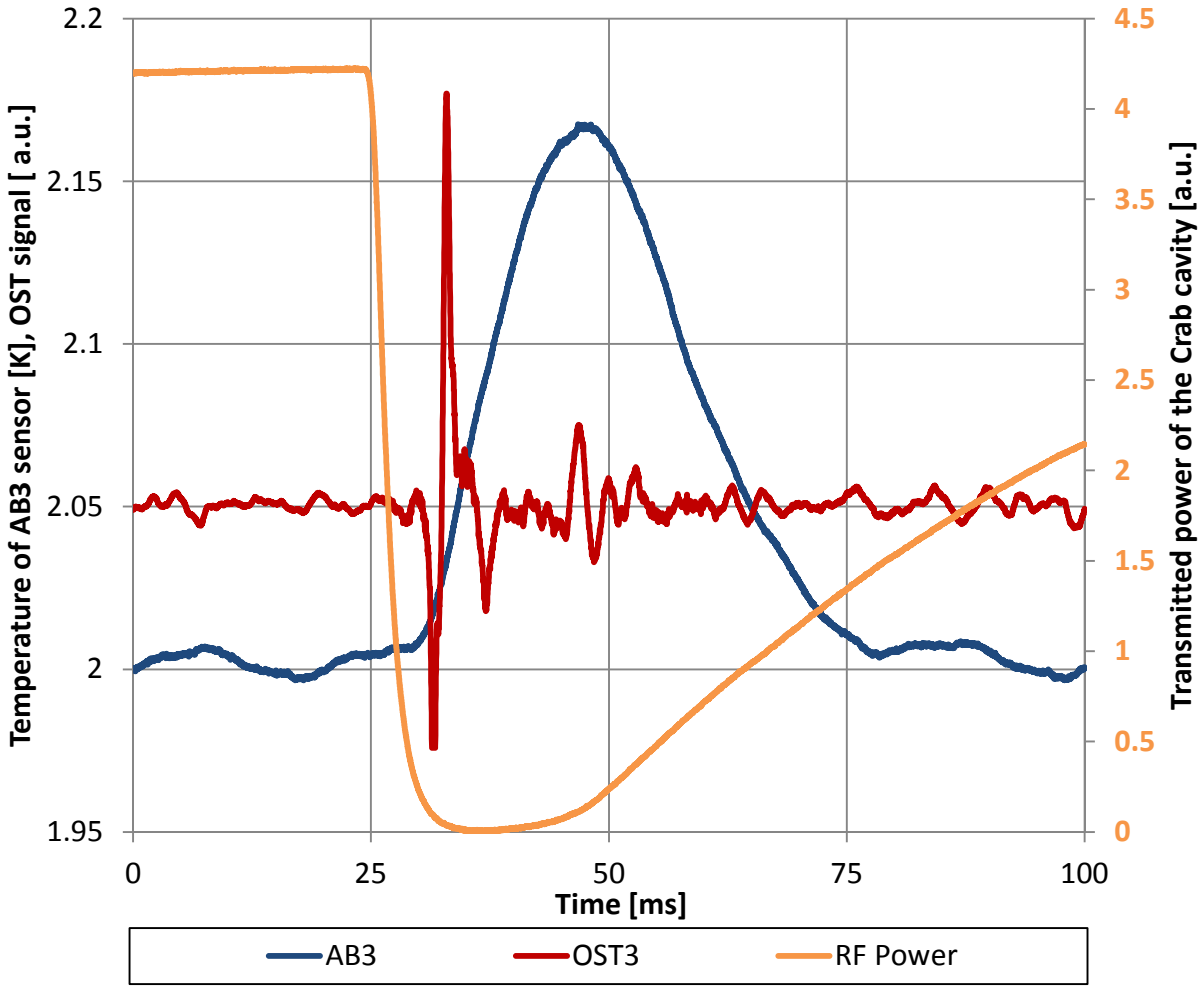

Figure 62: Transient measurement of the AB3 temperature and OST3 at the same quenching event.

Figure 62 shows the signal of OST 3, the Allen Bradley temperature sensor no 3 and the curve of the transmitted power for one quenching event. The response of the temperature sensor is much slower than the OST but gives temperature information. To get the temperature information the resistance of the Allen Bradley carbon resistors was monitored during the initial cooling down procedure and compared with calibrated Cernox™ temperature sensors. The temperature of the sensor rises from about 2 K bath temperature to 2.16 K within 20 ms after the quench. As the bath temperature was controlled by the pressure above the bath one could ask why any

temperature above 2 K did not cause boiling. The slight pressurisation by the helium above is the reason for a higher boiling temperature. This sub cooling by height is especially big for low temperatures and high cryostats. The Crab cavity was tested in an about 4 m deep cryostat so that quite high immersion depths are possible. The principle is depicted in the phase diagram of helium, see Figure 7. The needed liquid column above the crab cavity for a boiling temperature of 2.16 K is about 1.2 m, which could be the case for the test. Unfortunately the helium level reading was not accessible after the experiment anymore.

The transmitted power again shows the quenching event as it drops quickly at the 25 ms mark. The quench alters the properties of the cavity in such a way that the cavity reflects the power send to it. When the cavity becomes superconducting again the power fills the cavity again. The transmitted power curve depicts this as one can see the rise of this value only a few milliseconds after the quench.

4.6 Evaluation of Uncertainty in Measurement

Various methods allow the allocation of uncertainties to a certain measurement or calculated value. One of these methods is described in the guide to the expression of uncertainty in measurement (GUM) [54]. The GUM states that a measurement is an estimation of the value which one tries to determine (true value). The measurement has a certain accuracy. The GUM therefore assumes that the deviations from the true value can be described with a Gaussian distribution and is therefore only valid for statistical errors. Systematic errors are not included in this evaluation of uncertainty. One is not able to determine the true value but can give a range of confidence in which the true value can be found with a certain percentage. This is expressed by the combined standard uncertainty. This standard uncertainty states that in 68.27% the true value is within the given boundaries. Three times the standard uncertainty gives the boundaries to cover 99,73% of the true values. In this document all error bars represent three times the standard uncertainty.

The GUM differentiates two types of evaluations of uncertainty. Type A is a “method of evaluation of uncertainty by the statistical analysis of series of observations” (GUM 2.3.2). Whereas type B is described as a “method of evaluation of uncertainty by means other than the statistical analysis of series of observations” (GUM 2.3.3.).

Although many measurements were made for the presented work, the measurements with the same conditions were not made repeatedly so that they could be investigated by statistical means. Thus the evaluation of uncertainty was done with the type B method.

The measurements in the presented work were not limited by the tools of measurement but by the application of these tools. As no uncertainty values for the used methods could be found, upper and lower bounds were estimated (GUM 4.3.7).

Following this method the GUM advises to determine the standard uncertainty u by

$$u(x_i) = \sqrt{\frac{a^2}{3}} \tag{4.2}$$

where x_i describes the measured estimate of the true value X_i and a half the difference between upper and lower bound. For uncorrelated input quantities as used in this work the propagation of uncertainty for a function of the true values of $Y = f(X_1, X_2, \dots X_N)$ can be fused into a combined standard uncertainty $u_C(y)$ for the calculated value y

$$u_C(y) = \sqrt{\sum_{i=1}^{N} \left(\frac{\partial f}{\partial x_i}\right)^2 u^2(x_i)}\,. \tag{4.3}$$

The evaluated values in the presented work are velocities and temperatures.

The velocities were calculated by measuring a distance and determining a time of flight from an oscilloscope and dividing the distance by the time. The precision of the measuring instruments was not the limiting factor but the use of these tools. The uncertainty of the slide calliper is given with 0.02 mm but this value is not realistic as it was very hard to determine an accurate value for mounted experiments. To be still able to determine an uncertainty an upper and lower bound of 0.5 mm was estimated. The time of flight was determined by identifying the arrival of the second sound wave on an oscilloscope trace. The oscilloscope gives the measurements in 0.4 µs increments but the noise level is far too high to determine the beginning of a bending down curve that quickly. Therefore an upper and lower bound of 25 µs was chosen to determine the uncertainty of this measurement. The bounds of the pressure uncertainty were given by the specifications of the used pressure sensor. The used equations can be found in Appendix 8.2.1.

5 Conclusion

Refurbishment and extension of test stands. The experimental setup for Oscillating Superleak Transducers (OST) tests in the central cryogenic laboratory of CERN was successfully upgraded. An improved pressure measurement and control system tremendously increased the stability and accuracy of the helium bath temperature. A new temperature controlled heating system allowed faster warm-ups and avoided condensation of air humidity on the setup when the cryostat is opened. The use of RF heaters made it possible to apply about ten times higher heating powers (1 kW/cm^2), but they are still in the lower range of heat generation during a quenching event in a superconducting RF cavity.

Theory of heat transfer for quenches on superconducting cavities. The theory of the occurring thermal effects during quenches was discussed in detail. Their interaction and impact on the process was evaluated by a combination of simplified models and a literature study. The combined investigation of the behaviour of the second sound in three dimensional geometries and OST signals make it now possible to extract information about the heating duration and gradient from the OST signal. This enables a new way of cavity research and development focused on transient thermal effects in superfluid helium cooling.

Experimental investigation of heat transfer in helium. The high sensitivity and easy applicability of the OST as a second sound detection device was verified. The relationship between heating parameters and the OST signal was experimentally confirmed. The main focus was the fast signal propagation. Signals faster than the second sound velocity were reported in the literature. By a dedicated experiment with well-known parameters these publications could be confirmed for the first time. The observed change in second sound velocity was measured to be up to 10%, obviously much smaller than reported in other publications. A dependency of the applied heating powers on the propagation speed was observed. The theory of amplitude dependence by Temperly and Khalatnikov could be excluded as the solemn effect for this relationship.

6 Outlook

The presented work gives detailed insight into the occurring thermal phenomena during a quench of a superconducting radio frequency cavity. Therefore it is the basis for a subsequent research and development program. For the use of OSTs as sensors for cavity tests three main fields have to be investigated further.

Most of the effects during quenches in RF cavities are well known, but their interaction is not well understood. Therefore a theoretical model should be established, which combines heating, heat transport in the cavity material, across the solid-helium interfaces and in the superfluid helium itself. This would allow simulations that show the interplay of the occurring effects.

In the presented work signal propagation faster than second sound was verified. This raises the question what the causing effects are. A dedicated investigation is needed to gain further knowledge. The best starting point for such a research is probably a close look at the occurring boiling phenomena and interaction between first and second sound as theoretically predicted by Dessler [56].

The third field of further investigations are the OSTs and their behaviour. The following paragraphs concerns the upcoming questions and makes suggestions how to investigate them.

In literature the OSTs were proven to be very well suited for quench localisation but up to now only a fraction of the transported information of the signal is used. The signal bears information about boiling effects and the heat flux and therefore also the heated area. Further studies are needed to relate the OST signals to these effects.

As some measurements gave rise to the assumption that the OST signal was altered when it was not perpendicular to the heater, this effect should be studied. A setup was already built in the central cryogenic laboratory of CERN to allow such investigations.

Since 2008 the OSTs, which were used for quench localisation measurements, had always the same design governed by the size of the commercially available membranes. The diameter of the membranes, which is exposed to the helium II, is quite large with 19 mm. This could be a restriction for more precise quench localisations. One should try to cover a part of this area and compare whether the localisation can be improved. In general the behaviour of the OSTs should be investigated in more detail. As capacitor microphones have a similar working principle and very sophisticated studies have been performed for them, this knowledge should be used to improve the OST design.

To learn more about the response of boiling effects on the OST signals it would be very helpful to compare the response on heating pulses with and without boiling effects. As this is only helpful for the same hating power and the same bath temperature in both cases, the pressure is the only variable that can be changed. Higher pressures (than vapour pressure) should suppress boiling and can therefore give a good condition for such a test. This can be done in a two bath cryostat with a lambda plate that allows independent regulation of pressure and temperature in helium II. The Cryogenics Laboratory and Test Stations (LCSE) at CEA Saclay has such a cryostat that is available for such experiments.

Comparing the OST signal with the actual temperature of the bath would certainly be the biggest improvement for the understanding of the OST behaviour. This is the reason why a comparison of the OST signal with a fast response thermometer with low thermal mass such as a transition-edge-sensor would be highly beneficial. It would give detailed insight in the performance and restrictions of this highly sensitive device.

7 References

[1] Z. A. Conway, D. L. Hartill, H. S. Padamsee and E. N. Smith, “Oscillating Superleak Transducers For Quench Detection in Superconducting ILC Cavities Cooled with He-II”, TESLA Technology Collaboration, Ithaca, New York, 2008.

[2] CERN Council , “CERN - Convention,” 23 09 2010. [Online]. Available: http://council.web.cern.ch/council/en/EuropeanStrategy/ESConvention.html. [Accessed 19 05 2014].

[3] M. Georges, “TE-EPC-LPC LHC General,” 06 02 2014. [Online]. Available: http://te-epc-lpc.web.cern.ch/te-epc-lpc/machines/lhc/general.stm. [Accessed 19 05 2014].

[4] G. Passardi and L. Tavian, “How CERN keeps its cool,” *CERN Courier,* Nov 25, 2005.

[5] E. Rutherford, “The Scattering of α and β Particles by Matter and the Structure of the Atom”, *Philosophical Magazine,* vol. 21, pp. 669 - 688, 1911.

[6] E. Rutherford, “Adress of the president, Sir Ernest Rutherford O.M., at the Anniversary Meeting, November 30, 1927”, *Proc. R. Soc. Lond. A,* Vol. 117, pp. 300 - 316, 1928.

[7] R. Wideröe, “Über ein neues Prinzip zur Herstellung hoher Spannungen”, *Archiv für Elektrotechnik,* Vol. 21, no. 4, pp. 387 - 406, 1928.

[8] E. O. Lawrence and M. S. Livingston, “Communication to the American Physical Society in May”, *Phys. Rev.,* Vol. 37, 1931.

[9] The Royal Swedish Academy of Science, “Press Release The 1972 Nobel Prize in Physics”, October 1972. [Online]. Available: http://www.nobelprize.org/nobel_prizes/physics/laureates/1972/press.html. [Accessed 28 04 2014].

[10] W. Buckel and R. Kleiner, Superconductivity; Second, revised and enlarged edition, Weinheim: Wiley-VCH Verlag GmbH & Co. KGaA, 2004.

[11] R. J. Donnelly and C. F. Barenghi, “The Observed Properties of Liquid Helium at the Saturated Vapor Pressure”, University of Oregon, Donelly research group, 2004. [Online]. Available: http://darkwing.uoregon.edu/~rjd/vapor1.htm. [Accessed 18 12 2013].

[12] S. W. Van Sciver, Helium Cryogenics, New York, Dordrecht, Heidelberg, London: Springer, 2012.

[13] E. M. Lifshitz and L. P. Pitaevskii, Statistical Physics Part 2 Theory of the Condensed State, Oxford: Pergamon Press Ltd., 1980.

[14] J. F. Annett, Superconductivity, Superfluids and Condensates, Oxford: Oxford University Press, 2004.

[15] I. M. Khalatnikov, An Introduction to the Theory of Superfluidity, New York, Amsterdam: W.A. Benjamin, Inc., 1965.

[16] R. J. Donnelly, “The two-fluid theory and second sound in liquid helium”, *Physics today,* Vol. 62, pp. 34 - 39, 2009.

[17] C. Enss and S. Hunklinger, Low-Temperature Physics, Heidelberg: Springer-Verlag, 2005.

[18] L. D. Landau and E. M. Lifshitz, “Dynamics of superfluids”, in *Fluid Mechanics*, Oxford, Elsevier, 2004, p. 516.

[19] K. Schaber, "*Skriptum Technische Thermodynamik I*“, Karlsruhe, ITTK KIT, 2013, p. 103.

[20] Y. Maximenko and D. A. Sergatskov, “Quench dynamics in SRF cavities: Can we locate the quench origin with 2nd sound?”, in *Proceedings of the Partice Accelerator Confrence*, New York, 2011.

[21] J. Plouin, *Private Communication,* Paris, 2014.

[22] C. Gerthsen and H. Vogel, Physik, Berlin, Heidelberg: Springer, 1993.

[23] H. Padamsee, J. Knobloch and T. Hays, RF Superconductivity for Accelerators; second edition, Weinheim: Wiley-VCH Verlag GmbH &Co. KGaA, 2008.

[24] F. Koechlin and P. Dolegieviez, "Measurements of thermal conductivity of industrial niobium", in *Proceedings of the Fifth Workshop on RF Superconductivity*, Hamburg, 1991.

[25] A. Brown, M. W. Zemansky and H. A. Boorse, "The Superconducting and Normal Heat Capacities of Niobium", *Physical review,* Vol. 92, No. 1, pp. 52 - 58, 1953.

[26] A. Powell, *1-D Thermal Diffusion Equation and Solutions,* Cambridge, Massachusetts: MIT Open Courseware, 2003.

[27] I. N. Bronstein, K. A. Semendjajew, G. Musiol and H. Mühlig, Taschenbuch der Mathematik, Thun, Frankfurt am Main: Verlag Harri Deutsch, 2001.

[28] Y. Xie, "New Insights Into Quench Caused by Surface Pits in SRF Cavities", in *SRF2013: Proceedings of the 16th International Conference on RF Superconductivity* , Paris, 2013.

[29] S.-H. Kim, "Simulation of quench dynamics in SRF cavities under pulsed Operation", in *Proceedings of the Partice Accelerator Confrence*, Portland, 2003.

[30] Z. Liu, M. Kelly and A. Nassiri, "New method to improve the accuracy of quench position measurement on a superconducting cavity by a second sound method", *Physical Review Special Topics - Accelerators and Beams,* Vol. 15, pp. 092001-1 - 6, 2012.

[31] K. Liao and T. Junginger, *personal communication.*

[32] F. Pobell, Matter and Methods, Berlin, Heidelberg: Springer-Verlag, 2007.

[33] C. Kittel, Einführung in die Festkörperphysik, München: Oldenbourg Verlag, 2006.

[34] P. Zhang, M. Murakami, R. Z. Wang and H. Inaba, "Study of film boiling in He II by pressure and pressure oscillation measurements", *Cryogenics,* Vol. 39, pp. 609 - 615, 1999.

[35] V. Arp, "Heat transport through helium II", *Cryogenics,* Vol. 10, pp. 96 - 105, 1970.

[36] K. R. Atkins, Liquid Helium, Cambridge: Cambridge University Press, 1959.

[37] J. Wilks, The properties of liquid and solid helium, Oxford: Oxford University Press, 1967.

[38] L. Landau, "The Theory of superfluidity of helium II", *Journal of Physics,* Vol. 5, pp. 71 - 90, 1941.

[39] R. J. Atkin and N. Fox, "Spherical thermal shock waves in helium II", *J. Phys. C: Solid State Phys.,* Vol. 18, pp. 1585-1593, 1985.

[40] T. Worthington, J. Yan and J. U. Trefny, "Shape analysis of pulsed second sound", *Journal of Low Temperature Physics,* Vol. 22, pp. 293-300, 1976.

[41] P. Zhang and M. Murakami, "Three dimensionality of pulsed second sound waves in He II", *Physical Review B,* Vol. 74, pp. 024528-1 - 10, 2006.

[42] H. N. V. Temperley, "The Theory of the Propagation in Liquid Helium II of `Temperature-Waves' of Finite Amplitude", *Proc. Phys. Soc.,* Vol. A 64, pp. 105-114, 1951.

[43] D. V. Osborne, "Second sound in Liquid Helium II", *Proc. Phys. Soc.,* Vol. A 64, pp. 114-125, 1951.

[44] A. J. Dessler and W. M. Fairbank, "Amplitude dependence of the velocity of second sound", *Physical review,* Vol. 104, No. 1, pp. 6 - 12, 1956.

[45] I. M. Khalatnikov, “Discontinuities and high amplitude sound in helium II”, *Zh. ekspl. teor. Fiz. (U.S.S.R.),* Vol. 23, p. 253, 1952.

[46] H. Preston-Thomas, “The International Temperature Scale of 1990 (ITS-90)”, *meterologica,* Vol. 27, No. 107, pp. 3-10, 1990.

[47] R. Williams, S. E. Beaver, J. C. Fraser, R. S. Kagiwada and I. Rudnick, “The velocity of second sound near T_λ”, *Physics Letters A,* Vol. 29, No. 5, pp. 279 - 280, 1969.

[48] J. Hietanen, J. Stor-Pellmen, M. Luukkala, P. Mattila, F. Tsuzuki and K. Sansaki, “A Helmholtz resonator model for an electrostatic ultrasonic air transducer with a V-grooved backplate”, *Sensors and Acuators,* Vol. 39, pp. 129 - 132, 1993.

[49] A. Quadt, B. Schröder, M. Uhrmacher, J. Weingarten, B. Willenberg and H. Vennekate, “On the response of an OST to a Point-like Heat Source”, *Physical Review Special Topics - Accelerators and Beams,* Vol. 15, pp. 031001-1 - 9, 2012.

[50] N. H. Fletcher and T. D. Rossing, The physics of musical instruments, New York: Springer, 1998.

[51] R. E. Berg and D. G. Stork, The physics of sound, Upper Saddle River, New Jersey: Pearson Education, Inc., 2005.

[52] R. A. Sherlock and D. O. Edwards, “Oscillating Superleak Second Sound Transducers”, *The Review of Scientific Instruments,* Vol. 41, No. 11, pp. 1603 - 1609, 1970.

[53] CEA, “CEA - Identity - Facts and Figures,” October 2012. [Online]. Available: http://www.cea.fr/english-portal/cea/identity. [Accessed 24 March 2014].

[54] Working Group 1, Joint Comittee for Guides in Metrology, Evaluation of measurement data - Guide to the expression of uncertainty in measurement, Joint Comittee for Guides in Metrology, 2008.

[55] J. W. Ekin, Experimental Techniques for Low-temperature Measurements, Oxford: Oxford University Press, 2006.

[56] A. J. Dessler, “Interactions between First and Second Sound in Liquid Helium”, *The Physics of Fluids,* Vol. 2, No. 1, pp. 5 - 7, 1959.

[57] C. P. Poole, Handbook of Superconductivity, San Diego, London: Academic Press, 2000.

[58] A. Macpherson, “SPS Tests - first look at constraints and schedule,” in *LHC-CC13, 6th LHC Crab Cavity Workshop*, CERN, 2013.

[59] S. Meyers and P. Collier, “Executive Summary, LHC-CC11,” in *LHC-CC11, 5th LHC Crab Cavity Workshop*, CERN, 2011.

[60] National Physical Laboratory, “Fig on page 157,” [Online]. Available: http://www.kayelaby.npl.co.uk/general_physics/2_6/2_6_4a.html. [Accessed 28 04 2014].

[61] H. Vennekate, “Second sound for heat source localization,” II. Physikalisches Institut Universität Göttingen, Göttingen, 2011.

7.1 LIST OF FIGURES

7.2 LIST OF TABLES

8 Appendix

8.1 MATERIAL PROPERTIES

8.1.1 Helium as a cryogenic fluid

8.1.1.1 THE INTERNATIONAL TEMPERATURE SCALE OF 1990 (ITS 90)

In the range of 1.25 to 5.0 K the temperature is defined by equations describing the temperature in terms of the helium (^4He) vapour pressure. The temperature is described by the equation:

$$T_{90}/K = A_0 + \sum_{i=1}^{9} A_i \left[(ln(p/Pa) - B)/C\right]^i \tag{8.1}$$

The coefficients to be used are the following:

Table 3: Parameters of the1990 international temperature scale.

^4He	**From 1.25K to 2.1768K**	**From 2.1768K to 5.0K**
$\mathbf{A_0}$	1.392 408	3.146 631
$\mathbf{A_1}$	0.527 153	1.357 655
$\mathbf{A_2}$	0.166 756	0.413 923
$\mathbf{A_3}$	0.050 988	0.091 159
$\mathbf{A_4}$	0.026 514	0.016 349
$\mathbf{A_5}$	0.001 975	0.001 826
$\mathbf{A_6}$	-0.017 976	-0.004 325
$\mathbf{A_7}$	0.005 409	-0.004 973
$\mathbf{A_8}$	0.013 259	0
$\mathbf{A_9}$	0	0
B	5.6	10.3
C	2.9	1.9

Source for "8.1.1.1 The International Temperature Scale of 1990" is [46].

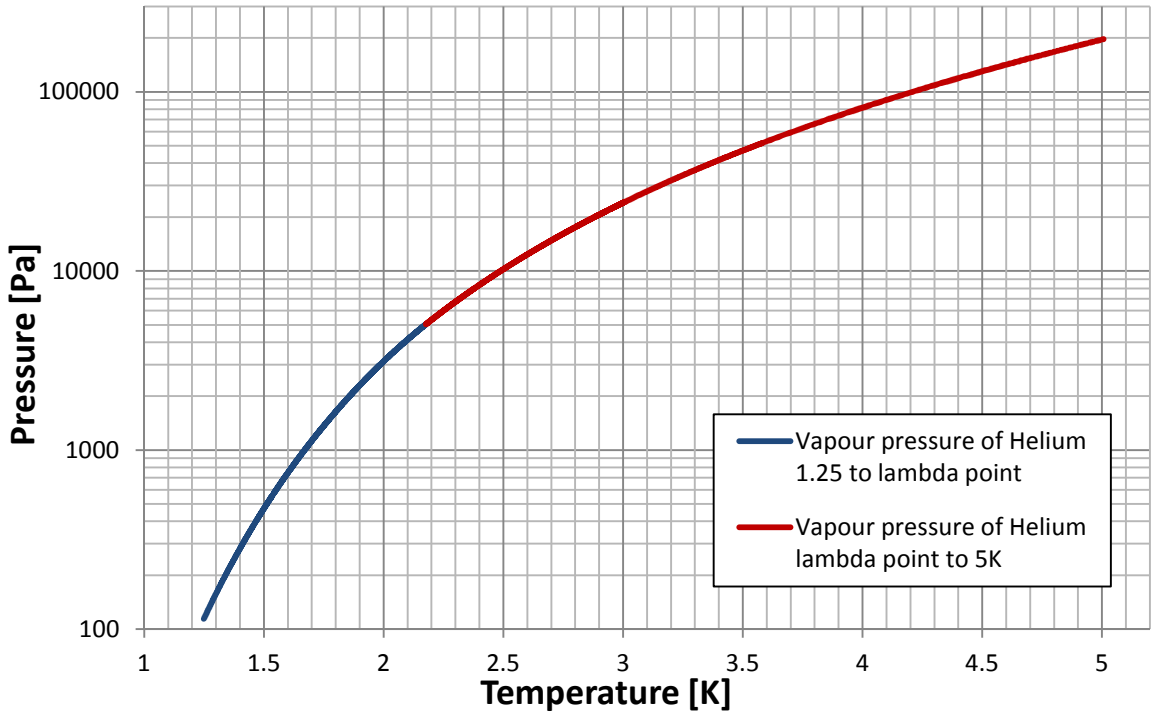

Figure 63: Temperature definition by the vapour pressure of Helium 4 in the range 1.25 K to 5K by the ITS 90.

8.1.2 Specific heat of helium at the lambda point

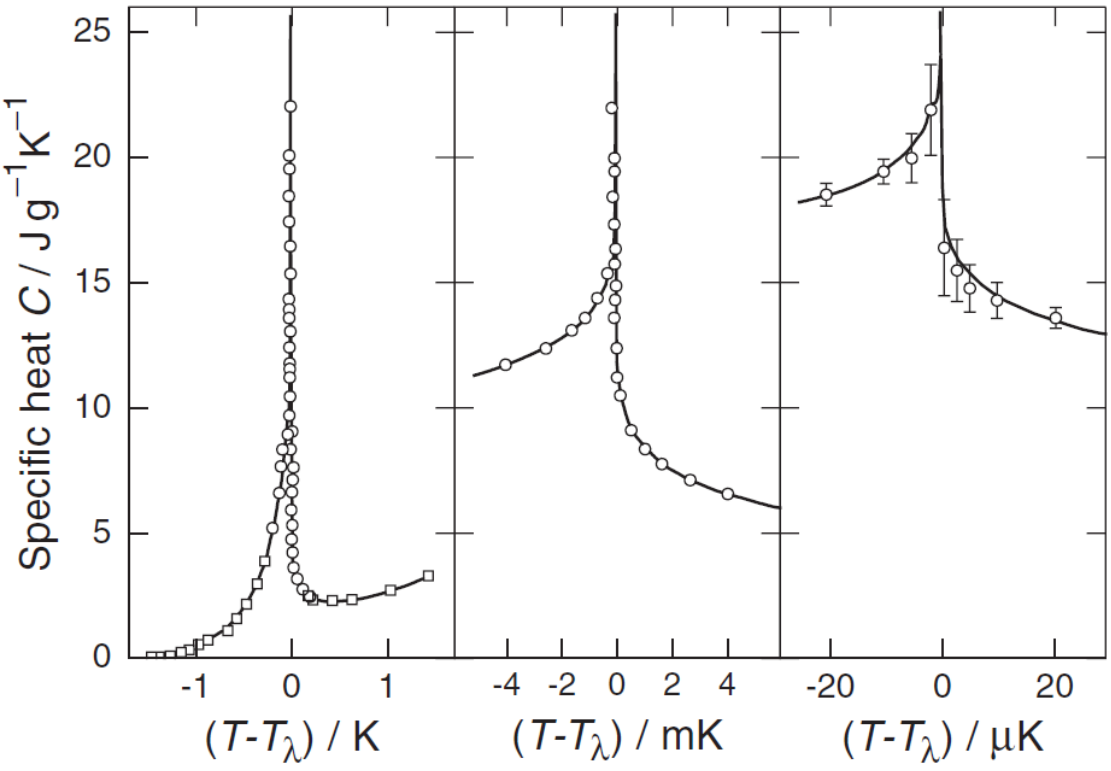

Figure 64: Specific heat of helium close to the lambda point [17].

h

8.1.3 De Broglie wavelength for helium

The de Broglie wavelength is defined as:

$$\lambda = \frac{h}{mv} \tag{8.2}$$

The speed of the helium atoms can be calculated equalizing the kinetic and thermal energy.

$$E_{kin} = E_{th} \tag{8.3}$$

$$\frac{1}{2}mv^2 = \frac{3}{2}kT \tag{8.4}$$

$$v = \sqrt{\frac{3kT}{m}} \tag{8.5}$$

Joining formula (8.2) and (8.5) one gets the formula for the thermal de Broglie wavelength.

$$\lambda = \frac{h}{\sqrt{3\,mkT}} \tag{8.6}$$

For the mass of a helium atom $m_{He} = 4.00\ \mathrm{u} = 6.65 \cdot 10^{-27}\mathrm{kg}$, a temperature of 2 K and the constants $h = 6.63 \cdot 10^{-34}\ \mathrm{m^2kg/s}$ and $k = 1.38 \cdot 10^{-23}\ \mathrm{m^2kg/s^2K}$, the wavelength is $\lambda = 8.93 \cdot 10^{-10}\mathrm{m}$.

The liquid density of helium is about $\rho = 125\ \mathrm{kg/m^3}$, with the molar mass $\widetilde{M}_{He} = 4.00\ \mathrm{g/mol}$, Avogadro number $N_A = 6.02 \cdot 10^{23}\ 1/\mathrm{mol}$ the average distance between the atoms can be calculated.

$$\mathrm{d} = \sqrt[3]{\frac{\widetilde{M}_{He}\,N_A}{\rho}} = 3.76 \cdot 10^{-10} m \tag{8.7}$$

8.1.4 Niobium

8.1.4.1 SKIN DEPTH

According to [23] the skin depth is defined as

$$\delta = \frac{1}{\sqrt{\pi f \mu_0 \sigma}} \tag{8.8}$$

In this case f is the frequency of the field, μ_0 the permeability of free space and σ the electrical conductivity of the material.

The electrical conductivity of niobium is $6.58 \cdot 10^6 \frac{1}{\Omega m}$ [57] and the permeability of free space is $4\pi \cdot 10^{-7} \frac{N}{A^2}$. For a frequency of 1.3 GHz this gives a skin depth of 17 µm.

8.2 THEORY

8.2.1 Calculating averaged factors for the amplitude dependence of second sound

The amplitude dependence of second sound is a well proven theory [44]. It states a change in the literature value of the second sound dependent on the heat flux of a pulse. All experiments quantifying this theory were done in small channels with a constant cross section in order to have a constant heat flux. As the experiments for the presented work in this thesis were done in a three dimensional setup, the theory has to be altered to be applicable.

In the conducted experiments the speed of second sound was obtained by measuring the time of flight over a known distance. In this way it is impossible to know the change of SSV at a certain point, but an averaged value over the whole distance is the result. The aim is to calculate a value for τ_2 for the average speed of second sound.

Based on the definition of

$$\tau_2 = \frac{v_2 - v_{2,0}}{v_n} = \frac{\Delta v_2}{v_n} \tag{8.9}$$

With the following relationship between heating power $\dot{Q}$ and normal fluid velocity v_n.

$$\dot{Q} = A \rho s T v_n \tag{8.10}$$

The basic simplification of this calculation is that the second sound wave is emitted as a semi-sphere from an also semi-spherical heater.

j

The radius of the heater is given as

$$r_0 = \sqrt{\frac{A_{heater}}{2\pi}} \qquad \text{(heater radius)} \tag{8.11}$$

To determine the heat flux density to calculate the velocity of the normal component, an area has to be known. For a given distance r_1 from the zero coordinate this area is calculated as:

$$A = 2\pi {r_1}^2 \tag{8.12}$$

If the Equations (8.9) and (8.10) are rearranged for v_n and set as equal, one obtains.

$$\Delta v_2 = \frac{\dot{Q}\tau_2}{\rho s T\ 2\pi r^2} \tag{8.13}$$

To be able to use an averaged second sound signal this formula has to be integrated over the covered distance and then divided by this distance.

$$\overline{\Delta v}_2 = \frac{1}{r_1 - r_0}\int_{r_0}^{r_1} \Delta v_2\ dr = \frac{\dot{Q}\tau_2}{\rho s T\ 2\pi(r_1 - r_0)}\int_{r_0}^{r_1} \frac{1}{r^2}\ dr \tag{8.14}$$

Solving this integral gives

$$\overline{\Delta v}_2 = \frac{\dot{Q}\tau_2}{\rho s T\ 2\pi\ r_1 r_0} \tag{8.15}$$

Rearranging for the amplitude dependence factor gives

$$\tau_2 = \frac{\overline{\Delta v}_2}{\dot{Q}} \rho s T\ 2\pi\ r_1 r_0. \tag{8.16}$$

In a similar way the amplitude dependence parameter Γ_2 can be obtained.

$$\Gamma_2 = \frac{\overline{\Delta v}_2}{\dot{Q}}\ 2\pi\ r_1 r_0. \tag{8.17}$$

8.3 MEASURING EQUIPMENT

8.3.1 Equations used for the evaluation of the uncertainty of measurement

Equations (4.2) and (4.3) build the basis of the uncertainty evaluation in this thesis. The actual used formulas are given in the following.

The distance between heater and OST are calculated by:

$$\mathrm{d} = \sqrt{\frac{a^2}{2} - \frac{c^2}{4} + \frac{b^2}{2}} \tag{4.1}$$

The associated uncertainty can be calculated by

$$u_{C,d} = \sqrt{\left(\frac{a}{2d}\right)^2 u_a{}^2 + \left(-\frac{c}{4d}\right)^2 u_c{}^2 + \left(\frac{b}{2d}\right)^2 u_b{}^2} \tag{8.18}$$

The velocity of the second sound is calculated by

$$v_2 = \frac{d}{t} \tag{8.19}$$

With the combined uncertainty of

$$u_{C,d} = \sqrt{\left(\frac{1}{t}\right)^2 u_{C,d}{}^2 + \left(-\frac{d}{t^2}\right)^2 u_t{}^2} \tag{8.20}$$

The temperature is calculated by the International Temperature scale of 1990:

$$T_{90}/K = A_0 + \sum_{i=1}^{9} A_i \left[(ln(p/Pa) - B)/C\right]^i . \tag{8.1}$$

The uncertainty of the temperature measurement is given by the uncertainty of the pressure.

$$u_{C,d} = \sqrt{\left(\frac{A_1}{p\,C} + \sum_{i=2}^{9} \frac{i\,A_i}{p}\left[\frac{(ln(p/Pa) - B)}{C}\right]^{i-1}\right)^2 u_p{}^2} \tag{8.21}$$

8.3.2 The broken RF heater

To obtain even larger heating powers than with the SMD resistor it was planned to use a RF heater. These heaters have a resistance of 50 Ω and are built to convert high frequency power into heat. The power is conducted via a coaxial cable to the heater. Normally the auxiliary equipment to use such a resistor as a heater is quite sophisticated and expensive. One needs a signal generator which can deliver a heat pulse with a certain frequency and well-defined amplitude as well as an amplifier for this frequency. Fortunately these devices are used to deliver power to cavities, so the equipment was available.

The used heater was an aluminium-nitride-ceramic resistor made by the company “Bourns”. It is specified for 250 W usage at room temperature.

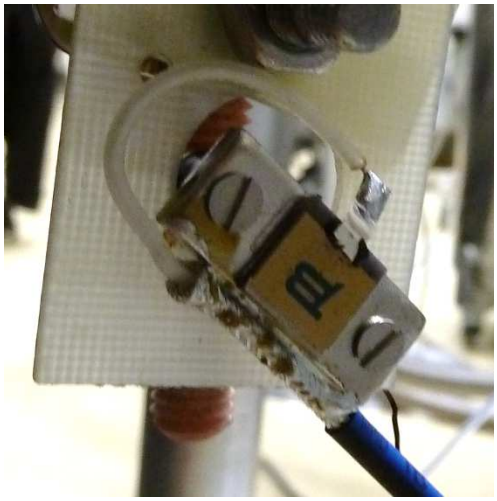

Figure 65: RF heater before test in LHe.

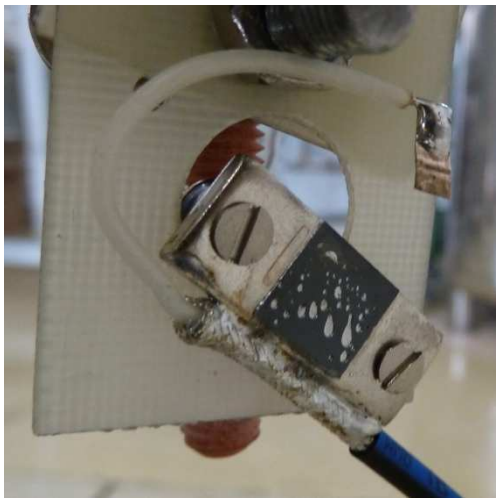

Figure 66: RF heater after test in LHe.

Most of these heaters are not specified for use in cryogenic conditions and if they are the rage only goes down to the temperature of liquid nitrogen (77 K). The experience shows that many resistors still work at LHe conditions and the applicable heating power is even higher than specified. This did not hold for the used heater. After a small testing pulse at the beginning of the experiment the resistance of the heater was unmeasurable high. After the experiment it was found that the resistive layer of the heater had come off the back body of the heater. It was found, split into two pieces at the bottom of the cryostat. Figure 65 and Figure 66 show a comparison of the main heater body before and after the experiment.

Probably the resistive layer (yellow with blue “B”) was glued to the back plate with small gas bubbles trapped in the glue. As superfluid helium can penetrate even the smallest gaps it probably crept behind the heater. When the heating was turned on it was vaporized and blasted the front part off.

8.3.3 Circuit layout of the OST Amplifiers

OST box inner circuit:

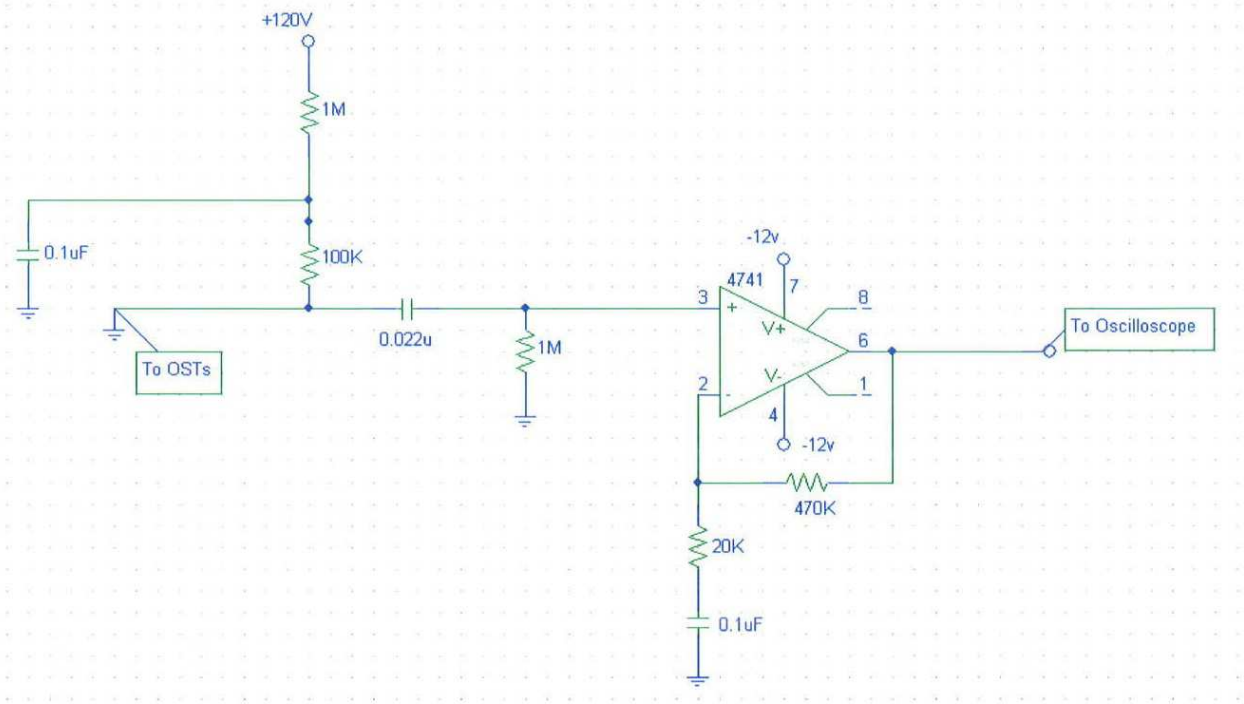

n